Alma Mater Studiorum · Università di Bologna

Scuola di Scienze
Dipartimento di Fisica e Astronomia
Corso di Laurea Magistrale in Fisica

Two Dimensional P-wave Superconductors with Long Range Interactions

Relatore:
Prof. Elisa Ercolessi

Correlatore:
Prof. Fabio Ortolani

Presentata da:
Roberto Saputo

Anno Accademico 2017/2018

grazie a tutti...

Abstract

L' interesse crescente che circonda lo studio delle proprietà topologiche della materia è profondamente collegato all' effetiva possibilità di verifica in laboratorio. Negli ultimi decenni infatti la fisica sperimentale degli atomi ultrafreddi ha raggiunto livelli di precisione prima inimmaginabili. Attraverso reticoli ottici si possono riprodurre sistemi multicorpo fortemente interagenti di cui si possono controllare in maniera quasi esatta i parametri fisici, come i potenziali. In questo contesto si inserisce il modello bidimensionale P-wave con interazioni a lungo raggio. Le interazioni in questo modello avvengono tra tutte le componenti, quindi in tutte le direzioni. Questo sistema fisico topologico inoltre è caratterizzato da una Hamiltoniana con potenziale di interazione che decade con la distanza secondo una legge di potenza per cui, per quanto detto, la sua realizzazione sperimentale è possibile. In questo lavoro abbiamo iniziato studiando lo spettro di questo sistema partendo da un approccio analitico. Dopo aver compreso il comportamento dei vari termini energetici abbiamo selezionato dei casi di studio per diversi range di interazione. In questi casi successivamente abbiamo analizzato le varie fasi e transizioni di fase tramite simulazioni numeriche. All' aumentare del range di interazione abbiamo visto l' emergere di nuovi fenomeni assenti nei modelli con interazione a corto raggio.

Contents

List of Figures

List of Abbreviations

APC: Antiperiodic Boundary Conditions
BCS: Bardeen-Cooper-Schrieffer
BdG: Bogoliubov-de Gennes
BZ: Brillouin Zone
CPT: Classical Phase Transition
FQH: Fractional Quantum Hall
LR: Long Range
OBC: Open Boundary Conditions
OO: Open Open
PBC: Periodic Boundary Conditions
PHS: Particle-Hole Symmetry
PP: Periodic Periodic
PRS : Particle-hole Reversal Symmetry
QPT: Quantum Phase Transition
SPP: Strong Pairing Phase
SPT: Symmetry Protected Topological
SR: Short Range
TRS: Time-Reversal Symmetry
WPP: Weak Pairing Phase

Introduction

A main theme in condensed matter physics concerns the classification of different states of matter and the characterization of systems in the vicinity of a phase transition. Classically a phase of matter is defined as a distinct form in which the constituents of a many-body system are organized with a distinct set of physical properties. Within a given phase, the properties of a system as functions of parameters such as temperature vary smoothly, while during transitions among different phases discontinuities are present in some of these parameters. But the discovery of a class of strongly correlated systems in the early '80s called the fractional quantum Hall (FQH) liquids [1] opened the way towards a new set of phases. The study of FQH systems has shown that the classification based on symmetry breaking is not complete and has revealed that phases of matter should also be distinguished based on their topological properties. In fact FQH states share the same symmetry even if they are separated by a phase transitions. It turns out that the differencies among FQH states arise from topology. In fact it was shown that the symmetry of a many-body system cannot be spontaneously broken at any finite temperature in dimensions $d \leq 2$. This result, which holds in systems with sufficiently short-range interactions, is called the Mermin–Wagner theorem [2]. But an alternative mechanism preserving symmetry involves the creation of topological defects that are finite energy distortions of the order parameter field that cannot be eliminated by any continuous change of it. The topological properties that define different phases of matter are intrinsically quantum mechanical and there are two main categories of topologically nontrivial quantum phases [3]. There are phases possessing states with short range topological order and phases with the so-called intrinsic topological order states. The short range order is characterized by the emergence of bulk excitations with fractional statistics and in this case the states require the presence of certain symmetries. These are called symmetry protected topological states and their topological properties are robust against adiabatic deformations of the Hamiltonian that preserve the symmetry. The intrinsic ordered phases states instead emerge in strongly interacting many-body systems and they are protected against any type of adiabatic deformation of the Hamiltonian. The standard example of intrinsic ordered quantum states is provided by the fractional quantum Hall effect (FQHE).
Note also that topological phases are often characterized by a gapped bulk and a gapless

boundary. However, gapless boundary modes are always present only in noninteracting topological systems and they are not required in interacting systems. The boundary modes of which we talked above were introduced in 1937 by Ettore Majorana and they are known as 'Majorana fermions' i.e. particles that constitute their own antiparticles. Nowadays Majorana fermions are central to diverse problems across modern physics. For what concerns condensed matter systems these are not fundamental particles as the constituents of matter are and this fact severely constrains the success in their search. In fact if a Majorana fermion is present in a solid state it must be in the form of non-trivial emergent excitations [4]. Then the unambiguous observation of Majorana fermions nevertheless remains an outstanding goal. Recent advances in the condensed matter search for Majorana fermions have led many in the field to believe that this quest may soon get an answer. The key insights that arose during the past few years regard the possibility to 'engineer' materials containing them in the laboratory by forming heterostructures of appropriate materials. Numerous proposals of this type have been made based on topological insulators, conventional semiconductors, ferromagnetic metals, and many others. Two of the best-studied systems are Sr_2RuO_4 and UPt_3 [5], which are superconductors thought to host Majorana fermions. Key signatures of these states are surface currents and chiral Majorana modes, Majorana states in vortex cores and the possibility of half-flux quantum vortices in the case of superconductive triplet pairing. The most interesting property of such states is that these are exotic quasiparticles with intrinsic topological protection and robustness against disorder. These characteristics make them the ideal candidates as building blocks in quantum computation and quantum information processing.

In the last two decades a lot of theoretical models describing short range ordered phases have been proposed in one ad two dimensions [6, 7] to explain the basic mechanisms of Majorana fermions and how to search for them but literature lacks of models describing strongly interacting systems. This is a striking argument to look at because as we explained above, the intrinsic topological ordered states have strong properties of robustness against all kind of Hamiltonian deformations. This gives importance to the study of these models in the long range. Then another important reason to study such models is linked to the outstanding goals reached by the ultracold atom physics on optical lattices [8]. In fact it is nowadays possible to reproduce quantum many-body interacting systems in laboratory [9] and to fine-control the parameters which decay as a power law.

Then following the previous works done by E. Ercolessi, D. Vodola and G. Pupillo [10, 11] our work inserts his self in this fascinating topic. In particular in Chapter 1 we start with a general description of the different kinds of phase transitions and classify the Hamiltonians on a symmetry basis. Then we explain some important concepts linked to topology in quantum systems, i.e. the Berry curvature and the topological invariants. Then in Chapter2 we introduce the 1D models starting from the p-wave superconductor which is a topological model that contains the principal hints of the subject. We then move on to the Kitaev model which is a simple but rather efficient case to understand

the different phases of a system. In the last part we talk about the long range p-wave superconductors, where new phenomena occur compared to the short range case. After that in Chapter3 we introduce the 2D models. We start by describing the p-wave chiral superconductor that supports boundary chiral gappless edge-states described by a quasi-1D approximation. Afterwards we show how to compactify the momentum space in order to calculate the the winding number for this model. Then we move on to the core of the work introducing the p-wave superconductor with long range interactions. We start from the energy spectrum analysis by means of analytical methods to understand the behaviour of its components when varying the interaction lenghts. Then by means of numerical methods we fix the hopping term to reproduce the short range kinetic term and we analyse the spectrum in some relevant cases with open boundary conditions in both directions. With these simulations we were able to catch the edge-states structure. Finally to test the correctness of the work we compared the results with simulations made with periodic boundary conditions in both directions where we do not expect to see any edge-states indeed none of them appeared.

Chapter 1

Phases Of Matter

Condensed matter physics deals with the behaviour of particles at finite density and at low temperatures. Depending on some parameters matter can reorganizes itself in different phases. Classically, we learn of phases such as crystal, liquid or vapor but the quantum theory predicts the existence of a great number of different states. There are superconductors, Bose-Einstein condensates, ferromagnets and antiferromagnets and many others. The main feature for characterizing them is called symmetry breaking. An order parameter with observable consequences acquires a finite expectation value in a certain state of matter that differentiates it from others. For example there is an overall magnetization in ferromagnet which breaks the rotational symmetry of the spin and picks a particular direction of the north pole. An antiferromagnet does not have an overall magnetization but develops a staggered-order parameter at some finite wavevector. The theory of phase transitions exposed by Landau [12] provides the phenomenological explaination of this mechanism. According to his theory, a system that is in a symmetric phase at high temperature passes through a phase transition at low temperature and goes to a less symmetric state. It describes this mechanism by the possibility to expand the free energy in the order parameter close to a phase transition and this is possible because the order parameter is small there. The limitation of Landau's theory is that it is related to a local order parameter. In fact it has become clear in the last decades that there exist phases of matter that do not have a local order parameter and its presence makes unclear how to develop a Landau-like theory.

1.1 Classical Phase Transitions

A classical phase transition (CPT) of a system is a change of its equilibrium state which modifies its physical properties. This is done by varying some externally controllable parameters such as temperature. The CPTs can be described by an order parameter, say g that is non-zero in the ordered phase (less symmetric) and vanishes in the disordered

one. We say that a transition is first-order if g is discontinuous at a critcal point while it is of second-order if g changes from a zero to a non-zero value in a continuous way. In the latter case, the correlation length diverges and the fluctuations are present at all length scale. So the system is scale invariant and the renormalization group method can be applied. A first order transitions happens when the first order derivative of the free energy with respect to a parameter is discontinuous at the transition point. Often this discontinuity is accompanied by a jump in the entropy, thus it involves a latent heat $Q = T\Delta S$ that implies an absorption or release of energy so it cannot occur instantaneously. On the contrary if all the first derivatives of the free energy are continuous but a second derivative has a discontinuity, the transition is classified as second order. Second order phase transitions happen because even if the thermodynamic average of the order parameter is zero for $T > T_c$, its fluctuations are non-zero. Then the spatial correlations of these fluctuations increase as the system is driven towards the transition and become long-ranged near the critical point. Away from T_c, the two-point correlation function typically decays exponetially:

$$C(\boldsymbol{x}_i, \boldsymbol{x}_j) \propto e^{-|\boldsymbol{x}_i - \boldsymbol{x}_j|/\xi}$$

where ξ is the correlation length. Close to T_c it diverges as:

$$\xi \sim |\epsilon_T|^{-\nu}$$

where $\epsilon_T = \frac{|T-T_c|}{T_c}$ estimates the distance from the critical point and ν is a critical exponent. In general, a critical exponent defines the scaling behaviour of a given quantity very close to the critical point of a continuous phase transition. In addition to a diverging correlation length, we also observe a diverging correlation time as $\epsilon_T \to 0$, in fact:

$$\tau_c \sim \xi$$

These two divergences are responsible for the so-called critical phenomena and allow to rescale the lengths of a system without changing its physical properties. Then the system is said to be scale-invariant. Phase transitions as we said can present a symmetry breaking, meaning that the state of the system is driven from a highly symmetric phase to a lower symmetric one. The more symmetrical phase is called disordered while the less symmetrical is called ordered. Then we say that a symmetry is spontaneously broken when the Hamiltonian exhibits all the possible symmetries in the disordered phase while it lacks some of them in the ordered one and say it is explicitly broken when some terms in the Hamiltonian do not respect the symmetry of the theory. Finally we would like to mention again Landau's theory of phase transitions which is not concerned with the microscopic details of the interactions but it is strictly related to symmetry. In fact systems described by different microscopic theories but sharing the same symmetries are similar within this picture. In particular the Landau theory applies to symmetry

breaking transitions concerning second order phase transitions and relies on the idea that the order parameter is small close to the phase transition. This observation suggests that a Taylor expansion of the free energy with respect to the order parameter can provide information about the behaviour of the system near the phase transition. Then once the order parameter of the theory has been identified one can proceed to construct the Landau free energy F as a function of the external parameters and the order parameter g:

$$F = F_0 + \sum_n F_n g^n$$

The F_0 term here represents the free energy of the disordered phase. The number of terms in the series can be restricted by symmetry considerations and the series is truncated as soon as the physics is captured. For a given set of external parameters, the stable state of the system is obtained by minimizing the free energy with respect to g

$$\frac{\partial F}{\partial g} = 0$$

Note that the physical properties of a system close to a second order phase transition are described by the critical exponents and these depend only on the symmetries of the system and the dimension of the space. This phenomenon is known as universality and systems which share the same critical exponents are said to belong to the same universality class. In fact, near criticality the microscopic details of the Hamiltonian become unimportant and Hamiltonians with the same symmetries show a similar behavior.

1.2 Quantum Phase Transitions

A quantum phase transition (QPT) is the transformation of a system from one phase of matter to another at zero temperature. It implies a change in the ground state due to quantum fluctuations. Unlike the CPT it is driven by a change in one or more physical parameters appearing in the hamiltonian, such as the magnetic field. Then while a CPT arises from thermal fluctuations and vanishes at zero temperature a QPT arises in this situation at the quantum critical point (QCP). Here quantum fluctuations diverge and become scale invariant in space and time. Even if zero temperature is not realizable in physical systems the transitions can be detected in the low-temperature regime. In this situation the system is in the so called quantum critical region (QCR) [13]. Here both the classical and quantum fluctuations are present but the quantum ones dominate the system until their energy scale is larger than $k_B T$ (k_B is the Boltzmann constant) and then they are completely destroyed. In order to establish the range of validity of the classical picture, one has to compare the typical classical energy scales with the parameter fluctuations. The energy of quantum fluctuations is $\hbar\omega$ where $\hbar$ is the reduced Planck constant while ω is the frequency characteristics of the lowest ecitation. We are

in a quantum regime when $k_B T < \hbar\omega$. Also QPTs can be classified as first or second order phase transitions. In first order phase transitions one does not observe diverging correlations while in second order phase transitions we observe that the characteristic energy scale of fluctuations above the ground state, say Δ vanishes for $g \to g_c$ and the characteristic length scale diverges. Then the behavior of the energy gap near the critical point could reveal the nature of the phase transition. In fact in second order phase transitions we have that:

$$\Delta \sim |g - g_c|^{z\nu}$$

Then his behavior holds for both $g > g_c$ and $g < g_c$ with the same critical exponent $z\nu$ but with different constants of proportionality. Noting that the correlation length diverges as:

$$\xi^{-1} \sim \Lambda |g - g_c|^{\nu}$$

we can conclude that $\Delta \sim \xi^{-z}$ then it is decaying as a power law.

1.3 Topological Phase Transitions

It is well known that in low dimensions, typically in 1D and 2D, the mechanism of spontaneously symmetry breaking is forbidden, at least if the interactions are short range, as stated by the so-called Mermin-Wagner theorems [2]. The existence of "topological phase transitions" and "topological states of matter", that escape such paradigm are known since the '80s, in connection with the integer and the fractional quantum Hall effect, or with the quantum spin-liquid state of integer-spin chains. A topological phase is a phase of matter whose low-energy field theory is a topological field theory. Recently, topological phases have been pursued because of their potential practical applications, in fact it has been proposed that a topological quantum computer could employ the 2D quasi-particles of superconductors whose world lines cross over one another rembering the way they did it. They follow the rules of a Braid Group and can form the logic gates making up the computer. The advantage of such a kind of computer when compared to one using trapped quantum particles is that the former encodes information non-locally and hence is less susceptible to local decoherence processes. The problem is that even if the concept of topological order has been discussed for more than a decade most examples involved complicated models. Meanwhile states of matter formed out of free fermions where thought to be topologically trivial because the Hamiltonian spectrum is exactly solvable. But there are two subsets of these states called topological insulators and topological superconductors that have interesting properties despite being made out of non-interacting fermions. For these systems it is possible to differenciate a trivial phase which has two bands separated by a gap, say $\Delta \neq 0$ from the non-trivial one which presents gapless surface or boundary gapless states that fill the energy gap thus linking the two energy bands. While the presence of gapless edge modes is a test but

it is not necessary to distinguish topological phases, the term topological implies the existence of a bulk invariant. This can either be one or a set of numbers that label different phases of matter having the same symmetries. Then we are now interested not only in which symmetries are broken during a phase transitions but which of them must be preserved for the stability of the state. A series of symmetries, the most important of which are time reversal and charge conjugation can be used to classify states of matter. In fact a periodic table classifying the topological insulators and superconductors has been created as we will show later on.

1.4 Classification of Topological Phases

The topological properties of a phase such as boundary modes in an open geometry are described by a set of quantized numbers called the topological invariants of the phase. These properties are found for gapped ground states of local Hamiltonians without boundaries at zero temperature. The quantization implies that these properties can not change adiabatically in fact the spectral gap allows to define an equivalence class of phases using the adiabatic theorem. The idea is that two gapped phases are the same if it possible to pass from one to the other by slowly changing the parameters of the Hamiltonian like the chemical potential without closing the gap. If this is not possible the two phases are topologically distinct. In the latter case the interface between the two phases will hosts a state in the bulk gap that can not be moved into the continuum of excited states. The topological phases are said to be protected or enriched by a symmetry when only transformations preserving it are allowed. Then symmetries define a topological classification of Symmetry Protected Topological (SPT) phases. Here the term Protected describes the fact that the boundary modes are robust against local perturbations that preserve the bulk symmetry. We will now describe the pricipal symmetries involved in the next chapters. Starting from the definitions of time-reversal and charge conjugation we classify the non-interacting fermionic Hamiltonians with Particle-Hole Symmetry (PHS) and Time-Reversal Symmetry (TRS) following [14, 15].
For a Hamiltonian which is invariant under the action of the time reversal operator T:

$$THT^{-1} = H$$

the time-evolution operator e^{-itH} changes as:

$$Te^{-itH}T^{-1} = e^{-TiT^{-1}tH} = e^{itH}$$

Then it is an antiunitary operator that can be represented as $T = \mathrm{T}K$, where K denotes the complex conjugation and T is a unitary operator. Note that applying it twice on any state must return the initial state up to an overall phase factor $e^{i\phi}$. From this consideration we have that:

$$e^{i\phi} = T^2 \implies T = e^{i\phi}T^T, \quad T^T = e^{i\phi}T$$

So we conclude that the eigenvalues of T^2 can be only ± 1.
For a Hamiltonian which is invariant under the action of the charge conjugation operator P:

$$PHP^{-1} = H$$

the minimal coupling $\boldsymbol{p} - ie\boldsymbol{A}$ changes to $\boldsymbol{p} + ie\boldsymbol{A}$, where $\boldsymbol{p}$ is the momentum operator and $\boldsymbol{A}$ is the electromagnetic gauge potential. This is done if:

$$PiP^{-1} = -i$$

Thus also P is an antiunitary operator writable as $P = \mathrm{P}K$ with P unitary. As before considering the overall phase change we conclude that the eigenvalues of P^2 can be only ± 1. In the mean-field theory of superconductivity under this symmetry a particle state becomes a hole state.
When both T and P are symmetries of a Hamiltonian, their product is also a symmetry. This unitary operator is called called Chiral Symmetry and it is defined as:

$$C = TP$$

Observe that a Hamiltonian can obey chiral symmetry even if it possesses neither of particle-hole symmetry nor time reversal symmetry.

1.5 Classification with Homotopy Groups

We can now move on to classify all the combinations of the symmetries P, T and C that a Hamiltonian can have accounting for the different signs of T^2 and P^2. There are in total ten classes, listed in Table 1.1. Then there are three possible cases of phases with protected edge modes on the $d-1$ dimensional boundary. If there is only one trivial phase, the entry is $\varnothing$, for two distinct phases (one trivial and one topological), $\mathbb{Z}_2$ is listed. Finally, if there exists a distinct topological phase for every integer, $\mathbb{Z}$ is listed.
Let us consider the situation where the system is translationally invariant and periodic boundary conditions are imposed. In second quantization the general Hamiltonian has the Bloch representation:

$$H = \int d^d\boldsymbol{p}\ \psi^\dagger_\alpha(\boldsymbol{p}) H_{\alpha,\alpha'}(\boldsymbol{p}) \psi_{\alpha'}(\boldsymbol{p}) \tag{1.1}$$

where $\psi^\dagger_\alpha(\boldsymbol{p})$ creates a fermion at momentum $\boldsymbol{p}$ in the Brillouin Zone (BZ) with $\alpha = 1, \ldots, N$ representing the degrees of freedom. The energy bands are obtained by diagonalizing the $N \times N$ Hamiltonian matrix using a unitary transformation $U(\boldsymbol{p})$:

$$U^\dagger(\boldsymbol{p}) H(\boldsymbol{p}) U(\boldsymbol{p}) = diag[\epsilon_{i+j}(\boldsymbol{p}), \ldots, \epsilon_j(\boldsymbol{p}), \ldots, \epsilon_1(\boldsymbol{p})] \tag{1.2}$$

	T^2	P^2	C^2	d	1	2	3	4	5	6	7	8
A	$\varnothing$	$\varnothing$	$\varnothing$		$\varnothing$	$\mathbb{Z}$	$\varnothing$	$\mathbb{Z}$	$\varnothing$	$\mathbb{Z}$	$\varnothing$	$\mathbb{Z}$
AIII	$\varnothing$	$\varnothing$	+		$\mathbb{Z}$	$\varnothing$	$\mathbb{Z}$	$\varnothing$	$\mathbb{Z}$	$\varnothing$	$\mathbb{Z}$	$\varnothing$
AII	-	$\varnothing$	$\varnothing$		$\varnothing$	$\mathbb{Z}_2$	$\mathbb{Z}_2$	$\mathbb{Z}$	$\varnothing$	$\varnothing$	$\varnothing$	$\mathbb{Z}$
DIII	-	+	+		$\mathbb{Z}_2$	$\mathbb{Z}$	$\mathbb{Z}$	$\varnothing$	$\varnothing$	$\varnothing$	$\mathbb{Z}$	$\varnothing$
D	$\varnothing$	+	$\varnothing$		$\mathbb{Z}_2$	$\mathbb{Z}$	$\varnothing$	$\varnothing$	$\varnothing$	$\mathbb{Z}$	$\varnothing$	$\mathbb{Z}_2$
BDI	+	+	+		$\mathbb{Z}$	$\varnothing$	$\varnothing$	$\varnothing$	$\mathbb{Z}$	$\varnothing$	$\mathbb{Z}_2$	$\mathbb{Z}_2$
AI	+	$\varnothing$	$\varnothing$		$\varnothing$	$\varnothing$	$\varnothing$	$\mathbb{Z}$	$\varnothing$	$\mathbb{Z}_2$	$\mathbb{Z}_2$	$\mathbb{Z}$
CI	+	-	+		$\varnothing$	$\varnothing$	$\mathbb{Z}$	$\varnothing$	$\mathbb{Z}_2$	$\mathbb{Z}_2$	$\mathbb{Z}$	$\varnothing$
C	$\varnothing$	-	$\varnothing$		$\varnothing$	$\mathbb{Z}$	$\varnothing$	$\mathbb{Z}_2$	$\mathbb{Z}_2$	$\mathbb{Z}$	$\varnothing$	$\varnothing$
CII	-	-	+		$\mathbb{Z}$	$\varnothing$	$\mathbb{Z}_2$	$\mathbb{Z}_2$	$\mathbb{Z}$	$\varnothing$	$\varnothing$	$\varnothing$

Table 1.1: Symmetry classes of non-interacting fermionic Hamiltonians. The columns contain: Cartan's name for the symmetry class, the square of the time reversal operator, the particle-hole operator and the chiral operator ($\varnothing$ means the symmetry is absent). Then we have the dimensions and on each Cartan's name row we have the corresponding index. The first two rows are called "complex classes", while the lower eight rows are the "real classes".

where the energies are ordered from the highest to the lowest and $i,\ j \in \mathbb{Z}$ with $i+j=N$. Assuming that there exists an energy gap between the bands i and $i+1$ with the chemical potential μ inside this gap:

$$\epsilon_i(\boldsymbol{p}) < \mu < \epsilon_{i+1}(\boldsymbol{p}) \quad \forall \boldsymbol{p} \in BZ$$

this allows us to adiabatically deform the Hamiltonian to:

$$Q(\boldsymbol{p}) = U(\boldsymbol{p}) \begin{pmatrix} \mathbb{I}_i & 0 \\ 0 & -\mathbb{I}_j \end{pmatrix} U^\dagger(\boldsymbol{p}) \tag{1.3}$$

$Q(\boldsymbol{p})$ is called flatband Hamiltonian and assigns the energy ± 1 respectively to the states above and under the gap. This deformation preserves the eigenstates and the degeneracy of its eigenspaces adds an extra $U(i) \times U(j)$ symmetry to $Q(\boldsymbol{p})$ and until $U(\boldsymbol{p})$ is an element of $U(i+j)\ \ \forall \boldsymbol{p}$ we can change the basis of the upper and lower bands by a $U(i)$ and $U(j)$ transformation. Then $Q(\boldsymbol{p})$ defines a map:

$$Q : BZ \to C_0 \qquad C_0 := \frac{U(i+j)}{U(i) \times U(j)} \tag{1.4}$$

and the number of topologically distinct Hamiltonians is given by:

$$\pi_d(C_0)$$

This is called homotopy group [16] and it is the group of equivalence classes of maps from the d-sphere to a target space. Note that the the BZ is not a sphere but a torus.

1.6 Topological Invariants

To understand in which topological sector a system with certain symmetries is, we have to compute topological invariants. These invariants are automatically numbers in the group of possible topological phases ($\mathbb{Z}$, $\mathbb{Z}_2$) and they are called Chern numbers for systems without chiral symmetry and winding numbers for systems with it. But before we can define them we need to briefly talk about Berry Curvature.

1.6.1 Berry Curvature

In differential geometry topology is described by the Gauss-Bonnet theorem. It states that for compact 2D Riemannian manifolds M without boundary, the integral over the Gaussian curvature defined as:

$$2(1-g) = \frac{1}{2\pi}\int_M d^2\boldsymbol{x} F(\boldsymbol{x}) \tag{1.5}$$

is an integer and a topological invariant. Here g is the genus, i.e. the number of handles of an orientable surface. $F(\boldsymbol{x})$ is the curvature and it is proportional to the angle mismatch mesured after parallel transporting a vector of the tangential plane at a given point on M around an infinitesimal closed loop. In the physical systems the manifold M is the BZ and the the tangent plane on M is a space spanned by the Bloch states of the occupied bands at a given momentum $\boldsymbol{p} \in BZ$. In this case we now have a generalized curvature form called Berry curvature F_{ij} which reads:

$$F_{i,j}(\boldsymbol{p}) := \partial_i A_j(\boldsymbol{p}) - \partial_j A_i(\boldsymbol{p}) + [A_i(\boldsymbol{p}), A_j(\boldsymbol{p})] \quad i,j = 1,\dots,d \tag{1.6}$$

$F_{ij}(\boldsymbol{p})$ is a $n \times n$ matrix of differential forms defined by A which is the Berry connection:

$$A_i^{\alpha\beta} := \sum_{\gamma=1}^{N} U^\dagger_{\alpha\gamma}(\boldsymbol{p})\partial_i U_{\gamma\beta}(\boldsymbol{p}) \quad \alpha,\beta = 1,\dots,n \quad i = 1,\dots,d \tag{1.7}$$

Under a local $U(n)$ gauge transformation in momentum space (1.2), that is parametrized by the $n \times n$ matrix $G(\boldsymbol{p})$:

$$U_{\gamma\alpha}(\boldsymbol{p}) \to U_{\gamma\beta}(\boldsymbol{p})G_{\beta\alpha}(\boldsymbol{p}) \quad \gamma = 1,\dots,N \quad \alpha = 1,\dots,n \tag{1.8}$$

the Berry curvature changes covariantly:

$$F \to G^\dagger F G \tag{1.9}$$

Then the trace of F is invariant under this transformation.

1.6.2 Chern Numbers

For the spatial dimension $d = 2$, the topological invariant was found by Chern and is defined as:

$$2C^1 := \frac{i}{2\pi}\int_{BZ} \mathrm{tr}F = \frac{i}{\pi}\int_{BZ} d^2\boldsymbol{p}\ \mathrm{tr}F_{12} \tag{1.10}$$

This is called the first Chern number and it can only take integer values. In order to obtain a topological invariant for any even dimension $d = 2s$ of space, we can use the s-th power of the Berry curvature form F to build a gauge invariant d-form that can be integrated over the BZ to obtain a scalar. Upon taking the trace, this scalar is invariant under the gauge transformation (1.8) and defines the s-th Chern number:

$$2C^s := \frac{1}{s!}(\frac{i}{2\pi})^s \int_{BZ} \mathrm{tr}[F^s] \tag{1.11}$$

where $F^s = F \wedge \cdots \wedge F$ is s times the wedge product of F. These will also be all integer numbers.

1.6.3 Winding Numbers

Now we will consider systems with chiral symmetry C. Their topological invariants are found by considering a different representation of the Chern numbers C^s, i.e. in terms of the flatband Hamiltonian (1.3) in fact:

$$C^s \propto \epsilon_{i_1\ldots i_d}\int_{BZ} d^d\boldsymbol{p} tr[Q(\boldsymbol{p})\partial_{i_1}Q(\boldsymbol{p})\ldots\partial_{i_d}Q(\boldsymbol{p})] \quad d = 2s \tag{1.12}$$

In this form we can interpret C^s as the winding number of the unitary transformation $Q(\boldsymbol{p})$ over the BZ. One verifies that $C^s = 0$ for systems with chiral symmetry by inserting $CC^\dagger$ in the expression and anticommuting C with all the Q, using the cyclicity of the trace. After $2s + 1$ anticommutations we have the original expression up to an overall minus sign so $C^s = -C^s$. Hence, all systems with chiral symmetry have vanishing Chern numbers. For odd dimensions instead, we can define an alternative topological invariant for systems with chiral symmetry by modifying (1.12) and using the chiral operator C:

$$W^s := \frac{(-1)^s s!}{2(2s+1)!}\Big(\frac{i}{2\pi}\Big)^{s+1}\epsilon_{i_1\ldots i_d}\int_{BZ} d^d\boldsymbol{p} tr[CQ(\boldsymbol{p})\partial_{i_1}Q(\boldsymbol{p})\ldots\partial_{i_d}Q(\boldsymbol{p})] \quad d = 2s+1 \tag{1.13}$$

Upon anticommuting the chiral operator C with all the matrices Q and using the cyclicity of the trace, one finds that the expression for W^s vanishes for even dimensions. We now have all the $\mathbb{Z}$ entries of Table 1.1.

Chapter 2

1D Superconducting Models

We will first consider a 1D wire with a p-wave superconductive pairing term and then move on to introduce the one dimensional Kitaev chain following [6, 14, 17]. Later on we will look at its long-range pairing version as studied in [10, 11, 18]. These models exhibit Majorana edge states and topological superconducting phases.

2.1 P-wave Superconductor

The simplest model of a topological superconductor is a mean-field Bogoliubov de Gennes Hamiltonian of spinless fermions with a pairing term (Appendix A). Spinless fermions can be either viewed as a simpler model compared to the spinful case or as fermions that are fully spin polarized. The 1D metal of spinless fermions with momentum dependent p-wave potential reads:

$$H = H + H_\Delta = \sum_p c_p^\dagger (\frac{p^2}{2m} - \mu) c_p + \frac{1}{2}(\Delta p c_p^\dagger c_{-p}^\dagger + \Delta^* p c_{-p} c_p) \tag{2.1}$$

This Hamiltonian can be rewritten in the BdG form:

$$H = \frac{1}{2}\sum_p \Psi_p^\dagger H_{\text{BdG}} \Psi_p \qquad \Psi_p = (c_p \; c_{-p}^\dagger)^T \tag{2.2}$$

where H_{BdG} is a 2×2 matrix:

$$H_{\text{BdG}}(p, \Delta) = \begin{pmatrix} \frac{p^2}{2m} - \mu & \Delta p \\ \Delta^* p & -\frac{p^2}{2m} + \mu \end{pmatrix} \tag{2.3}$$

There are two energy bands because we doubled the degrees of freedom and the spectrum is shown in Fig.2.1:

$$E_\pm = \pm\sqrt{\epsilon^2(p) + |\Delta|^2 p^2} \qquad \epsilon(p) = \frac{p^2}{2m} - \mu \tag{2.4}$$

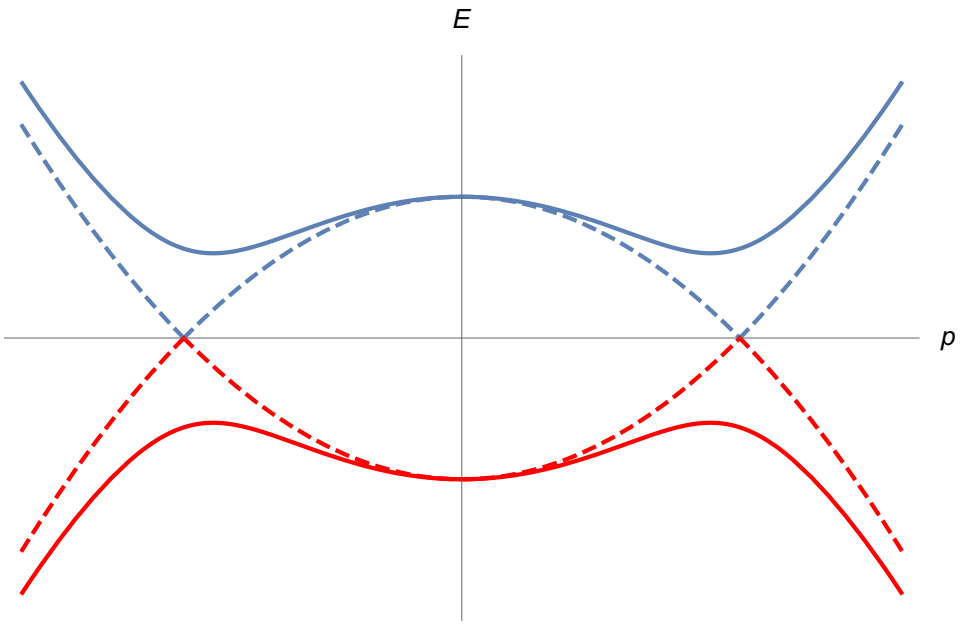

Figure 2.1: Plot of the dispersion relation for the positive (blue) band and the negative (red) band for a l-D p-wave superconductor for $m = 1$, $\mu = 0.2$. The dashed lines represent the $\Delta = 0$ case while the full lines represent the $\Delta \neq 0$ case.

The critical point $\mu_c = 0$ separates two phases:

$$\begin{cases} \text{weak-pairing phase (WPP)} & \mu > 0 \\ \text{strong-pairing phase (SPP)} & \mu < 0 \end{cases} \tag{2.5}$$

The WPP is a BCS-like superconducting phase ($\Delta \neq 0$) while the SPP is a gapped insulating phase even without pairing ($\Delta = 0$) and does not fit the usual weak-pairing BCS instability picture. Now we are going to look for majorana edge-states which represent one way to test the topological nature of a model. After that, if any of these states exist, we will see which of the phases is topological.

2.1.1 Majorana Edge States

We will start by considering the BdG Hamiltonian (2.3) in the limit $m \to \infty$ when the matrix structure becomes a massive 1D Dirac Hamiltonian, see [19]:

$$H_{\text{BdG}}(p) = (\text{Re}\Delta)p\tau^x - (\text{Im}\Delta)p\tau^y - \mu\tau^z \tag{2.6}$$

where $\tau^i,\ i = x, y, z$ are Pauli matrices. As we are considering only one superconductor, we can use the global phase rotation of $\Delta = |\Delta|e^{i\theta}$ to make it real and then absorb the

phase in the creation and annihilation operators:

$$c_p \to e^{-i\theta/2} c_p \ ; \ c_p^\dagger \to e^{i\theta/2} c_p^\dagger \tag{2.7}$$

So the Hamiltonian is now:

$$H_{\mathrm{BdG}}(p) = |\Delta| p \sigma^x - \mu \sigma^z \tag{2.8}$$

Let us assume that $\mu \equiv \mu(x)$ and:

$$\begin{cases} \mu(+\infty) > 0 \\ \mu(-\infty) < 0 \end{cases} \tag{2.9}$$

We will look for a localized zero-energy solution that is a $|\Psi\rangle$ such that: $H_{\mathrm{BdG}} |\Psi\rangle = 0 |\Psi\rangle$. Taking the ansatz:

$$|\Psi(x)\rangle = \exp\left(-\frac{1}{|\Delta|} \int_0^x \mu(x') dx' \right) |\phi_0\rangle \tag{2.10}$$

with $|\phi_0\rangle$ constant and normalized we then need to solve:

$$\begin{gathered} H_{\mathrm{BdG}} |\Psi(x)\rangle = \\ \begin{pmatrix} -\mu(x) & -i|\Delta| d/dx \\ -i|\Delta| d/dx & \mu(x) \end{pmatrix} |\Psi(x)\rangle = \\ \begin{pmatrix} -\mu(x) & i\mu(x) \\ i\mu(x) & \mu(x) \end{pmatrix} |\Psi(x)\rangle = 0 |\Psi(x)\rangle \end{gathered} \tag{2.11}$$

Thus $|\phi_0\rangle$ is simply $\frac{1}{\sqrt{2}}(1 \ -i)^T$ and the zero-energy solution reads:

$$|\Psi(x)\rangle = \frac{1}{\sqrt{2}} \exp\left(-\frac{1}{|\Delta|} \int_0^x \mu(x') dx' \right) \begin{pmatrix} 1 \\ -i \end{pmatrix} \tag{2.12}$$

The field operator that destroys this zero mode has the form:

$$\gamma_0 = \frac{1}{N} \int dx \, \exp\left(-\frac{1}{|\Delta|} \int_0^x \mu(x') dx' \right) \frac{1}{\sqrt{2}} (c(x) - i c^\dagger(x)) \tag{2.13}$$

where $c(x)$ destroys a fermion state at the point x and N is a normalization factor. Note that γ_0, $\gamma_0^\dagger$ follow fermionic anticommutation relations. Multiplying this state by a global $U(1)$ phase: $\bar{\gamma_0} \equiv e^{i\pi/4} \gamma_0$, we find that $\bar{\gamma_0}^\dagger = \bar{\gamma_0}$. So we have a 0D Majorana fermion-bound state, i.e. a localized fermion state which is its own antiparticle and does not propagate. Knowing that there is a low-energy fermion on a domain well between vacua with opposite Dirac masses is a sign of a topological phase.

2.1.2 Topological Phase

We can now determine which phase is topological. In the $m \to \infty$ limit we cannot distinguish the phases because the energy spectra in the SPP ($\mu < 0$) and in the WPP ($\mu > 0$) are identical. If we first set $\Delta = 0$ both phases are gapped for $\mu \neq 0$. The situation does not change if we set $\Delta \neq 0$, in fact the system will still be gapped so we can adiabatically connect the two phases. In order to differenciate the two phases we must pick a finite m so that the bands dispers upward and downward in energy for $m > 0$. Now there is a difference between $\mu < 0$ and $\mu > 0$. In the first case the trivial insulator phase ($\Delta = 0$) is adiabatically connected with the spectrum of the gapped superconductor phase ($\Delta \neq 0$), see Fig.2.2. In the second for $\Delta = 0$, the system is gapless and becomes gapped only when $\Delta \neq 0$, see Fig.2.3. Then we cannot adiabatically connect the two phases without passing through a gapless point or region. The zero-energy states are only present in the WPP.

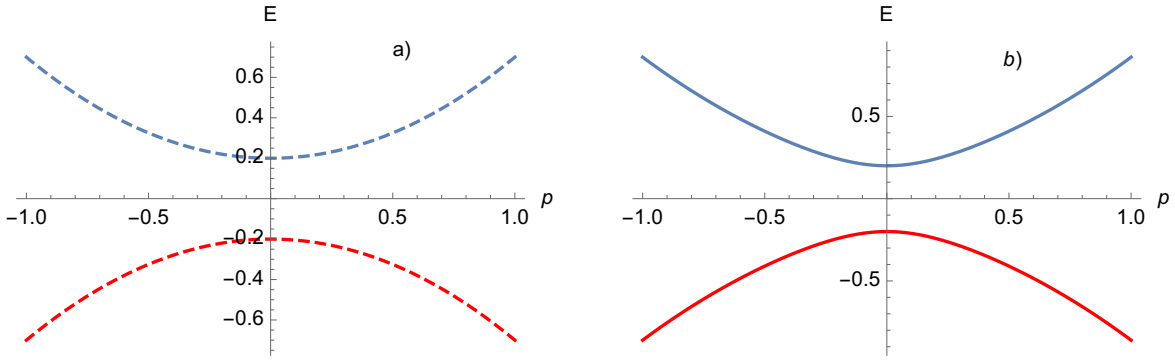

Figure 2.2: Plot of the energy spectrum in the SPP($\mu = -0.2$) and: a)$\Delta = 0$, b)$\Delta = 0.5$

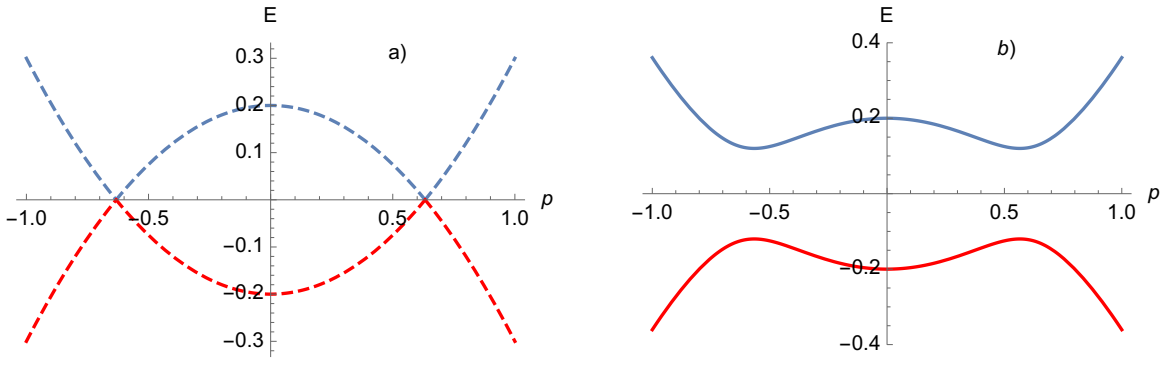

Figure 2.3: Plot of the energy spectrum in the WPP($\mu = 0.2$) and: a)$\Delta = 0$, b)$\Delta = 0.2$

2.2 Kitaev Chain

Now we will consider a simple lattice model for a topological superconductor that has been studied by Kitaev. The setup is a 1D chain with one spinless fermion on each site. Superconductivity is encoded in the pairing terms $c_i^\dagger c_{i+1}^\dagger$ that do not conserve particle number. The particular mechanism of superconductivity is not important, we may just think that our quantum wire lies on the surface of a 3D superconductor. Consider a chain consisting of $N \gg 1$ sites with each site empty or occupied by an electron. The Hamiltonian is:

$$H_{1D} = \sum_{j=1}^{N} \Big(-t(c_j^\dagger c_{j+1} + c_{j+1}^\dagger c_j) - \mu c_j^\dagger c_j + \Delta^* c_j c_{j+1} + \Delta c_{j+1}^\dagger c_j^\dagger \Big). \tag{2.14}$$

Here t is a hopping amplitude, μ a chemical potential and $\Delta = |\Delta| e^{i\theta}$ the induced superconducting gap of amplitude $|\Delta|$ and complex phase θ. We can perform a straightforward lattice Fourier transform (Appendix B) to write the Hamiltonian in the BdG form (2.2) where in this case:

$$H_{\mathrm{BdG}}(p, \Delta) = \begin{pmatrix} -2t\cos p - \mu & 2i\Delta \sin p \\ -2i\Delta^* \sin p & 2t\cos p + \mu \end{pmatrix} \tag{2.15}$$

The energy spectrum is:

$$E_\pm = \sqrt{(2t\cos p + \mu)^2 + 4|\Delta|^2 \sin^2 p} \tag{2.16}$$

For $|\Delta| \neq 0$ this model exhibits critical points when $2t\cos p + \mu$ and $\sin p$ vanish at the same time. This happens when $(p, \mu) = (0, -2t)$ or $(p, \mu) = (\pi, 2t)$. The spectrum is the same of (2.3) when expanded around $p \sim 0$ (but shifted) and it is the situation we will analyse. The critical point $\mu_c = -2t$ separates two gapped superconducting phases as before:

$$\begin{cases} \mu < \mu_c & \text{trivial phase} \\ \mu > \mu_c & \text{topological phase} \end{cases} \tag{2.17}$$

We know that the fermionic operators of the lattice Hamiltonian (2.14) obey the algebra:

$$\{c_i^\dagger, c_j\} = 2\delta_{ij} \tag{2.18}$$

and it is possible to represent the operators $c_j^\dagger$ and c_j on every site j with two Majorana operators a_i, b_i and hide the dependence on the phase parameter θ into their own definition:

$$a_j = e^{-i\frac{\theta}{2}} c_j + e^{i\frac{\theta}{2}} c_j^\dagger, \quad b_j = \frac{1}{i}(e^{-i\frac{\theta}{2}} c_j - e^{i\frac{\theta}{2}} c_j^\dagger) \qquad (j = 1, \ldots, N) \tag{2.19}$$

These operators obey the algebra:

$$\{a_i, a_j\} = \{b_i, b_j\} = 2\delta_{ij} \quad \{a_i, b_j\} = 0 \quad \forall i, j \tag{2.20}$$

Note that it is always possible to separate a complex fermion operator on a lattice site into its real and imaginary parts. In terms of this operators, the Hamiltonian (2.14) becomes:

$$H_{1D} = \frac{i}{2}\sum_{j}^{N}\Big(-\mu a_j b_j + (t + |\Delta|)b_j a_{j+1} + (-t + |\Delta|)a_j b_{j+1}\Big). \tag{2.21}$$

Let us consider two special cases:

a) The trivial case $\mu < \mu_c = -2t$, with $|\Delta| = t = 0$ so the Hamiltonian becomes:

$$H_{1D} = -\mu\frac{i}{2}\sum_{j} a_j b_j$$

The Majorana operators a_j, b_j from the same site j are paired together. In terms of the physical complex fermions, it is the ground state with all sites either occupied or empty. A representation of this Hamiltonian is shown in Fig.2.4(a). The Hamiltonian physically describes the atomic limit, which is another way to see that the ground state is trivial. If the chain has open boundary conditions there will be no low-energy states on the end of the chain.

b) The topological phase $\mu > \mu_c = -2t$ with $|\Delta| = t > 0$ for $\mu = 0$ so that the Hamiltonian becomes:

$$H_{1D} = it\sum_{j} b_j a_{j+1}.$$

The Majorana operators from the same site j are now decoupled while the a_{j+1}, b_j operators from different sites are paired together and a_1, b_N are not coupled to the rest of the chain, see Fig.2.4 (b). In this limit the existence of two Majorana zero modes localized on the ends of the chain is manifest.

These two limits give the simplest representations of the trivial and non-trivial phases. By tuning away from these limits the Hamiltonian will have some mixture of couplings. However, since the two Majorana modes are localized at different ends of a gapped chain, the coupling between them will be exponentially small in the length of the wire and they will remain at zero energy. In fact, in the non-trivial phase the zero modes will not be destroyed until the bulk gap closes at a critical point. The edge modes do not have a defined charge being a superposition of particle and hole but they preserve fermion parity. The nonlocal fermionic mode formed by two Majorana edge modes is envisioned to work as a qubit (a quantum-mechanical two-level system) that stores quantum information (its state) in a way that is protected against local noise and decoherence.

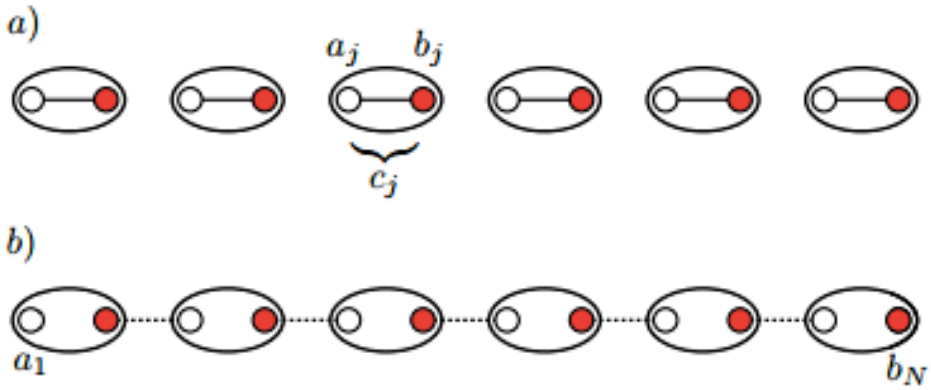

Figure 2.4: Schematic representation of: (a) trivial phase and (b) nontrivial phase with a zero mode on each end of the chain, taken from [14]

2.3 Long Range Kitaev Superconductor

We are now going to anylise a generalization of the 1D Kitaev chain (2.14). This model is obtained by considering LR interactions described by a pairing which decays as distance to the power of α. The lattice Hamiltonian is:

$$H_{LR} = \sum_{j=1}^{N}\Big(-t(c_j^\dagger c_{j+1} + c_{j+1}^\dagger c_j) - \mu c_j^\dagger c_j\Big) + \Delta\sum_{j=1}^{N}\sum_{l=1}^{N-1} d_l^{-\alpha}\Big(c_j c_{j+l} + c_{j+l}^\dagger c_j^\dagger\Big) \tag{2.22}$$

where $c_j^\dagger$ and c_j are spinless fermionic creation and annihilation operators on site j, $d_l = |l-j|$ is the distance, t is a hopping amplitude, μ is a chemical potential and Δ is a real pairing strength. We can perform a lattice Fourier transform similarly as done in AppendixB on a closed ring where $d_l = \min(l, N-l)$ to obtain:

$$H_{\mathrm{BdG}} = \begin{pmatrix} -2t\cos p - \mu & 2i\Delta\sum_l d_l^{-\alpha}\sin(pl) \\ -2i\Delta\sum_l d_l^{-\alpha}\sin(pl) & 2t\cos p + \mu \end{pmatrix} \tag{2.23}$$

Then the energy spectrum is:

$$E_\pm = \pm\sqrt{(2t\cos p + \mu)^2 + (\Delta f_\alpha(p))^2} \tag{2.24}$$

where $f_\alpha(p) = \sum_l d_l^{-\alpha}\sin(pl)$ is the function containing the LR information and can be evaluated in the thermodynamic limit $N \to \infty$, see [20, 21]. For $\alpha \to \infty$ we recover the SR Kitaev model and until $\alpha > 1$ the spectrum is gapless for $|\mu_c| = 2t$. The differences

arise for $\alpha \leq 1$ when along the $\mu_c = -2t$ line the model becomes massive thus it loses the phase transition that survives only along the $\mu_c = 2t$ line. To see these results we have to consider the energy spectrum (2.24) in the thermodynamic limit when $f_\alpha(p)$ becomes a sum of polylogarithms, see[18]:

$$f_\alpha^\infty(p) = -i[\mathrm{Li}_\alpha(e^{ik}) - \mathrm{Li}_\alpha(e^{-ik})] \tag{2.25}$$

There are two different situations depending on the value of α:

a) When $\alpha > 1$

$$\begin{cases} f_\alpha^\infty(p)|_{p=0} = 0 \\ f_\alpha^\infty(p)|_{p=\pi} = 0 \end{cases}$$

so both $\mu = 2t$ and $\mu = -2t$ are critical.

b) when $\alpha < 1$

$$\begin{cases} f_\alpha^\infty(p) \to \infty \text{ for } p \to 0 \\ f_\alpha^\infty(p)|_{p=\pi} = 0 \end{cases}$$

so only $\mu = -2t$ is critical while the gap does not close anymore for $\mu = -2t$.

Starting from the lattice model (2.22) on a closed chain($d_l = N/2$) with $\Delta = 2t = 1$ we want to see if Majorana edge states are supported by means of numerical diagonalization, see [22]. The quadratic Hamiltonian reads:

$$H = \sum_{ij}^{N} c_i^\dagger A_{ij} c_j + (c_i^\dagger B_{ij} c_j^\dagger + \text{h.c.}) \tag{2.26}$$

where the matrix A_{ij} is real and symmetric while B_{ij} is real and antisymmetric. The complete matrix can be rewritten in diagonal form:

$$H = \sum_{i=1}^{N} \lambda_i \eta_i^\dagger \eta_i \qquad \lambda_i \geq 0 \tag{2.27}$$

This is done by means of a Bogoliubov transformation:

$$\begin{pmatrix} \boldsymbol{\eta} \\ \boldsymbol{\eta}^\dagger \end{pmatrix} = \begin{pmatrix} \boldsymbol{g} & \boldsymbol{h} \\ \boldsymbol{h} & \boldsymbol{g} \end{pmatrix} \begin{pmatrix} \boldsymbol{c} \\ \boldsymbol{c}^\dagger \end{pmatrix} \tag{2.28}$$

where $\boldsymbol{c} = (c_1, c_2, \ldots, c_N)^T$, $\boldsymbol{\eta} = (\eta_1, \eta_2, \ldots, \eta_N)^T$ and $\boldsymbol{g}$, $\boldsymbol{h}$ are $N \times N$ matrices. To get $\boldsymbol{\lambda} = (\lambda_1, \lambda_2, \ldots, \lambda_N)^T$ and $\boldsymbol{g}$, $\boldsymbol{h}$ we can use a singular value decomposition of $A + B$:

$$\boldsymbol{\lambda} = \boldsymbol{\psi}(A + B)\boldsymbol{\phi}^{\boldsymbol{T}} \quad \boldsymbol{\psi} = \boldsymbol{g} - \boldsymbol{h} \quad \boldsymbol{\phi} = \boldsymbol{g} + \boldsymbol{h} \tag{2.29}$$

If there is a zero energy mode we will find a minimum λ_{n_0} vanishing in the gapped region in the thermodynamic limit. To verify it is not zero because we are at a critical point we can look at the exact dispersion relation (2.24) (same bulk properties when $L \to \infty$ for a closed ring and a closed chain). The critical lines are $\mu = 1$ for $\alpha < 1$ and $\mu = \pm 1$ for $\alpha > 1$. Thus if we find a $\lambda_{n_0} = 0$ for $\mu \neq \pm 1$ it will be a correct zero mode. In the region $|\mu| < 1$ and for $\alpha > 1$ the model supports zero energy modes as shown in Fig.2.5. Instead for $\alpha < 1$ the modes become massive as shown in Fig.2.6.

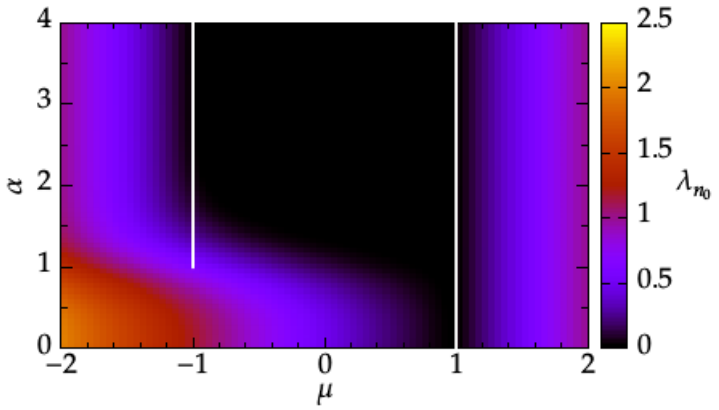

Figure 2.5: Plot of λ_{n_0} for $N = 200$ with the $|\mu| = 1$ gapless lines in white, taken from[18]. Note that for $|\mu| > 1$ and $\alpha > 1$, $\lambda_{n_0} \neq 0$ even if it seems to be black. It is a matter of color scaling.

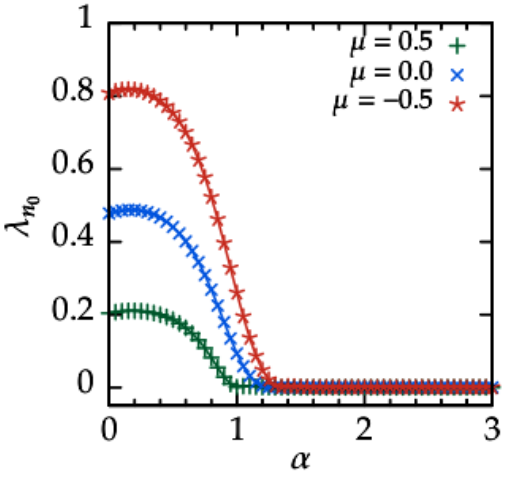

Figure 2.6: Plot of λ_{n_0} for $L \to \infty$. When $\alpha < 1$ it becomes finite in the thermodynamic limit so the zero energy mode disappears,taken from [18].

Chapter 3

2D Superconducting Models

We can now move on to 2D models. We will start from the lattice and momentum-sapce Hamiltonians of the SR 2D Superconductor of which we are going to analyse the phases, the winding number and the edge-modes following [14, 17, 23].

3.1 P-wave Chiral Superconductors

The lattice Hamiltonian of spinless interacting fermions can be written as:

$$H = \sum_{m,n} -t(c^\dagger_{m+1,n}c_{m,n}+c^\dagger_{m,n+1}c_{m,n})-(\mu-4t)c^\dagger_{m,n}c_{m,n}+(\Delta c^\dagger_{m+1,n}c^\dagger_{m,n}+i\Delta c^\dagger_{m,n+1}c^\dagger_{m,n}+\text{h.c.}) \tag{3.1}$$

The operators $c^\dagger_{m,n}$, $c_{m,n}$ create and annihilate spinless fermions on the (m,n) site. The pairing term is anisotropic with an additional $i = e^{i\pi/2}$ phase along the y-direction. We can rewrite this Hamiltonian in the BdG form, similarly as done in Appendix B and that reads:

$$H_{BdG} = \begin{pmatrix} \epsilon(\boldsymbol{p}) & f(\boldsymbol{p}) \\ -f^*(\boldsymbol{p}) & -\epsilon(\boldsymbol{p}) \end{pmatrix} \tag{3.2}$$

where:

- $\epsilon(\boldsymbol{p}) = -2t(\cos(p_x) + \cos(p_y)\ ) - (\mu - 4t)$
- $f(\boldsymbol{p}) = 2i\Delta(\sin(p_x) + i\sin(p_y))$

It is useful to make a gauge transformation on the operators $c^\dagger_{\boldsymbol{p}} \to e^{i\theta/2}c^\dagger_{\boldsymbol{p}}$, $c_{\boldsymbol{p}} \to e^{-i\theta/2}c_{\boldsymbol{p}}$ to absorb the pairing amplitude phase of $\Delta = |\Delta|e^{i\theta}$. Then the Bloch Hamiltonian reads:

$$H_{BdG} = \epsilon(\boldsymbol{p})\tau^z - 2|\Delta|\sin(p_x)\tau^y - 2|\Delta|\sin(p_y)\tau^x \tag{3.3}$$

Here the τ^α where $\alpha = x, y, z$ are Pauli matrices in the particle/hole basis and from their anticommutation properties the spectrum is easily found to be:

$$E_\pm = \pm\sqrt{\epsilon(\boldsymbol{p})^2 + 4|\Delta|^2(\sin(p_x)^2 + \sin(p_y)^2)} \tag{3.4}$$

Setting $|\Delta| = t = 1/2$ we can see that the spectrum is gapped unless (p_x, p_y, μ) is equal to:

- $(0, 0, 0)$
- $(\pi, 0, 2)$ or $(0, \pi, 2)$
- $(\pi, \pi, 4)$

So there are three three critical lines and four different phases. We now want to determine which of them are topological.

3.1.1 Winding Number

Let us consider (3.3) in the $\boldsymbol{p} \to 0$ limit which reads:

$$H_{BdG_0} = \begin{pmatrix} \frac{p^2}{2m} - \mu & 2i|\Delta|(p_x + ip_y) \\ -2i|\Delta|(p_x - ip_y) & -\frac{p^2}{2m}\mu \end{pmatrix} \tag{3.5}$$

where we set $t = \frac{1}{2m}$ and absorbed the phase in the operators. This is a massive 2D Dirac Hamiltonian in fact:

$$H = \frac{1}{2}\sum_{\boldsymbol{p}} \Psi^\dagger_{\boldsymbol{p}} H_{Bdg_0} \Psi_{\boldsymbol{p}} = \frac{1}{2}\sum_{\boldsymbol{p}} \Psi^\dagger_{\boldsymbol{p}} d_\alpha \tau^\alpha \Psi_{\boldsymbol{p}} \tag{3.6}$$

with $d_\alpha = (-2|\Delta|p_y, -2|\Delta|p_x, \frac{p^2}{2m} - \mu)$. For this Hamiltonian the topological invariant is the winding number defined as:

$$N_w = \frac{1}{8\pi}\int d^2p\ \epsilon^{ij}\hat{d} \times (\partial_{p_i}\hat{d} \cdot \partial_{p_j}\hat{d}) \tag{3.7}$$

where $\hat{d} = \boldsymbol{d}/|\boldsymbol{d}|$. This integral is equal to the degree of the mapping from momentum space (p_x, p_y) onto the 2-sphere given by $|\hat{d}|^2 = 1$. As we mentioned before (p_x, p_y) are not defined on a sphere so we need to change the domain by an equivalent compact one. Noting that:

$$\lim_{p\to 0} \hat{d} = (0, 0, 1)$$

that is indipendent from the direction of the limit on the plane we can perform a one-point compactification of $\Re^2$. Now the domain is $\Re^2 \cup \{\infty\}$ and it has the same topology of the 2-sphere. Finally we can calculate the winding number:

$$N_w = \frac{1}{8\pi}\int d^2p\ |\boldsymbol{d}|^{-3/2}\ [(-2|\Delta|p_y, -2|\Delta|p_x, \frac{p^2}{2m}-\mu)\cdot(-4|\Delta|p_y/m, -4|\Delta|p_x/m, -8|\Delta|^2)] = \frac{1}{\pi}\int d^2p \frac{|\Delta|^2(\frac{p^2}{2m}+\mu)}{[(\frac{p^2}{2m}-\mu)^2+4|\Delta|^2p^2\ ]^{3/2}} \tag{3.8}$$

and its values are:

- $N_w = 0$ for $\mu < 0$
- $N_w = 1$ for $\mu > 0$

For the other phases the winding number has to be calculated from (3.3) , see [23] and it is found that:

- $0 < \mu < 2$ is a topological phase with $N_w = 1$
- $2 < \mu < 4$ is a topological phase with $N_w = -1$
- $\mu > 4$ is a trivial phase with $N_w = 0$

Thus we have two topological phases with opposite chirality.

3.1.2 Majorana Edge-States

We will consider the low energy physics around $\boldsymbol{p} = 0$ for the $\mu = 0$ phase transition. From here is possible to show that there exist gapless, propagating fermion-states preventing us from continuously connecting the $\mu < 0$ to the $\mu > 0$ phase. Let us consider a domain wall $\mu = \mu(x)$ such that $\mu(x) = -\mu_0$ for $x < 0$ and $\mu(x) = +\mu_0$ for $x > 0$ with a constant $\mu_0 > 0$. This is a translationa1ly invariant interface along the y-direction so we can consider the momentum p_y as a quantum number in order to simplify the calculation. The quasi-1D Hamiltonian (3.5), neglecting the p^2 terms is then:

$$\hat{H}_{BdG_0} = \begin{pmatrix} -\mu(x) & 2i|\Delta|(-i\frac{d}{dx}+ip_y) \\ -2i|\Delta|(-i\frac{d}{dx}-ip_y) & \mu(x) \end{pmatrix} \tag{3.9}$$

We will take as ansatz for the gapless interface states:

$$|\psi_{p_y}(x,y)\rangle = e^{ip_y y}\exp\left(-\frac{1}{2|\Delta|}\int_0^x \mu(x')dx'\right)|\phi_0\rangle \tag{3.10}$$

where $|\phi_0\rangle$ is a constant, normalized spinor. For the zero energy mode $p_y = 0$ we need to solve:

$$\hat{H}_{BdG_0} |\psi_0(x,y)\rangle = \begin{pmatrix} -\mu(x) & -\mu(x) \\ \mu(x) & \mu(x) \end{pmatrix} |\psi_0(x,y)\rangle = 0 \tag{3.11}$$

so $|\phi_0\rangle = \frac{1}{\sqrt{2}}(1 \ -1)^T$ solves the secular equation. For $p_y \neq 0$ we have:

$$\hat{H}_{BdG_0} |\psi_{p_y}(x,y)\rangle = \begin{pmatrix} 0 & -2|\Delta|p_y \\ -2|\Delta|p_y & 0 \end{pmatrix} |\psi_{p_y}(x,y)\rangle \tag{3.12}$$

This matrix has eigenvalues $E_{p_y} = \pm 2|\Delta|p_y$ and is proportional to τ^x. So noting that $|\phi_0\rangle$ is the eigenvector corresponding to the negative eigenvalue of τ^x we then found a set of gapless chiral edge states with energy $E_{p_y} = -2|\Delta|p_y$. They have negative group velocity and are "half" of a Majorana fermion, its real or imaginary part, with the chirality defined by the Winding number. The edge-modes of the other phases are found by plotting the energy dispersion relation on a cylindrical geometry with OBC in one direction and PBC in the other, see [14, 23]

3.2 Long Range Superconductors

We are now going to study the 2D LR chiral superconductors starting from [24, 25]. This model presents both similarities and differences compared to the SR case. We would like to analyse the energy spectrum and see when the model supports edge-states. The idea is to see if we lose a phase transition when passing from a SR like model ($\alpha, \beta \to \infty$) to a "real" LR model (e.g. $\alpha \leq 2$, $\beta \to \infty$) as it happens in the 1D LR case. To this end we will first derive the energy spectrum, then study its properties both by analytical and numerical methods. In particular we will use the DMRG [26] software to directly diagonalize the lattice Hamiltonian and analyse how the low-energy modes change at different α.

3.3 P-wave Chiral Superconductor

We consider a 2D lattice Hamoltonian of spinless fermions with long-range hopping and pairing amplitude:

$$H = \sum_{\substack{m,n \\ r,s}}{}' \Big(-\frac{t}{d^\beta} c^\dagger_{m+r,n+s} c_{m,n} + \frac{\tilde{\Delta}(r,s)}{d^\alpha} c^\dagger_{m+r,n+s} c^\dagger_{m,n} + \text{h.c.} \Big) - (\mu - 4t) \sum_{m,n} c^\dagger_{m,n} c_{m,n} \tag{3.13}$$

Here the sum $\sum'_{r,s}$ runs over all integers r and s except $r = s = 0$, $d(r,s) = \sqrt{r^2 + s^2}$ is the Euclidean distance between fermions and μ is the chemical potential. The hopping

term decreases as d to the power of β while the pairing term:

$$\tilde{\Delta}(r,s) = \frac{\Delta}{d}(r+is) \tag{3.14}$$

decays as d to the power of α. Performing a lattice Fourier transform we can rewrite this Hamiltonian in the BdG form, see Appendix C.1 :

$$H_{BdG} = \begin{pmatrix} -\sum_{\boldsymbol{d}}{}' \frac{2t}{d^\beta}\cos(\boldsymbol{p}\cdot\boldsymbol{d}) - (\mu - 4t) & \sum_{\boldsymbol{d}}{}' 2i\sin(\boldsymbol{p}\cdot\boldsymbol{d})\frac{\tilde{\Delta}}{d^\alpha} \\ -\sum_{\boldsymbol{d}}{}' 2i\sin(\boldsymbol{p}\cdot\boldsymbol{d})\frac{\tilde{\Delta}^*}{d^\alpha} & \sum_{\boldsymbol{d}}{}' \frac{2t}{d^\beta}\cos(\boldsymbol{p}\cdot\boldsymbol{d}) + (\mu - 4t) \end{pmatrix} \tag{3.15}$$

where $\boldsymbol{p} = (p_x, p_y)$ and $\boldsymbol{d} = (r, s)$. At large values of the decaying exponents ($\alpha, \beta \to \infty$) the Hamiltonian (3.13) has a well-defined limit and we recover the short-range chiral p-wave Hamiltonian [14, 23]. In fact in that limit we are only left with the two terms $r = \pm 1$, $s = 0$ and $r = 0$, $s = \pm 1$. The single-particle energy spectrum is given by:

$$E = \pm\sqrt{\epsilon_\beta(\boldsymbol{p})^2 + 4\Delta^2(f_\alpha(\boldsymbol{p})^2 + g_\alpha(\boldsymbol{p})^2)} \tag{3.16}$$

where we have defined:

$$\begin{aligned} \epsilon_\beta(\boldsymbol{p}) &= -\sum_{\boldsymbol{d}}{}' \frac{2t}{d^\beta}\cos(\boldsymbol{p}\cdot\boldsymbol{d}) + (\mu - 4t) \\ f_\alpha(\boldsymbol{p}) &= \sum_{\boldsymbol{d}}{}' \sin(\boldsymbol{p}\cdot\boldsymbol{d})\frac{r}{d^{\alpha+1}} \\ g_\alpha(\boldsymbol{p}) &= \sum_{\boldsymbol{d}}{}' \sin(\boldsymbol{p}\cdot\boldsymbol{d})\frac{s}{d^{\alpha+1}} \end{aligned} \tag{3.17}$$

3.4 Energy Spectrum Analysis

In the following section we will analyse in particular $f_\alpha(\boldsymbol{p})$ to understand how does the interaction range influences the critical lines and thus the topological phase transitions. In fact it is easy to see that for a certain α, $f_\alpha(\boldsymbol{p})$ is going to diverge in some points and there will be no phase transition there. In fact we expect that for a certain α the series is not converging to 0 in the $\boldsymbol{p} \to \boldsymbol{0}$ limit and this situation has different interpretations. In principle we should lose the critical line $\boldsymbol{p} = \boldsymbol{0}$, but it seems that in some cases massive edge-states are still present [24, 27]. In the Appendix C.2 we study the convergence properties of $f_\alpha(\boldsymbol{p})$, which converges absolutely for $\alpha > 2$ while it diverges for $\alpha < 2$, see Appendix C.3. Then we were able to write it in an integral form made by two parts of which the first (f_{0,p_x}) encodes the "long range" interactions while the second (f_{1,p_x}) encodes the "short range" ones.

Let us start from:

- $f_\alpha(\boldsymbol{p}) = \sum_{\boldsymbol{d}}{}' \sin(\boldsymbol{p}\cdot\boldsymbol{d})\frac{r}{d^{\alpha+1}}$
- $f_\alpha(\boldsymbol{p}) = f_{0,p_x} + f_{1,p_x}$ where:

$$f_{0,p_x} = \Re e\Big\{\frac{\pi}{\Gamma((\alpha+1)/2)}\sum_{\boldsymbol{d}}(p_x/2-\pi r)E_{(\alpha-1)/2}\big((\ \boldsymbol{p}/2-\pi\boldsymbol{d})^2\big)\Big\}$$

$$f_{1,p_x} = \Re e\Big\{\frac{2}{\Gamma((\alpha+1)/2)}\sum_{\boldsymbol{d}>\boldsymbol{0}} r\sin(\boldsymbol{p}\cdot\boldsymbol{d})\ \varphi_{(\alpha+1)/2}(d^2)\Big\}$$

$E_n(x)$ is the General Exponential Integral [28] while $\varphi_n(x)$ is a function introduced in [29], as we discuss in Appendix C.2. We will be going to analyse three cases that are:

- $\alpha = 10$ SR behaviour, low LR effects
- $\alpha = 3$ higher LR effects but still SR behaviour
- $\alpha = 2$ strong LR effects, $f_\alpha(\boldsymbol{p})|_{\boldsymbol{p}\to\boldsymbol{0}} \neq 0$

For each case we will plot $f_\alpha(\boldsymbol{p})$ in both forms to see if its behaviour follows what we found in Appendix C.2 and to understand how the LR effects affect the model.

3.4.1 $\alpha = 10$

The first case is useful as we already know how it works, in fact from Fig.3.1 and Fig.3.2 we can see that $f_\alpha(\boldsymbol{p})$ converges to 0 in the four points of interest. Now we can also understand how its parts, f_{1,p_x} and f_{0,p_x} encode the "short" and "long" range interactions. In fact looking at Fig.3.3 we can appreciate the smooth behaviour of f_{1,p_x} and in Fig.3.5 the low LR effects labeled by f_{0,p_x} that has a positive peak around $(\pi/2, 0)$. The $\boldsymbol{d} = \boldsymbol{0}$ term of f_{0,p_x} that is:

$$\frac{\pi}{2\Gamma(11/2)}p_x E_{9/2}[p^2/4] = \frac{16\sqrt{\pi}}{945}p_x E_{9/2}[p^2/4]$$

is ~ 0 almost everywhere.

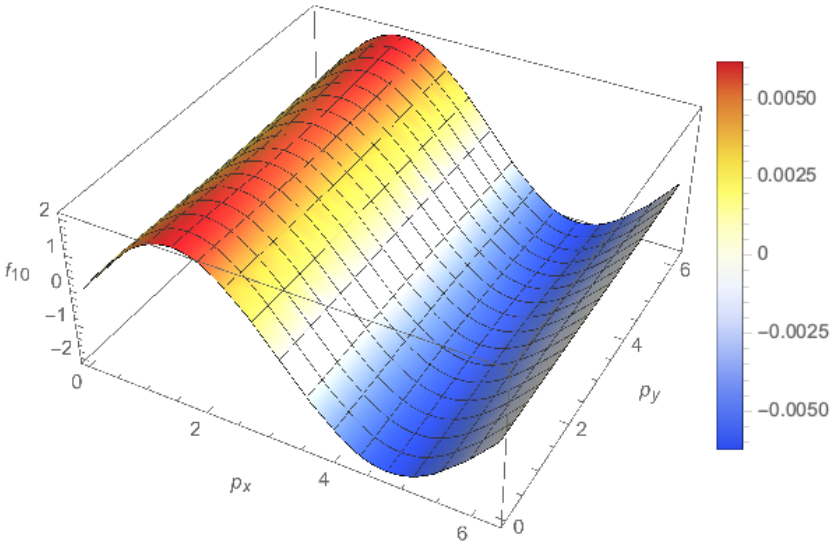

Figure 3.1: Plot of $f_{10}(\boldsymbol{p})$, [30]

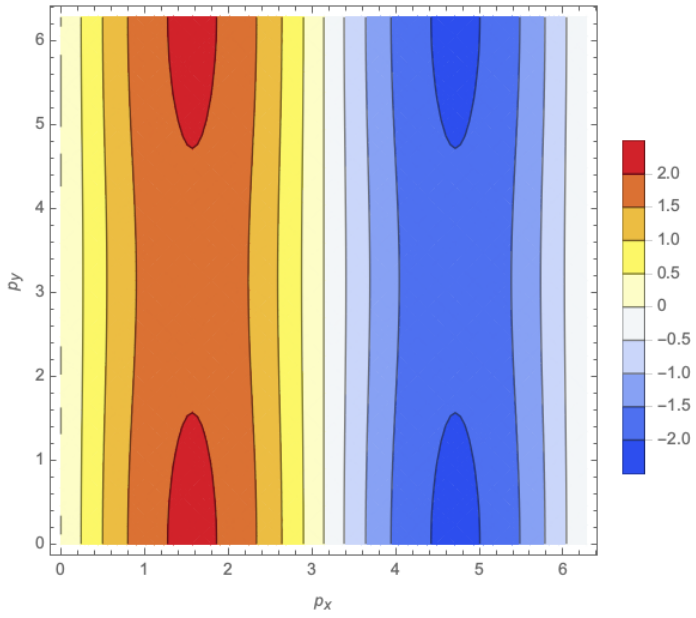

Figure 3.2: Contour plot of $f_{10}(\boldsymbol{p})$, [30]

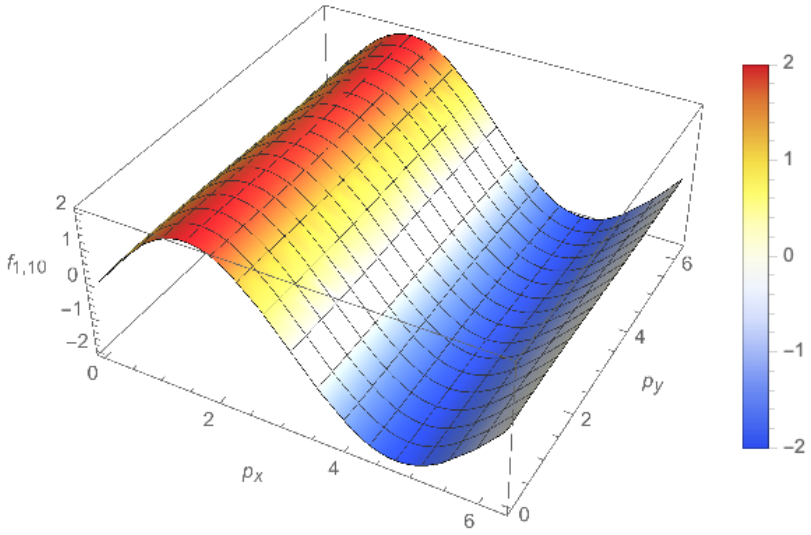

Figure 3.3: Plot of $f_{1,\alpha} = f_{1,10}$, [30]

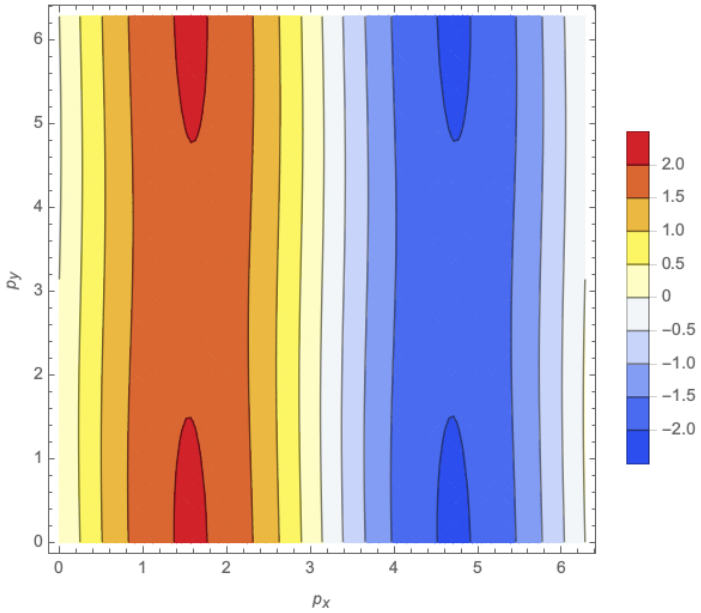

Figure 3.4: Contour plot of $f_{1,\alpha} = f_{1,10}$, [30]

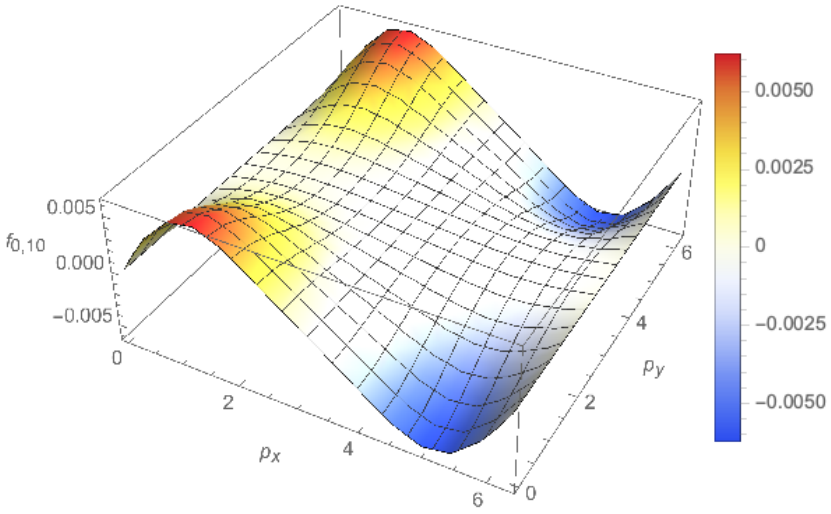

Figure 3.5: Plot of $f_{0,\alpha} = f_{0,10}$, [30]

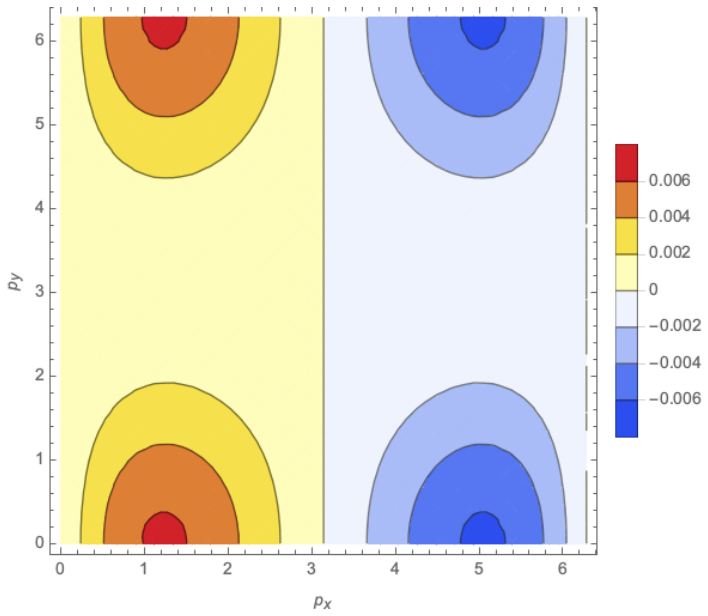

Figure 3.6: Contour plot of $f_{0,\alpha} = f_{0,10}$, [30]

3.4.2 $\alpha = 3$

In the second case looking at Fig.3.7 and Fig.3.8 we can see that the series is still convergent in the points we are considering but the peak is shifting towards $(0, 0)$ and getting higher meaning that the series is starting to converge slower than before. Looking at Fig.3.9 we can again see the smooth behaviour of f_{1,p_x} while in Fig.3.11 we see how f_{0,p_x} now contributes to the peak we observe also in $f_3(\boldsymbol{p})$. This behaviour is linked to the fact that the $x \to 0$ term of $E_n(x)$ gets higher when we decrease n. In fact the $\boldsymbol{d} = \boldsymbol{0}$ term of f_{0,p_x} in the $\boldsymbol{p} \to \boldsymbol{0}$ that reads:

$$\lim_{\boldsymbol{p}\to\boldsymbol{0}} \frac{\pi}{2\Gamma(2)} p_x E_1[p^2/4] = 0$$

is still defined, but note that $E_1(0) = \infty$

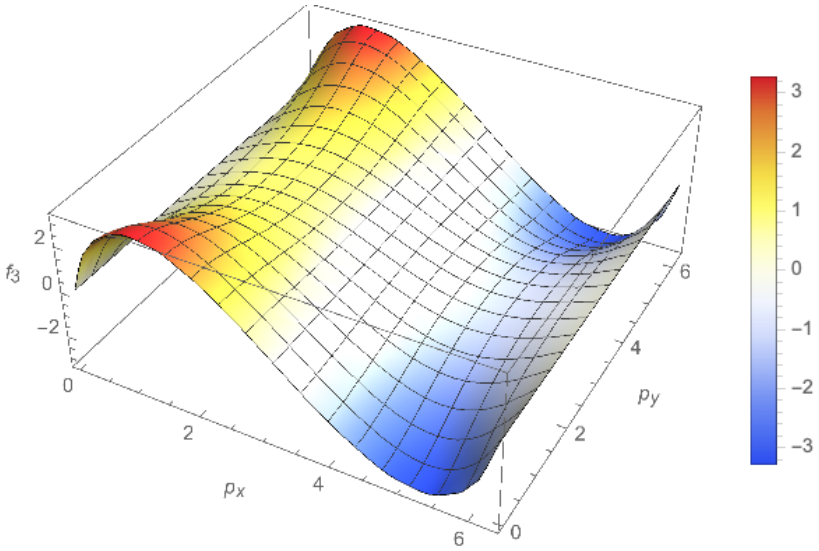

Figure 3.7: Plot of $f_3(\boldsymbol{p})$, [30]

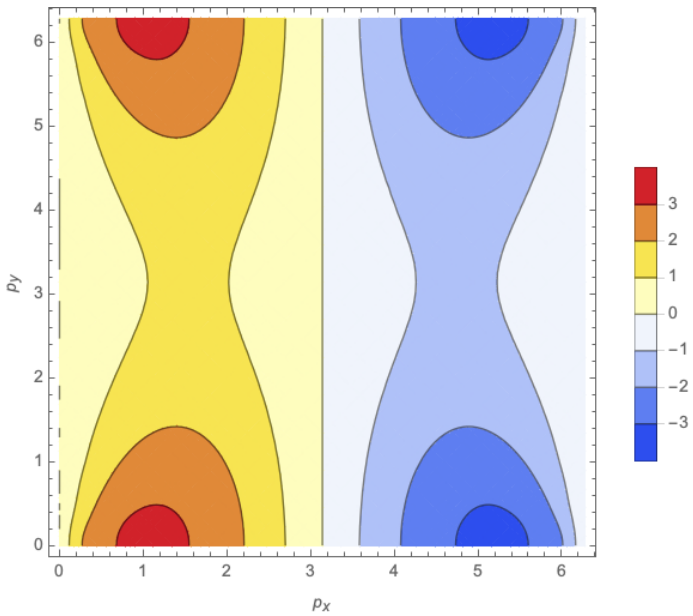

Figure 3.8: Contour plot of $f_3(\boldsymbol{p})$, [30]

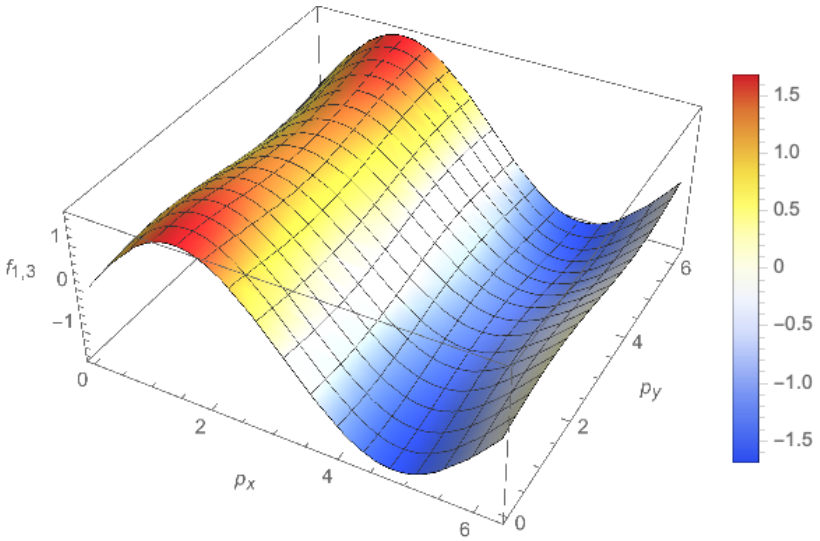

Figure 3.9: Plot of $f_{1,\alpha} = f_{1,3}$, [30]

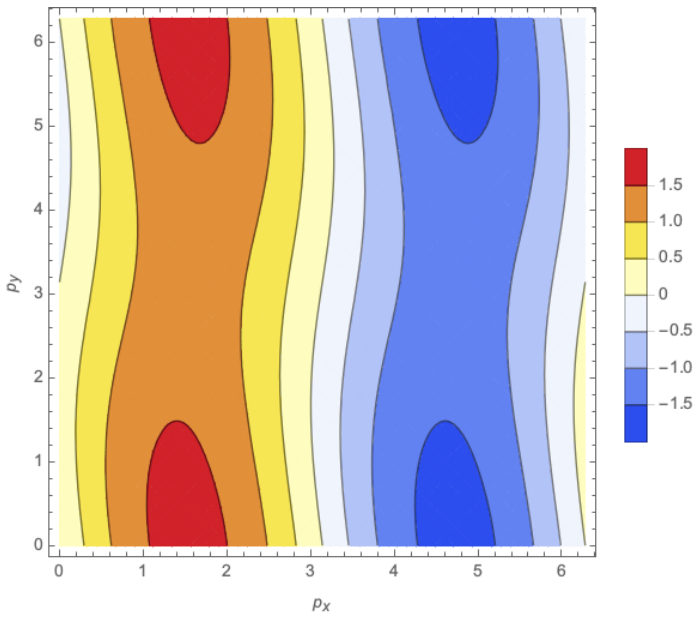

Figure 3.10: Contour plot of $f_{1,\alpha} = f_{1,3}$, [30]

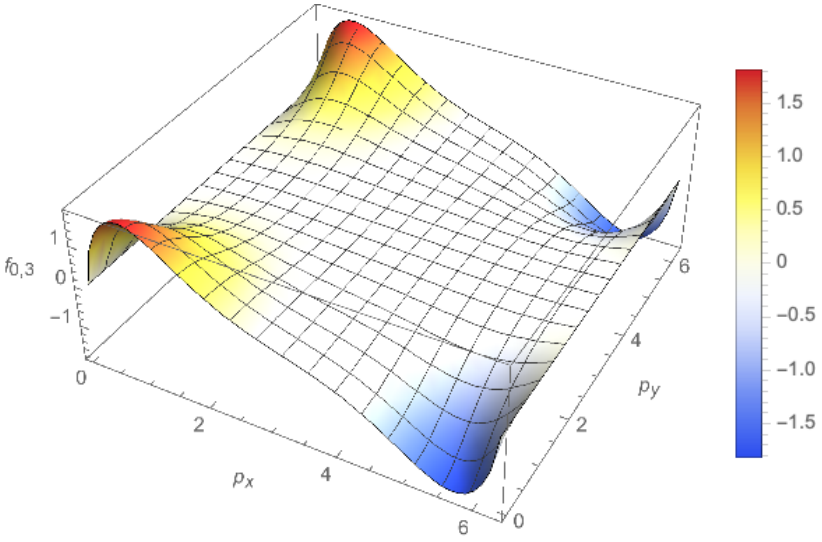

Figure 3.11: Plot of $f_{0,\alpha} = f_{0,3}$, [30]

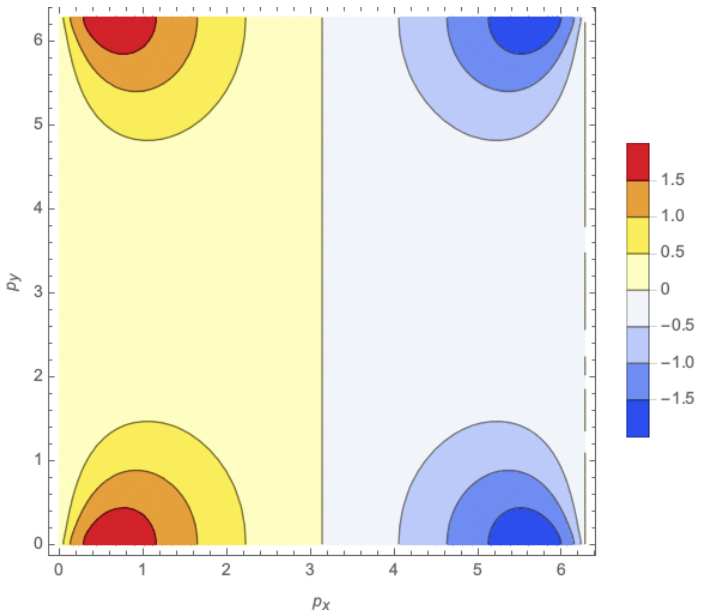

Figure 3.12: Contour plot of $f_{0,\alpha} = f_{0,3}$, [30]

3.4.3 $\alpha = 2$

In the last case that is the most relevant, by looking at Fig.3.13 and Fig.3.14 we can see that the series now has an high peak (2π) in the limit $\boldsymbol{p} \to \boldsymbol{0}$. In Fig.3.15 we observe the usual behaviour of f_{1,p_x} but now f_{0,p_x} is dominant in fact looking at Fig.3.17, we note that its shape is basically the same of $f_2(\boldsymbol{p})$. If we now extract the $\boldsymbol{d} = \boldsymbol{0}$ term of f_{0,p_x} in the $\boldsymbol{p} \to \boldsymbol{0}$ we have that:

$$\begin{aligned} \lim_{x\to 0^{\pm}} \lim_{y\to 0} \frac{\pi}{2\Gamma(3/2)} p_x \; E_{1/2}\Big(\frac{p_x^2+p_y^2}{4}\Big) = \pm 2\pi \\ \lim_{y\to 0} \lim_{x\to 0} \frac{\pi}{2\Gamma(3/2)} p_x \; E_{1/2}\Big(\frac{p_x^2+p_y^2}{4}\Big) = 0 \end{aligned} \tag{3.18}$$

so the limit is undefined as it depends on the path. The behaviour described above can be better seen in Fig.3.19 and Fig.3.20 where we set $p_y = 0$ and plot $f_\alpha(p_x, 0)$ and $f_{0,p_x}(p_x, 0)$. This kind of situation could represent that we are losing the $\boldsymbol{p} = \boldsymbol{0}$ critical line. A way to test it is to see if edge-modes are still present that is what we are going to do next.

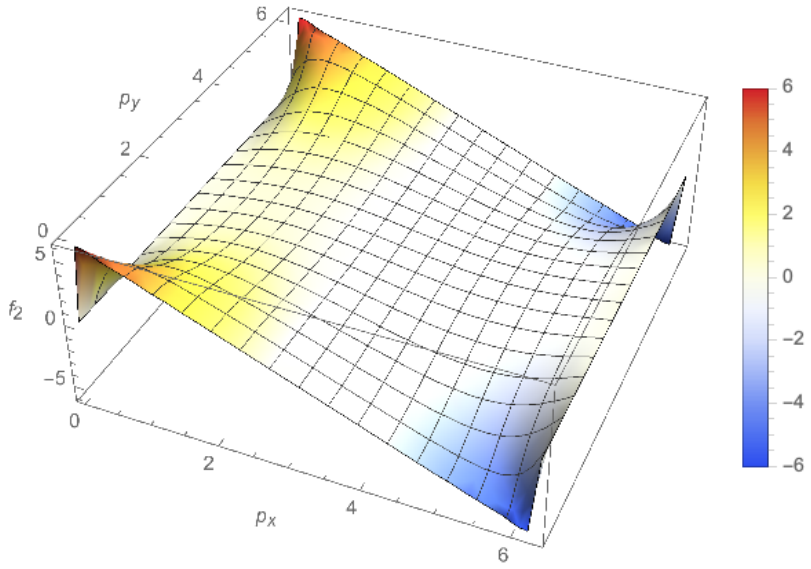

Figure 3.13: Plot of $f_2(\boldsymbol{p})$, [30]

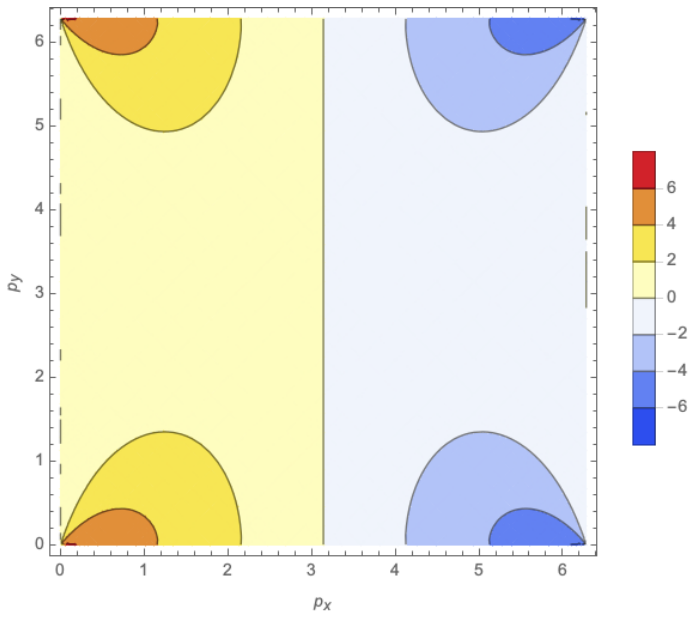

Figure 3.14: Contour plot of $f_2(\boldsymbol{p})$, [30]

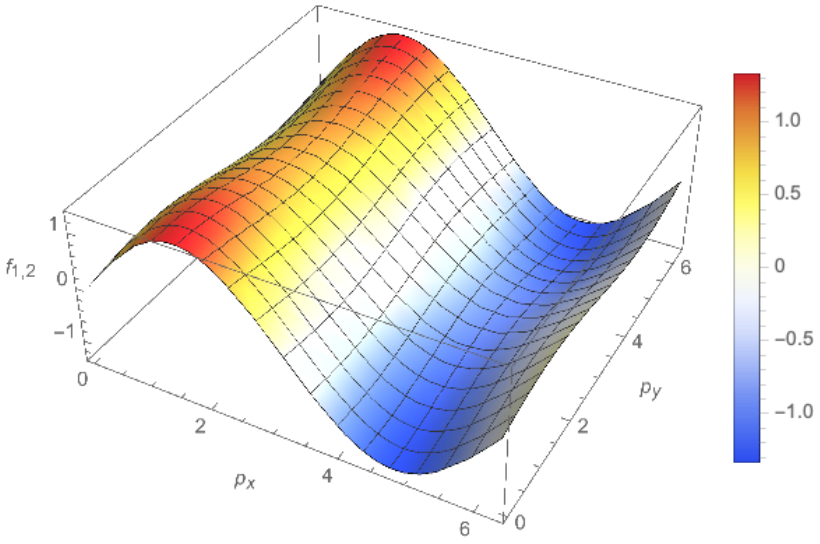

Figure 3.15: Plot of $f_{1,\alpha} = f_{1,2}$, [30]

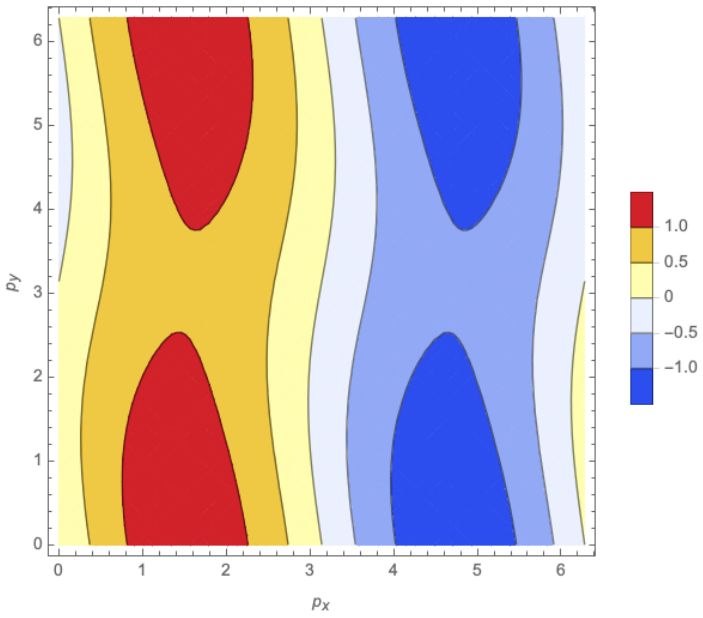

Figure 3.16: Contour plot of $f_{1,\alpha} = f_{1,2}$, [30]

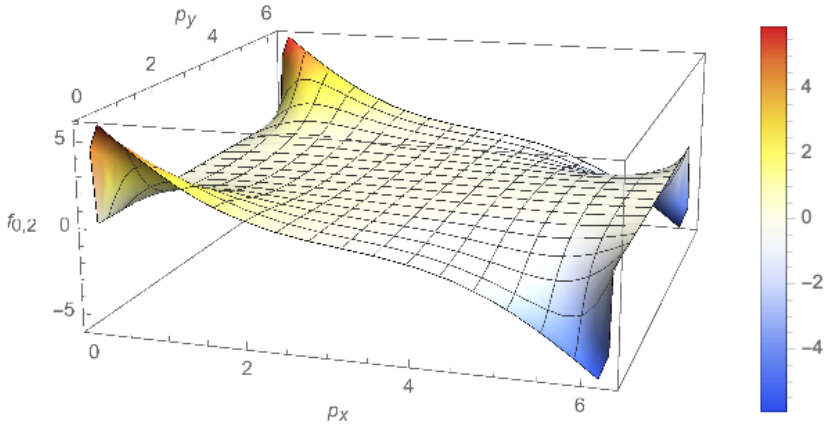

Figure 3.17: Plot of $f_{0,\alpha} = f_{0,2}$, [30]

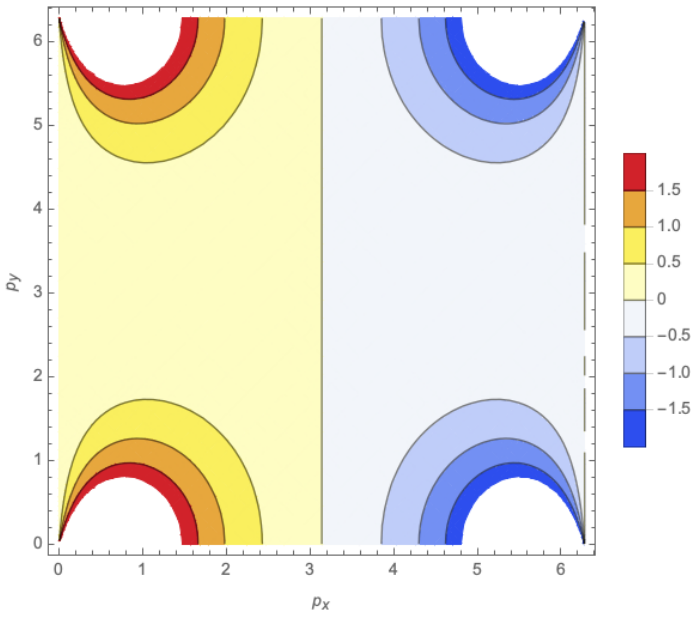

Figure 3.18: Plot of $f_{0,\alpha} = f_{0,2}$, [30]

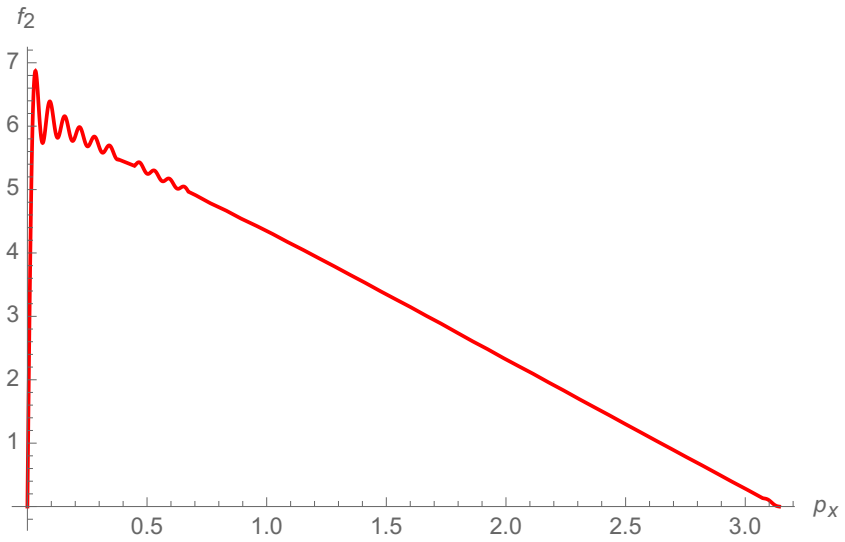

Figure 3.19: Plot of $f_2(p_x, 0)$, [30]

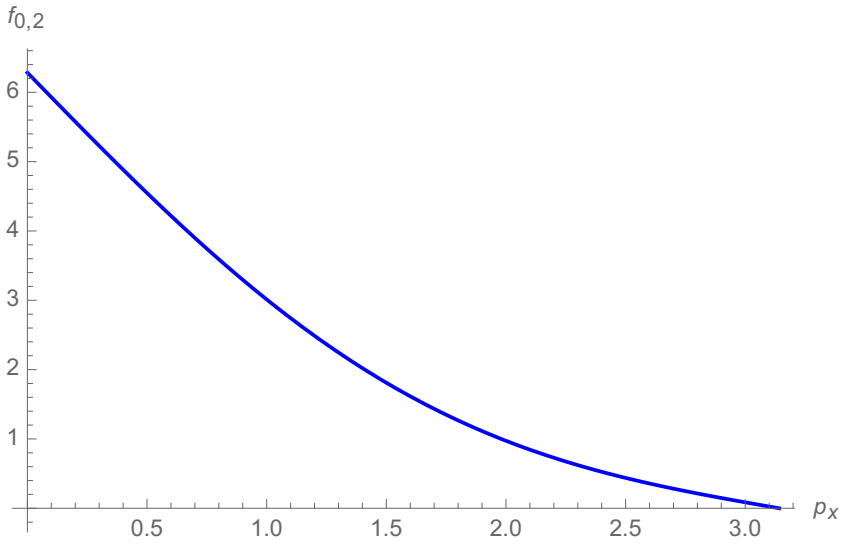

Figure 3.20: Plot of $f_{0,\alpha}(p_x, 0) = f_{0,2}(p_x, 0)$, [30]

3.5 Diagonalization and Edge-Modes

We start from the lattice Hamiltonian (3.13) and rewrite it in a matrix form of the kind:

$$H = \sum_{\boldsymbol{l}} \sum_{\boldsymbol{d}} c^{\dagger}_{\boldsymbol{l}} A_{(\boldsymbol{l},\boldsymbol{l}+\boldsymbol{d})}\ c_{\boldsymbol{l}+\boldsymbol{d}} + \frac{1}{2}(c^{\dagger}_{\boldsymbol{l}} B_{(\boldsymbol{l},\boldsymbol{l}+\boldsymbol{d})}\ c^{\dagger}_{\boldsymbol{l}+\boldsymbol{d}} + \text{h.c.}) \tag{3.19}$$

After dropping out a constant term this matrix reads:

$$H = \frac{1}{2} \sum_{\boldsymbol{l}} \sum_{\boldsymbol{d}} \Psi^{\dagger} \begin{pmatrix} -\mu + 4t & -t/d^{\beta} & 0 & \frac{2\Delta}{d^{\alpha+1}}(r+is) \\ -t/d^{\beta} & -\mu + 4t & -\frac{2\Delta}{d^{\alpha+1}}(r+is) & 0 \\ 0 & -\frac{2\Delta}{d^{\alpha+1}}(r-is) & \mu - 4t & t/d^{\beta} \\ \frac{2\Delta}{d^{\alpha+1}}(r-is) & 0 & t/d^{\beta} & \mu - 4t \end{pmatrix} \Psi \tag{3.20}$$

where $\Psi = (c_{\boldsymbol{l}+\boldsymbol{d}},\ c_{\boldsymbol{l}},\ c^{\dagger}_{\boldsymbol{l}+\boldsymbol{d}},\ c^{\dagger}_{\boldsymbol{l}})^T$ with $\boldsymbol{l} = (m,n)$, $\boldsymbol{d} = (r,s)$ and we set $\Delta = t = 1/2$. Using the DMRG software with OBC along both directions (oo in the figures stands for "open open") we will diagonalize the Hamiltonian in the $\beta \to \infty$ limit varying α. Thus we are going to obtain its single-particle energy spectrum and then we will analyse it. We are able to study a maximum lattice of $N = 35 \times 35$ sites where $N = L_x \times L_y$ and $L_x,\ L_y$ are the number of sites along the x and y directions. This is due to the fact that the matrix has $2N \times 2N$ elements so it soon requires an high computational cost. We will look at the same cases studied in the last section:

- $\alpha = 10$
- $\alpha = 3$
- $\alpha = 2$

for $-1 \geq \mu \leq 5$. We expect that in the first and second case the model is similar to the SR one, so it should:

- have a gap in the $\mu = -1$ and $\mu = 5$ trivial phases
- be gapless at the critical chemical potentials $\mu = 0$, $\mu = 2$ and $\mu = 4$
- have a gap in the $\mu = 1$ and $\mu = 3$ topological phases filled by a set of gapless edge-states energies (3.1.2) linking the two bands.

Then in the third case we would like to see if edge-states are present even if the spectrum is not 0 for $\mu = 0$ meaning that the gap is not closing and in principle there is no phase transition there. After that, we will test the correctness of the program in the topological phases using PBC in both directions (pp in the figures stands for "periodic periodic"), in fact with these conditions we do not expect to see edge-states in the topological phases.

3.5.1 $\alpha = 10$

• $\mu = -1$
Let us start from the energy spectrum given in Fig.3.21. As we can see, the energy range is correct as we expect from the 2D SR eigenenergies (as we are in the $\beta \to \infty$ limit):

$$E_{SR} = \pm\sqrt{(\cos(p_x) + \cos(p_y) + \mu - 2)^2 + \sin^2(p_x) + \sin^2(p_y)} \tag{3.21}$$

that in this case is equal to 5 in $(p_x, p_y) = (\pi, \pi)$ and 1 in $(p_x, p_y) = (0, 0)$. So we are in a trivial gapped phase of the model.

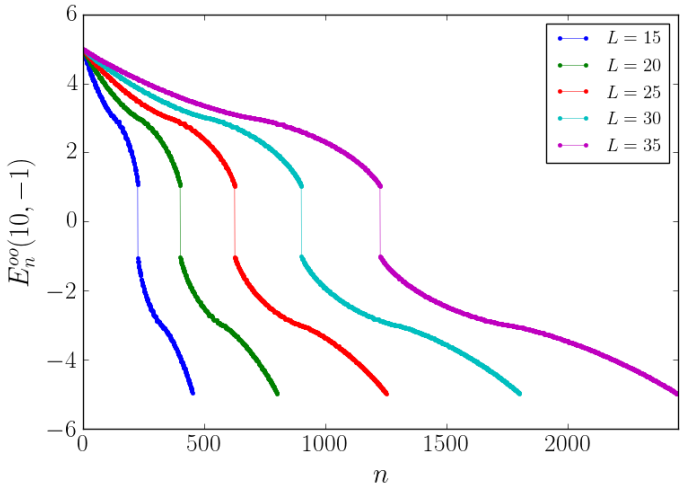

Figure 3.21: Plot of $E_n^{oo}(\alpha, \mu) = E_n^{oo}(10, -1)$,[31]

• $\mu = 0$
Now we move on to $\mu = 0$, where we expect that the gap closes as the system is in a critical point. Looking at Fig.3.22 we can see that in this case the spectrum is equal to 4 in $(p_x, p_y) = (\pi, \pi)$ and ~ 0 in $(p_x, p_y) = (0, 0)$ as it should following (3.21). Numerically the exact 0 eigenvalue is not found as we can see from the extrapolation in Fig.3.23. This happens because the system we are considering is finite so we did a fit for $L \to \infty$ to see if the lower positive eigenvalue scales to 0 and it does as we can see in Fig.3.24. Note

also that the momentum is discretized as: $(p_x, p_y) = (\frac{\pi}{L_x+1}i, \frac{\pi}{L_y+1}j)$ where $i = 1, \ldots, L_x$ and $j = 1, \ldots, L_y$ then with OBC we are not able to catch exactly the $(0, 0)$ values. In the PBC spectrum instead we find exactly the 0 eigenvalue because in this case we have that: $(p_x, p_y) = (\frac{2\pi}{L_x}i, \frac{2\pi}{L_y}j)$ where $i = 1, \ldots, L_x$ and $j = 1, \ldots, L_y$

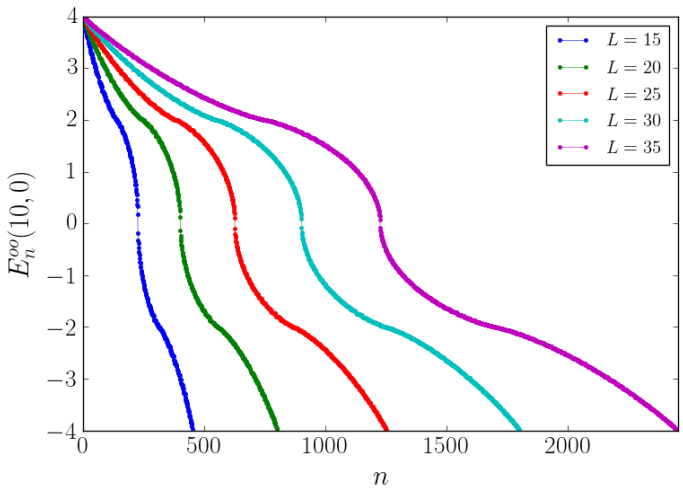

Figure 3.22: Plot of $E_n^{oo}(\alpha, \mu) = E_n^{oo}(10, 0)$, [31]

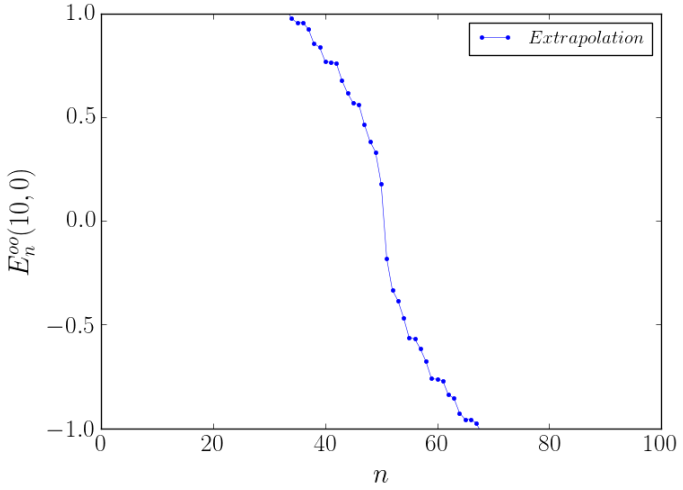

Figure 3.23: Extrapolation of the lower $E_n^{oo}(\alpha, \mu) = E_n^{oo}(10, 0)$, [31]

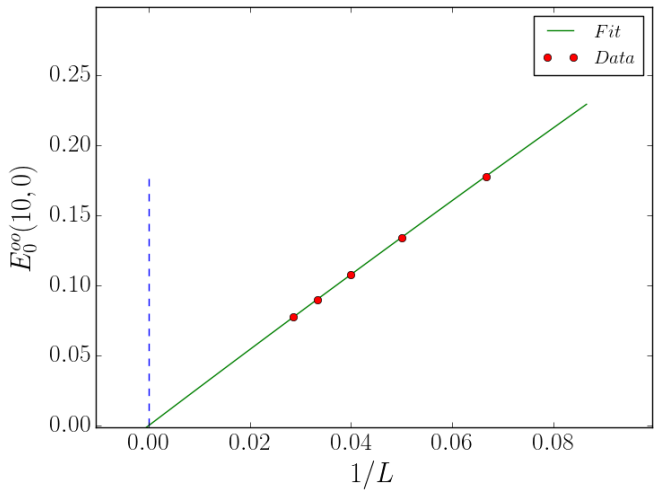

Figure 3.24: Fit of $E_0^{oo}(\alpha,\mu) = E_0^{oo}(10,0)$ for $L \to \infty$, [31]

• $\mu = 1$

In this case we now expect a certain number of edge-states filling the gap. Looking at the spectrum in Fig.3.25 we see that in this case it is equal to 3 in $(p_x, p_y) = (\pi, \pi)$ and 1 in $(p_x, p_y) = (0, 0)$ according to (3.21) but we effectively see that the gap is filled with a certain number of edge-states energies. Now we can compare this spectrum with the PBC one and test the program. In Fig.3.26 we can see that the spectrum is now gapped and no edge-states are present. Thus the program is correct and the system supports edge-states in this phase, which is topological.

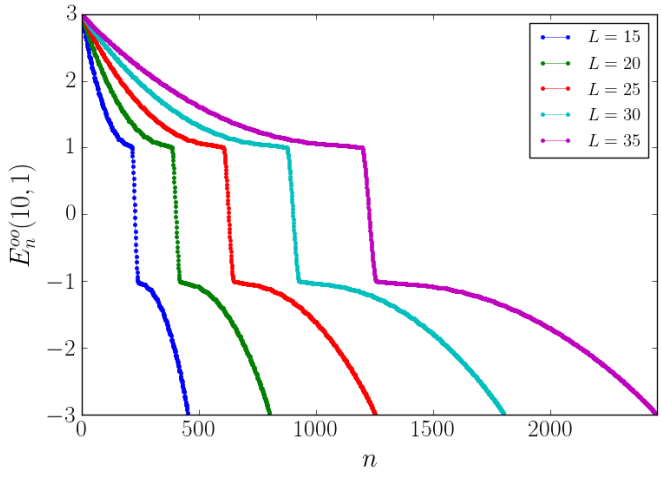

Figure 3.25: Plot of $E_n^{oo}(\alpha,\mu) = E_n^{oo}(10,1)$, [31]

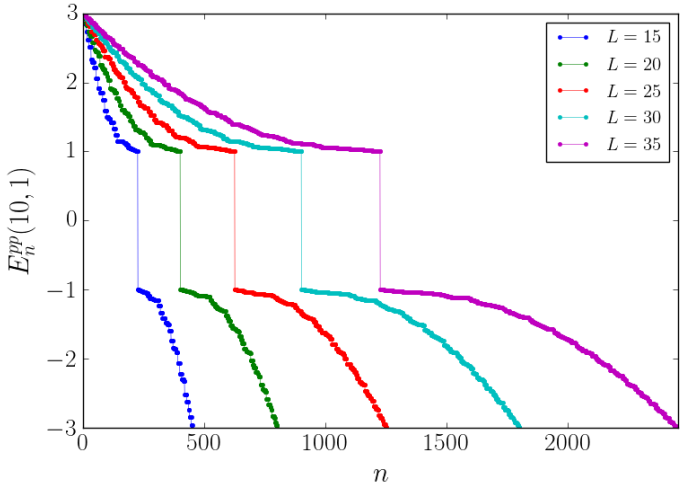

Figure 3.26: Plot of $E_n^{pp}(\alpha, \mu) = E_n^{pp}(10, 1)$, [31]

• $\mu = 2$

In this case we expect the gap to close being the system in a critical point. Looking at the spectrum in Fig.3.27 we see that it is equal to 2 in $(p_x, p_y) = (\pi, \pi)$ and ~ 0 in $(p_x, p_y) = (\pi, 0)$ as follows from (3.21. As before it does not close exactly in particular for the even lenghts of the lattice. In this case the $(\pi, 0)$ point is approximated by: $(p_x, p_y) = (\frac{\pi}{L_x+1} L_x, \frac{\pi}{L_y+1})$ and numerically the contribution is higher for even lenghts. Then we need to do a fit for the even lenghts because also from the extrapolation in Fig.3.23 we see that the gap is not exactly 0. As we can see from Fig.3.29, $E_0^{oo}(10, 2)$ scales to 0 in the $L \to \infty$ limit. In the PBC spectrum the situation is reversed, i.e. the gap gets an higher contribution from the odd lenghts because in this case $(\pi, 0)$ is approximated by: $(p_x, p_y) = (\frac{2\pi}{L_x} \frac{L_x+1}{2}, \frac{2\pi}{L_y} L_y)$ but still $E_0^{pp}(10, 2)$ scales to 0 in the odd sector.

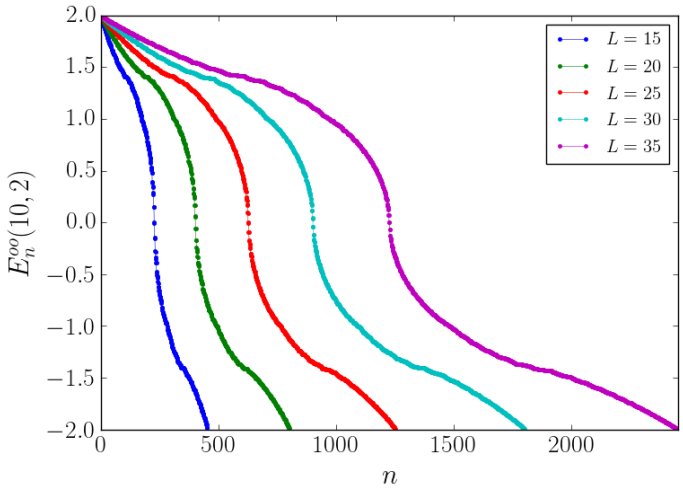

Figure 3.27: Plot of $E_n^{oo}(\alpha, \mu) = E_n^{oo}(10, 2)$, [31]

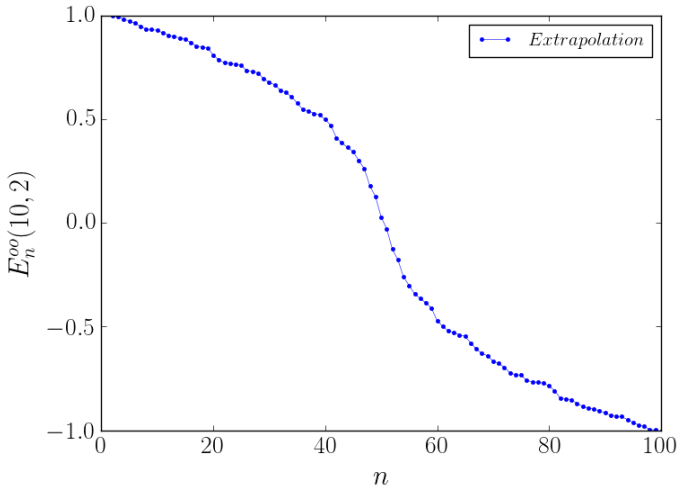

Figure 3.28: Extrapolation of the lower $E_n^{oo}(\alpha, \mu) = E_n^{oo}(10, 2)$, [31]

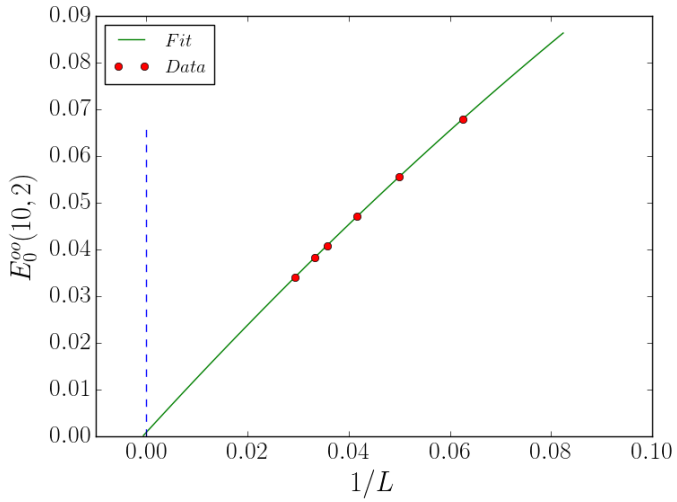

Figure 3.29: Fit of $E_0^{oo}(\alpha,\mu) = E_0^{oo}(10,2)$ for $L \to \infty$, [31]

• $\mu = 3$

This is the second topological phase, then there should be gapless-edge states filling the gap as in the $\mu = 1$ phase. Again we plot the energy spectrum in Fig.3.30 for OBC and then compare it with the PBC one as shown in Fig.3.31. Here the range of energies varies from 3 in $(p_x, p_y) = (0,0)$ to 1 in $(p_x, p_y) = (0,\pi)$ (3.21). We can appreciate the presence of edge-states in the first case while they disappear in the latter one as we expected. Thus we are effectively in a topological phase.

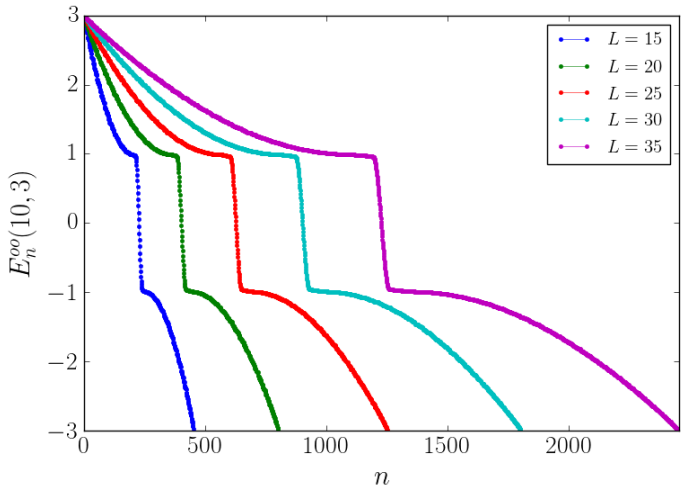

Figure 3.30: Plot of $E_n^{oo}(\alpha,\mu) = E_n^{oo}(10,3)$, [31]

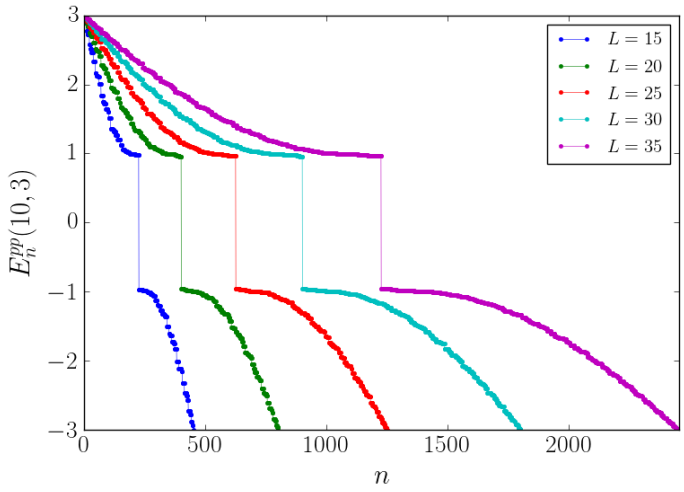

Figure 3.31: Plot of $E_n^{pp}(\alpha, \mu) = E_n^{pp}(10, 3)$, [31]

• $\mu = 4$
This is the third critical point with a spectrum varying from 4 in $(p_x, p_y) = (0, 0)$ to ~ 0 in $(p_x, p_y) = (\pi, \pi)$ (3.21). Again here the spectrum is not exactly 0 as we can see from Fig.3.32 and Fig.3.33 for similar reasons as explained above. In this case (π, π) is approximated by: $(p_x, p_y) = (\frac{\pi}{L_x+1}L_x, \frac{\pi}{L_y+1}L_y)$ then the approximation with OBC is independent from the parity of the lattice size like in the $\mu = 0$ case and it scales to 0 in the $L \to \infty$ limit as shown in Fig.3.34. In the PBC case instead we have a parity dependence of the lower energy as the (π, π) point in the odd sector is labeled by: $(p_x, p_y) = (\frac{2\pi}{L_x}\frac{L_x+1}{2}, \frac{2\pi}{L_y}\frac{L_y+1}{2})$ then it can not reach the exact point.

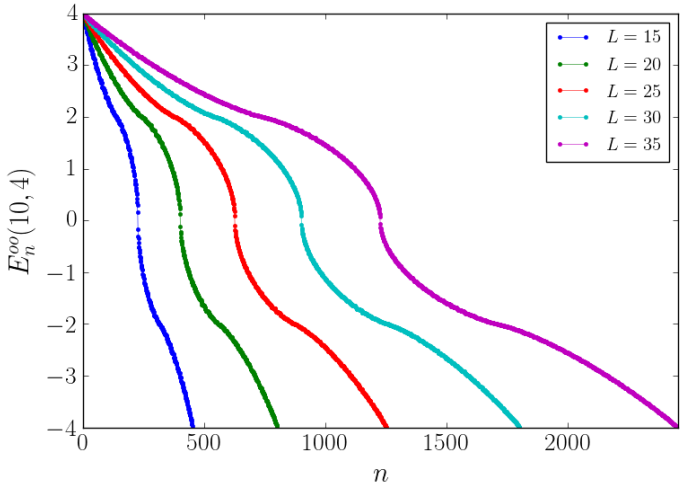

Figure 3.32: Plot of $E_n^{oo}(\alpha, \mu) = E_n^{oo}(10, 4)$, [31]

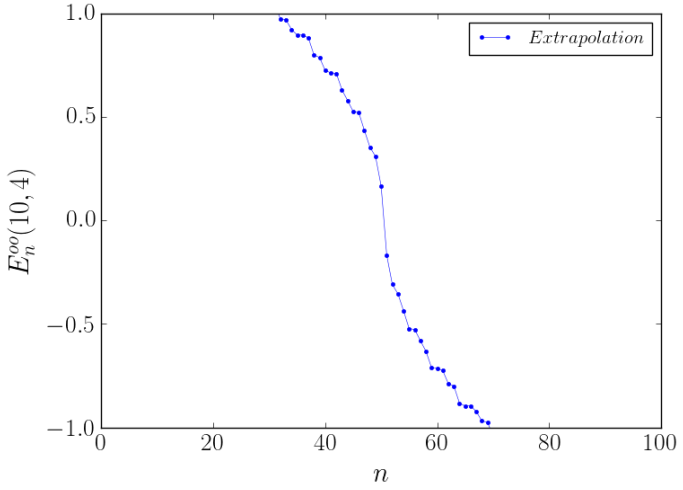

Figure 3.33: Extrapolation of the lower $E_n^{oo}(\alpha, \mu) = E_n^{oo}(10, 4)$, [31]

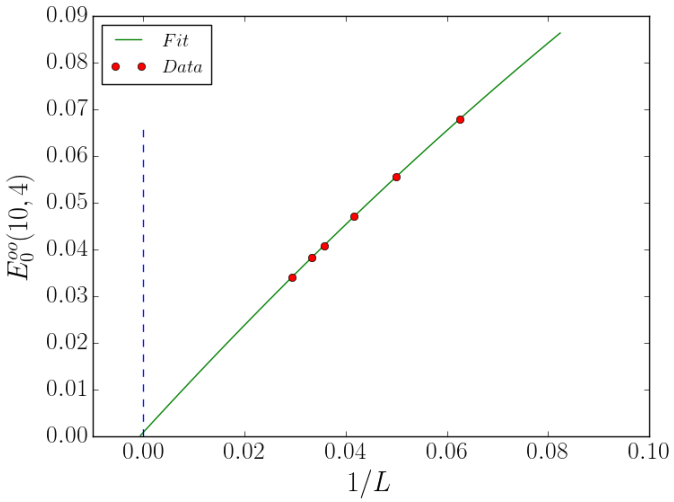

Figure 3.34: Plot of $E_n^{oo}(\alpha,\mu) = E_n^{oo}(10,4)$, [31]

• $\mu = 5$

The last case we are going to analyse for $\alpha = 10$ is a trivial phase which varies from 5 in $(p_x, p_y) = (0,0)$ to 1 in $(p_x, p_y) = (\pi,\pi)$ (3.21) and as we can see from the spectrum in Fig.3.35 it is a trivial gapped phase. Thus we finished the analysis of the "SR" like model and everything works as it should. Then we can move on to study the phases of the more interesting LR cases, $\alpha = 3$ and $\alpha = 2$ and see how the growing interactions influence the phase diagram.

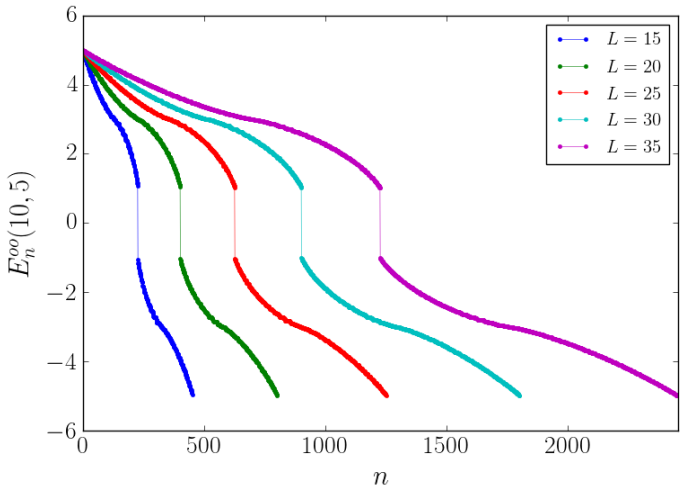

Figure 3.35: Plot of $E_n^{oo}(\alpha,\mu) = E_n^{oo}(10,5)$, [31]

3.5.2 $\alpha = 3$

• $\mu = -1$
Starting from the energy spectrum given in Fig.3.36 we can see that the energy range is still in agreement with (3.21) and in fact $E_n^{oo}(3,-1)$ goes from ~ 1 to 5. The gap is a bit larger now due to discretization but in the PBC spectrum 3.41 we see the jump from the first energy that is of order 1 in $(0,0)$ to the second in $\sim (0,0)$.
Note that now the eigenenergies are of LR type:

$$E_{LR} = \pm\sqrt{(\cos(p_x)+\cos(p_y)+\mu-2)^2 + \Big(\sum_{\boldsymbol{d}} \frac{r}{d^3}\sin(\boldsymbol{p}\cdot\boldsymbol{d})\Big)^2 + \Big(\sum_{\boldsymbol{d}} \frac{s}{d^3}\sin(\boldsymbol{p}\cdot\boldsymbol{d})\Big)^2} \tag{3.22}$$

so the two series will influence the spectrum expecially for $(p_x, p_y, \mu = (0,0,0))$ as we studied in section 3.4.2.

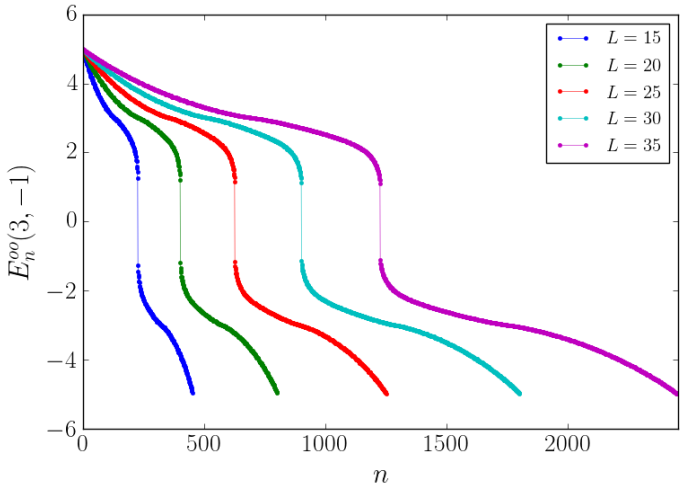

Figure 3.36: Plot of $E_n^{oo}(\alpha,\mu) = E_n^{oo}(3,-1)$,[31]

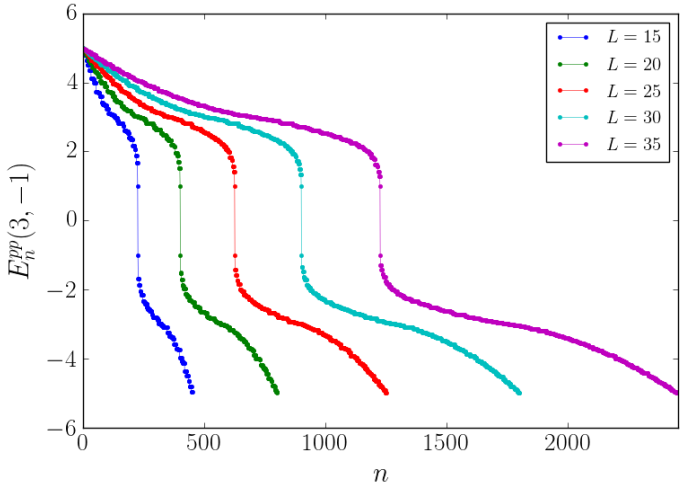

Figure 3.37: Plot of $E_n^{pp}(\alpha, \mu) = E_n^{pp}(3, -1)$,[31]

• $\mu = 0$

As we mentioned above also in this case, looking at Fig.3.38 there seems to be a large gap even if we expect that it closes. This is again linked to the finitness of the system and to the discretization of momenta as in the $\alpha = 10$ cases. But now the contributions of the sine series in $(0, 0)$ are high as they start to converge slowly in that point. We need a very large lattice for the gap to close. In the PBC spectrum in Fig.3.39 we can better understand this point. There the gap closes exactly as we expect but the second eigenvalue is quite bigger and this is due to the peak we see in $f_{0,p_x}(3, 0)$ as shown in Fig.3.12 around $(p_x, p_y) \gtrsim (0, 0)$. So by this considerations, we can conclude that even if the gap still closes in this case we already observe high long range effects acting on the system.

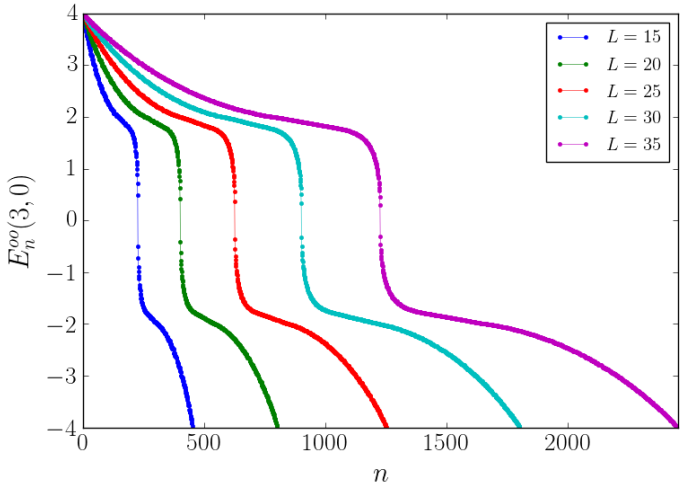

Figure 3.38: Plot of $E_n^{oo}(\alpha, \mu) = E_n^{oo}(3, 0)$, [31]

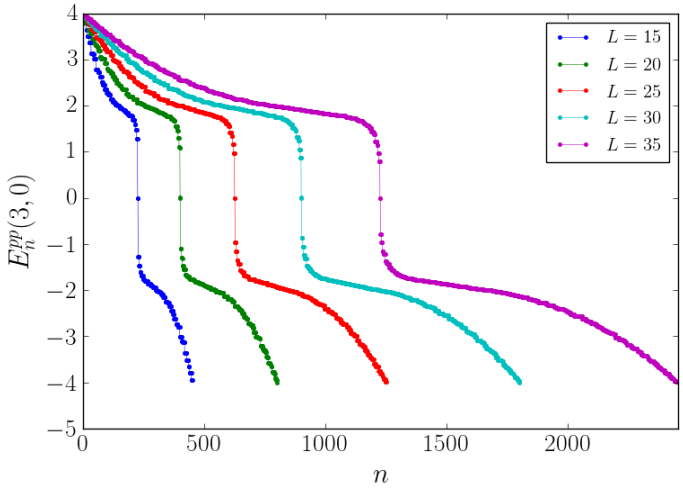

Figure 3.39: Plot of $E_n^{pp}(\alpha, \mu) = E_n^{pp}(3, 0)$, [31]

• $\mu = 1$

We now move on to a topological phase starting from the spectrum in Fig.3.40. We have that $E_n^{oo} \in [1, 3]$ and we see that the gap is filled with a certain number of edge-states energies. In the PBC spectrum instead, see Fig.3.41 no edge-states are present as we expected. Thus the model supports edge-states in this toplogical phase.

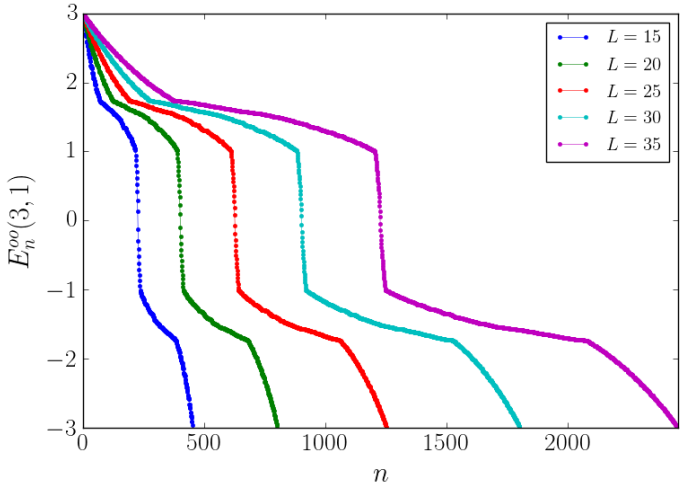

Figure 3.40: Plot of $E_n^{oo}(\alpha, \mu) = E_n^{oo}(3,1)$, [31]

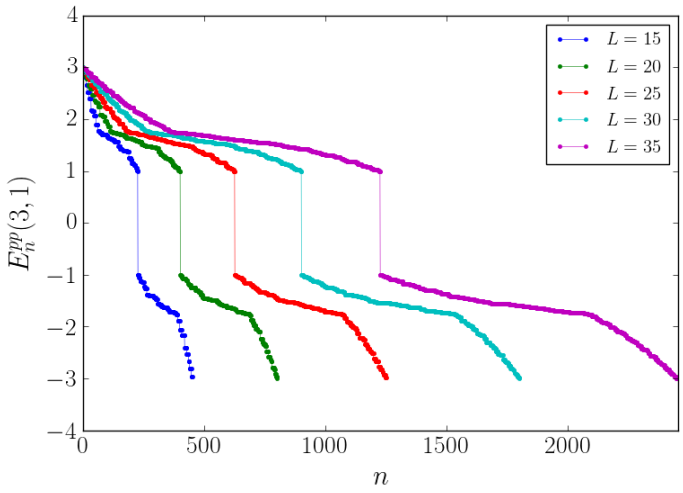

Figure 3.41: Plot of $E_n^{pp}(\alpha, \mu) = E_n^{pp}(3,1)$, [31]

• $\mu = 2$

In this case we expect the gap to close being the system in a critical point. Looking at the spectrum in Fig.3.42 we see that $E_n^{oo}(3,2) \in [0,2]$. The gap does not close exactly, see Fig.3.43. In particular the contribution comes from the even lenghts of the lattice as in the $\alpha = 10$. $\mu = 2$ case. So we did a fit of $E_0^{oo}(3,2)$ in the even sector and it scales to 0, see Fig.3.44. Then model is in a critical point.

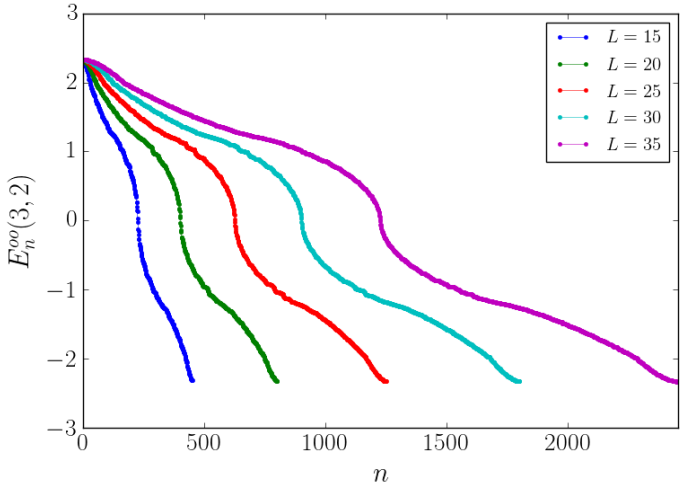

Figure 3.42: Plot of $E_n^{oo}(\alpha, \mu) = E_n^{oo}(3, 2)$, [31]

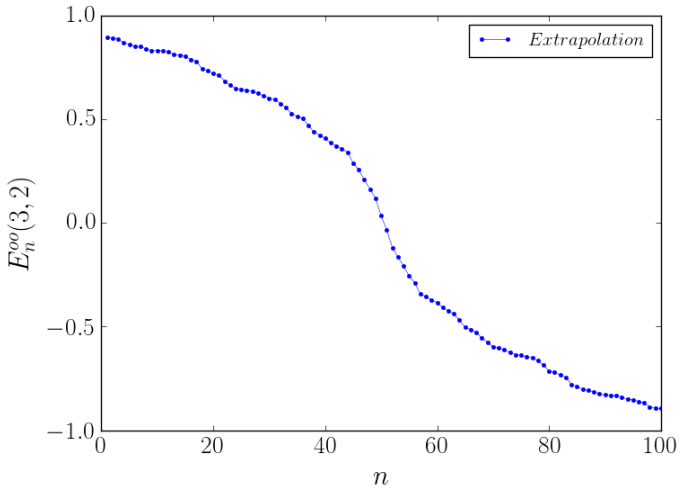

Figure 3.43: Extrapolation of the lower $E_n^{oo}(\alpha, \mu) = E_n^{oo}(3, 2)$, [31]

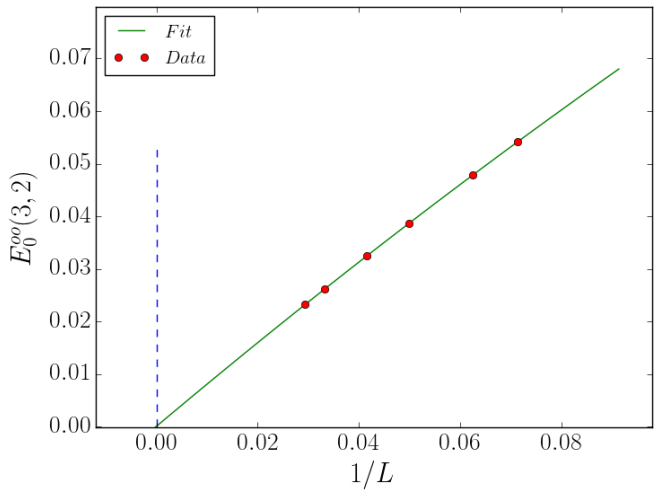

Figure 3.44: Fit of $E_0^{oo}(\alpha,\mu) = E_0^{oo}(3,2)$ for $L \to \infty$, [31]

• $\mu = 3$
This is the second topological phase and here $E_n^{oo}(3,3) \in [0,3]$ so we have gapless-edge states filling the gap, see 3.45. Again we plot the energy spectrum with PBC in Fig.3.46 and note how the gap is now empty. Thus we are effectively in a topological phase supporting edge-states.

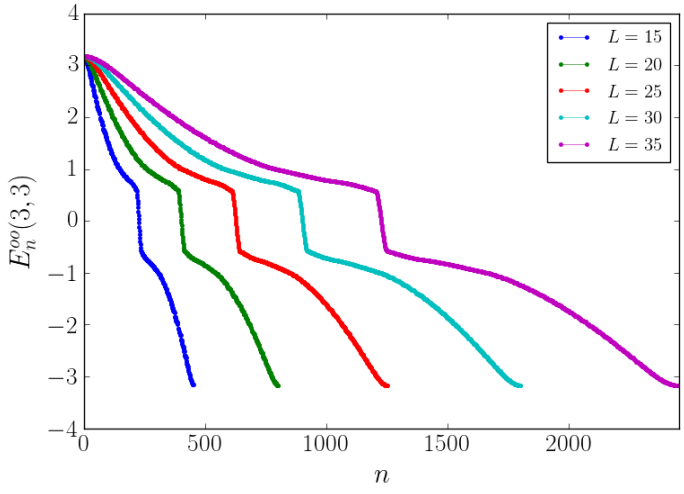

Figure 3.45: Plot of $E_n^{oo}(\alpha,\mu) = E_n^{oo}(3,3)$, [31]

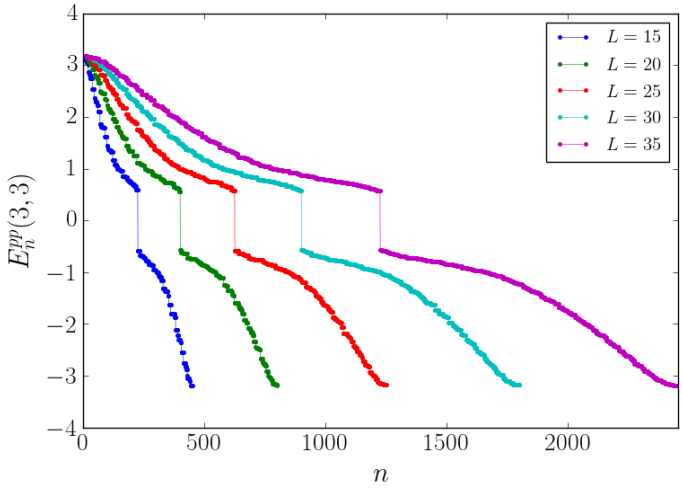

Figure 3.46: Plot of $E_n^{pp}(\alpha, \mu) = E_n^{pp}(3, 3)$, [31]

• $\mu = 4$
This is the third critical point where $E_n^{oo}(3, 4) \in [0, 4]$. The spectrum is not exactly 0 as we can see from Fig.3.47 and Fig.3.48 for similar reasons as in the $\alpha = 10$, $\mu = 4$ case. The plot is independent from the parity of the lattice size and $E_0^{oo}(3, 4)$ scales to 0 in the $L \to \infty$ limit as shown in Fig.3.49.

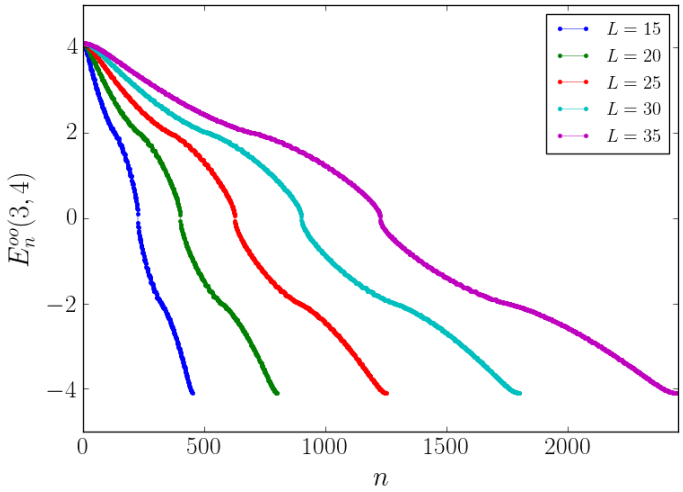

Figure 3.47: Plot of $E_n^{oo}(\alpha, \mu) = E_n^{oo}(3, 4)$, [31]

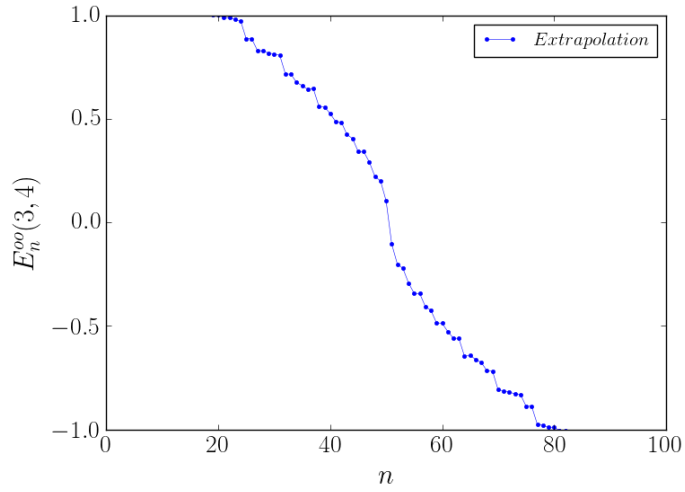

Figure 3.48: Extrapolation of the lower $E_n^{oo}(\alpha,\mu) = E_n^{oo}(3,4)$, [31]

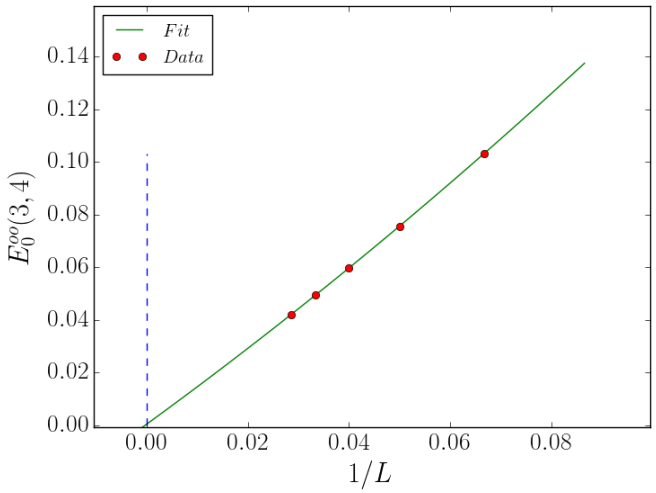

Figure 3.49: Fit of $E_0^{pp}(\alpha,\mu) = E_0^{pp}(3,4)$, [31]

• $\mu = 5$

The last case is a trivial gapped phase with $E_n^{oo}(3,5) \in [1,5]$ as we can see from the spectrum in Fig.3.50. Thus we finished the analysis $\alpha = 3$ case and as we saw the system still preserves the phases and edge-states structure of the SR model. Now we can go on and study the phases of the $\alpha = 2$ case.

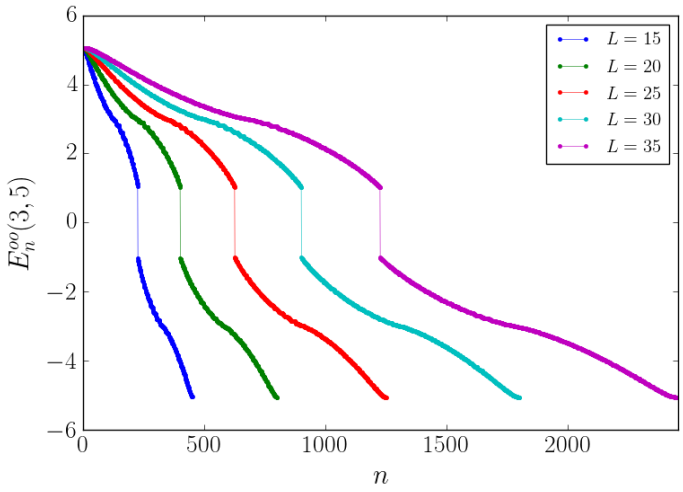

Figure 3.50: Plot of $E_n^{oo}(\alpha, \mu) = E_n^{oo}(3, 5)$, [31]

It is interesting to note that as we predicted the model still behaves quite exactly as in the short range case expecially when the minimum of the energy is reached in a point containing a π where the spectrum seems to converge even for $\alpha < 2$

3.5.3 $\alpha = 2$

• $\mu = -1$

Looking at the energy spectrum given in Fig.3.51 we can see that there is a gap as we expected so we are in a trivial phase. Note that as in the $\alpha = 3$, $\mu = -1$ case the minimum energy has increased. Looking at Fig.3.52 we see only one energy state (that is a numerical effect) and then there is a gap of order 2. As argued in [24] then the states present near 2 in the OBC spectrum could also be protected states.

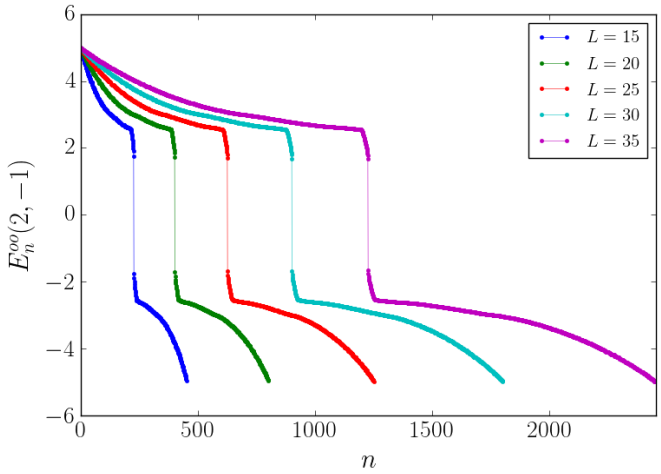

Figure 3.51: Plot of $E_n^{oo}(\alpha, \mu) = E_n^{oo}(2, -1)$,[31]

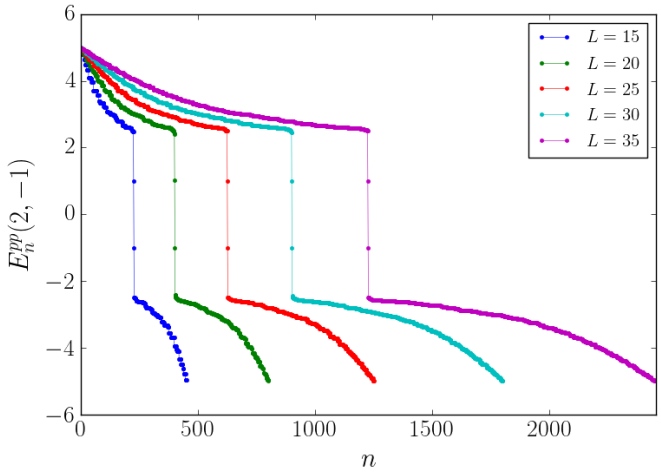

Figure 3.52: Plot of $E_n^{oo}(\alpha, \mu) = E_n^{oo}(2, -1)$,[31]

• $\mu = 0$

In this case, looking at Fig.3.53 we now clearly see that the gap is open. The tail of states partially filling the gap could be linked to the boundary conditions and the values of $f_{0,p_x}(2,0)$ that affect the spectrum but we see that the gap is nearly constant when increasing L and it gets more dense of states. Then looking at the PBC spectrum in Fig.3.54 we clearly see an empty gap of order 2 (the 0 energy as before is just a numerical effect as the program is able to pick exactly the $(p_x, p_y) = (2\pi, 2\pi)$ point but the spectrum is not well defined there). Then we can argue that something like a phase transition could be happening.

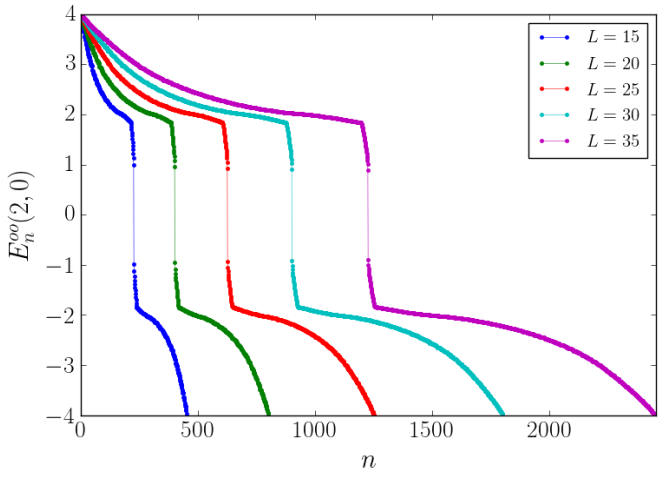

Figure 3.53: Plot of $E_n^{oo}(\alpha, \mu) = E_n^{oo}(2,0)$, [31]

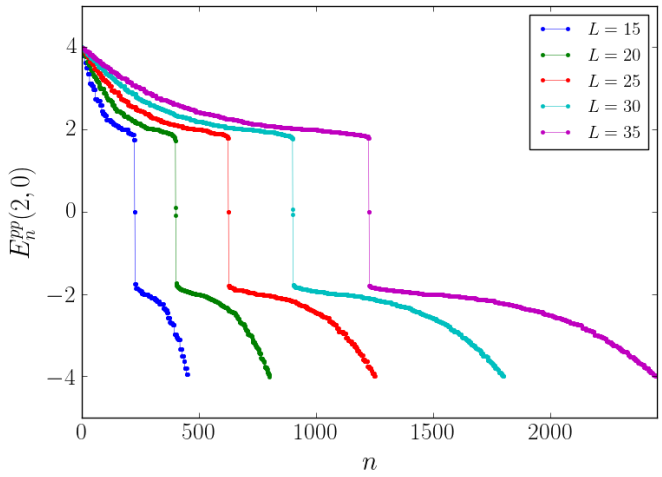

Figure 3.54: Plot of $E_n^{pp}(\alpha, \mu) = E_n^{pp}(2, 0)$, [31]

• $\mu = 1$

We now move on to a phase that was topological to see what happens now. Starting from the spectrum in Fig.3.55 it seems that there is a set of massive states partially filling the gap. In fact looking at the PBC spectrum in Fig.3.56 we do not see these states anymore, not even the two ones present in the $\alpha = 3$, $\mu = 1$ case. These could be a sort of topological massive-edge states. Then we can say that for $\alpha = 2$ we loose the $(p_x, p_y, \mu) = (0, 0, 0)$ phase transition but massive edge-states probably are still supported by the model that could now then be in a gapped topological phase.

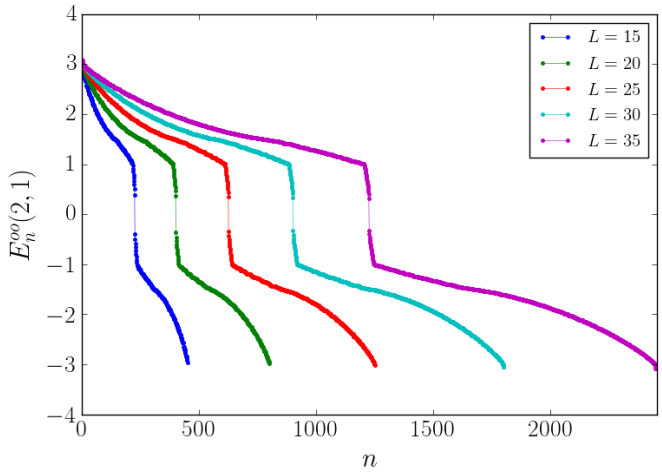

Figure 3.55: Plot of $E_n^{oo}(\alpha, \mu) = E_n^{oo}(2, 1)$, [31]

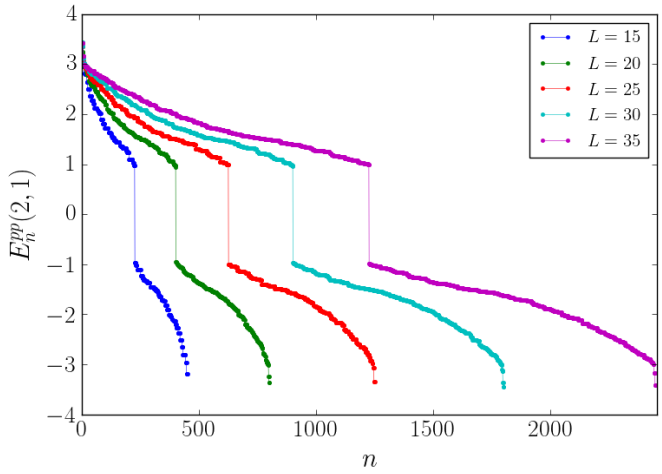

Figure 3.56: Plot of $E_n^{pp}(\alpha, \mu) = E_n^{pp}(10, 1)$, [31]

• $\mu = 2$
Looking at the spectrum in Fig.3.57 we see that the gap closes even if not exactly, see Fig.3.58. Also in this case the contribution to the gap comes from the even lenghts of the lattice. So we did a fit of $E_0^{oo}(2, 2)$ and this scales to 0, see Fig.3.59. So the model is in a critical point.

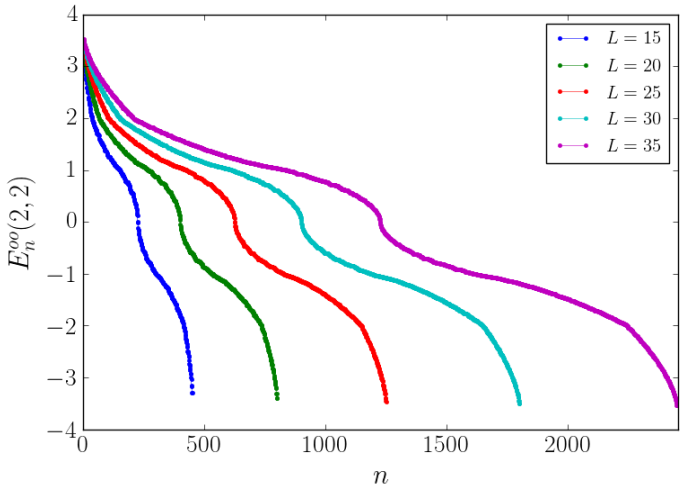

Figure 3.57: Plot of $E_n^{oo}(\alpha, \mu) = E_n^{oo}(2, 2)$, [31]

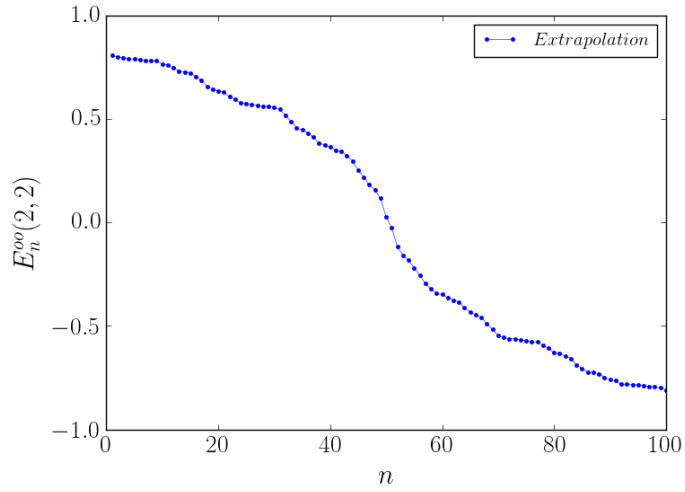

Figure 3.58: Extrapolation of the lower $E_n^{oo}(\alpha,\mu) = E_n^{oo}(2,2)$, [31]

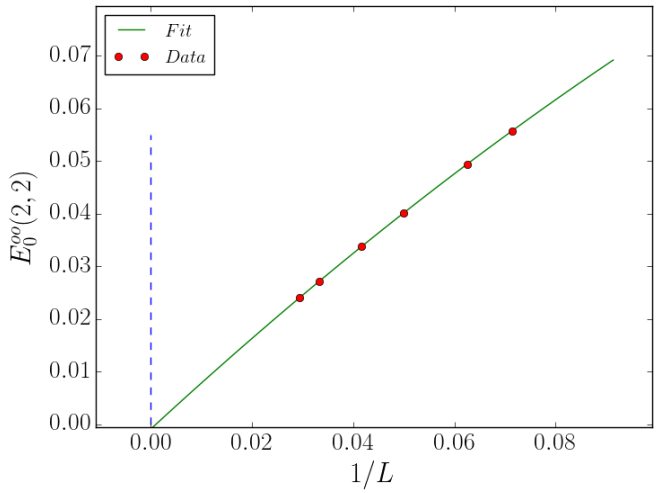

Figure 3.59: Fit of $E_0^{oo}(\alpha,\mu) = E_0^{oo}(2,2)$ for $L \to \infty$, [31]

• $\mu = 3$

This is now the first effective topological phase as we can see from Fig.3.60. We can in fact appreciate a set of gapless-edge states filling the gap. We also plot the energy spectrum for PBC in Fig.3.61 and there the gap is empty so we are effectively in a topological phase.

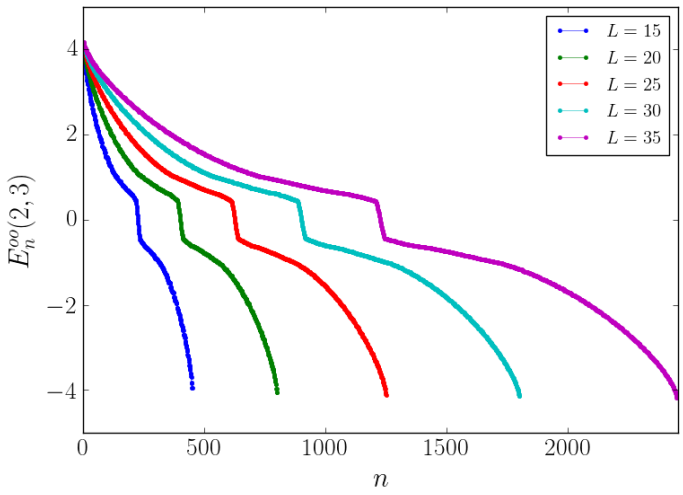

Figure 3.60: Plot of $E_n^{oo}(\alpha, \mu) = E_n^{oo}(2, 3)$, [31]

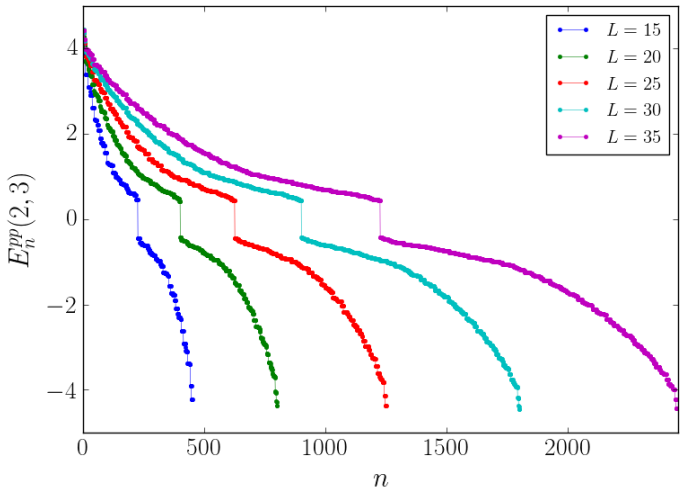

Figure 3.61: Plot of $E_n^{pp}(\alpha, \mu) = E_n^{pp}(2, 3)$, [31]

• $\mu = 4$

We now move on to the second critical point of which we plot the spectrum in Fig.3.62. This is not exactly closing as we can see from Fig.3.63. The plot is independent from the parity of the lattice size and $E_0^{oo}(2, 4)$ scales to 0 in the $L \to \infty$ limit as shown in Fig.3.64. So this is still a critical point as we expected.

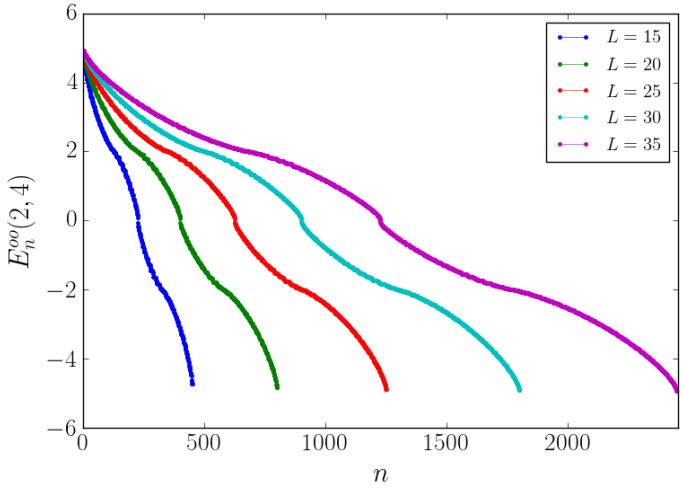

Figure 3.62: Plot of $E_n^{oo}(\alpha, \mu) = E_n^{oo}(2, 4)$, [31]

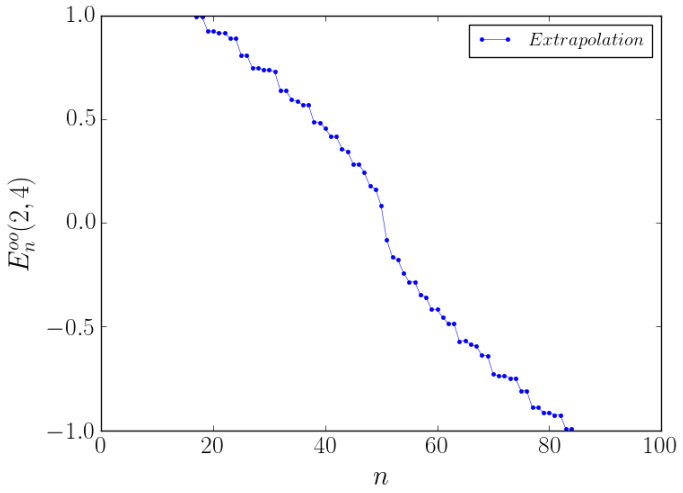

Figure 3.63: Extrapolation of the lower $E_n^{oo}(\alpha, \mu) = E_n^{oo}(2, 4)$, [31]

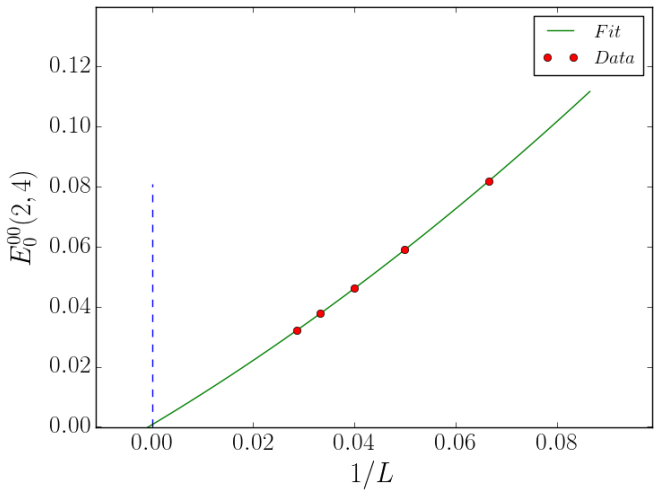

Figure 3.64: Fit of $E_0^{pp}(\alpha,\mu) = E_0^{pp}(2,4)$, [31]

• $\mu = 5$

The last case is a trivial gapped phase as we can see from the spectrum in Fig.3.50. Thus we finished the analysis for $\alpha = 2$ and as we saw the system loses a critical point but the edge-states linked to the topological phase at $0 < \mu < 2$, now massive, seem to be supported by the model.

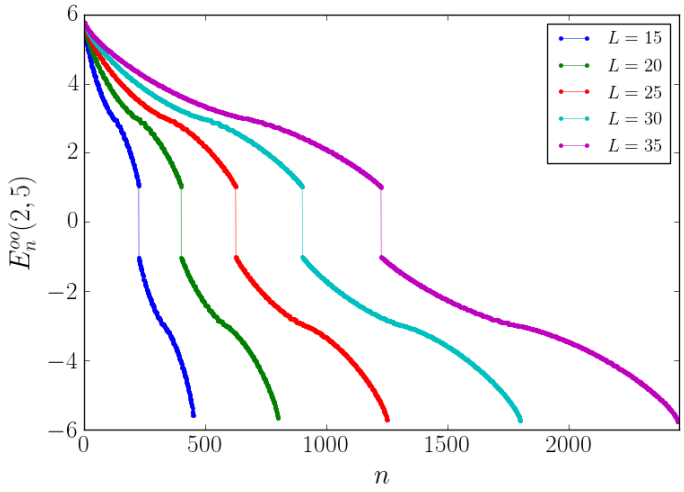

Figure 3.65: Plot of $E_n^{oo}(\alpha,\mu) = E_n^{oo}(2,5)$, [31]

Conclusions

We analysed the model analitically and gained knowledge on the behaviour of both the kinetic and pairing terms of the spectrum varying α and β. Then we simulated the spectrum with DMRG fixing the hopping decay at $\beta \to \infty$ to reproduce the SR kinetic term $\epsilon(\boldsymbol{p})$ while we varied the interaction decay α. We found that LR effects start to influence the system already in the $\alpha = 3$ case but they do not alter the SR phase diagram. On the contrary when we reach the critical exponent $\alpha = 2$ novel phenomena appear. It seems that a topological-like phase is present for $\mu = 1$ even without a real transition in $\mu = 0$ and this could be linked to cross-over phenomena. In fact in the $\mu = 1$ phase we see a set of gapped states partially filling the band. These could be massive edge-states. So it would be interesting to really undestand if these are edge-states, and if they are, to comprehend their nature. In particular we are interested to know if these exitations are Majorana-like states. Also it would be interesting to calulate the Chern number, to understand what happens to it in such a cross-over region. Right after the next step could be the study of this $\mu = 0$ "phase-transition". Then would follow the DMRG analysis of the spectrum for open-periodic and periodic-open conditions as in principle we could have different results. The next step would be the analysis of the model in the other possible configurations of α and β with the aid of the analytical formulas to have a hint of when new phenomena could occur. Then finally we would simulate the spectrum for these new cases and if new phenomena seem to appear we could begin a new analysis.

Appendix A

Bogoliubov de Gennes Formalism

Here we will describe the mean-field formulation of the quasiparticle physics for a conventional s-wave Bardeen-Cooper-Schrieffer (BCS) superconductor [17, 32]. We start with a simple metal with spin-degeneracy given by the many-body system, second quantized Hamiltonian:

$$H_\epsilon = \sum_{\boldsymbol{p},\sigma} c^\dagger_{\boldsymbol{p}\sigma}(\frac{p^2}{2m} - \mu)c_{\boldsymbol{p}\sigma} \equiv \sum_{\boldsymbol{p},\sigma} c^\dagger_{\boldsymbol{p}\sigma}\epsilon(\boldsymbol{p})c_{\boldsymbol{p}\sigma} \tag{A.1}$$

where $c^\dagger_{\boldsymbol{p}\sigma}$, creates a quasiparticle with momentum p and spin σ. The ground state is obtained simply by filling in all the levels below the Fermy energy:

$$|\Omega\rangle = \prod_{\boldsymbol{p}:\epsilon(p)<0} \prod_{\sigma} c^\dagger_{\boldsymbol{p}\sigma} \tag{A.2}$$

We can rewrite the Hamiltonian as:

$$\begin{aligned} &\frac{1}{2}\sum_{\boldsymbol{p},\sigma}(c^\dagger_{\boldsymbol{p}\sigma}\epsilon(\boldsymbol{p})c_{\boldsymbol{p}\sigma} - c_{\boldsymbol{p}\sigma}\epsilon(\boldsymbol{p})c^\dagger_{\boldsymbol{p}\sigma}) + \frac{1}{2}\sum_{\boldsymbol{p}}\epsilon(\boldsymbol{p}) = \\ &\frac{1}{2}\sum_{\boldsymbol{p},\sigma}(c^\dagger_{\boldsymbol{p}\sigma}\epsilon(\boldsymbol{p})c_{\boldsymbol{p}\sigma} - c_{-\boldsymbol{p}\sigma}\epsilon(-\boldsymbol{p})c^\dagger_{-\boldsymbol{p}\sigma}) + \frac{1}{2}\sum_{\boldsymbol{p}}\epsilon(\boldsymbol{p}) \end{aligned} \tag{A.3}$$

where we used $\{c^\dagger_{\boldsymbol{p}\sigma}, c_{\boldsymbol{p}'\sigma'}\} = \delta_{\boldsymbol{p}\boldsymbol{p}'}\delta_{\sigma\sigma'}$ and relabeled the sum index p in the second term to $-p$. Introducing the spinor $\Psi \equiv (c_{\boldsymbol{p}\uparrow}c_{\boldsymbol{p}\downarrow}c_{-\boldsymbol{p}\uparrow}c_{-\boldsymbol{p}\downarrow})^T$ we have a compact form for the Hamiltonian:

$$H_\epsilon = \sum_{\boldsymbol{p}} \Psi^\dagger_{\boldsymbol{p}} H_{\mathrm{BdG}}(\boldsymbol{p})\Psi_{\boldsymbol{p}} + const. \tag{A.4}$$

BdG stands for Bogoliubov-de-Gennes and after dropping the constant we have that:

$$H_{\mathrm{BdG}}(\boldsymbol{p}) = \frac{1}{2}\begin{pmatrix} \epsilon(\boldsymbol{p}) & 0 & 0 & 0 \\ 0 & \epsilon(\boldsymbol{p}) & 0 & 0 \\ 0 & 0 & -\epsilon(-\boldsymbol{p}) & 0 \\ 0 & 0 & 0 & -\epsilon(-\boldsymbol{p}) \end{pmatrix} \tag{A.5}$$

Note that the Bloch Hamiltonian $H_{\mathrm{BdG}}(\boldsymbol{p})$ is invariant under the particle-hole symmetry:

$$H_{\mathrm{BdG}}(\boldsymbol{p}) = -CH_{\mathrm{BdG}}(-\boldsymbol{p})^T C^{-1} \qquad C = \tau^x \otimes I_{2x2} \qquad \tau^x = \begin{pmatrix} 0 & 1 \\ 1 & 0 \end{pmatrix} \tag{A.6}$$

Here τ^x is a Pauli matrix in the particle-hole degrees of freedom. In fact we introduced a redundancy into our description of this noninteracting metal doubling the degrees of freedom. Instead of having one band and two spins the H_{BdG} has two bands and four spins. So we now have four energy eigenvalues, namely two copies of $\epsilon(\boldsymbol{p})$ and two of $\epsilon(-\boldsymbol{p})$. Note that only two out of the four bands give independent quasiparticle states. This formalism represents the easiest way to solve the quasiparticle bands of a mean-field superconductor. Now we add the conventional s-wave, singlet pairing potential of the form:

$$\begin{gathered} H_\Delta = \Delta c^\dagger_{\boldsymbol{p}\uparrow} c^\dagger_{-\boldsymbol{p}\downarrow} + \Delta^* c_{-\boldsymbol{p}\downarrow} c_{\boldsymbol{p}\uparrow} = \\ \frac{1}{2}[\Delta(c^\dagger_{\boldsymbol{p}\uparrow} c_{-\boldsymbol{p}\downarrow} - c^\dagger_{-\boldsymbol{p}\downarrow} c^\dagger_{\boldsymbol{p}\uparrow}) + \Delta^*(c_{-\boldsymbol{p}\downarrow} c_{\boldsymbol{p}\uparrow} - c_{\boldsymbol{p}\uparrow} c_{-\boldsymbol{p}\downarrow})] \end{gathered} \tag{A.7}$$

where Δ is a complex number representing the superconducting order parameter. This terms, at the mean-field level leads to a nonconservation of charge, i.e., charge is conserved only modulo 2e. This terms capture the physics of either two electrons combining to form a Cooper pair or holes breaking it apart into its constituents. The total Hamiltonian is then:

$$H = H_\epsilon + H_\Delta = \sum_{\boldsymbol{p}} \Psi^\dagger_{\boldsymbol{p}} H_{\mathrm{BdG}}(\boldsymbol{p}, \Delta) \Psi_{\boldsymbol{p}} \tag{A.8}$$

where:

$$H_{\mathrm{BdG}}(\boldsymbol{p}, \Delta) = \frac{1}{2} \begin{pmatrix} \epsilon(\boldsymbol{p}) & 0 & 0 & \Delta \\ 0 & \epsilon(\boldsymbol{p}) & -\Delta & 0 \\ 0 & -\Delta^* & -\epsilon(-\boldsymbol{p}) & 0 \\ \Delta^* & 0 & 0 & -\epsilon(-\boldsymbol{p}) \end{pmatrix} \tag{A.9}$$

We can finally rewrite H_{BdG} in the Bloch form:

$$H_{\mathrm{BdG}}(\boldsymbol{p}, \Delta) = \epsilon(\boldsymbol{p}) \tau^z \otimes I_{2x2} - (Re\Delta)\ \tau^y \otimes \sigma^y - (Im\Delta)\ \tau^x \otimes \sigma^x \tag{A.10}$$

Here $\tau^\alpha,\ \sigma^\alpha$ with $\alpha = x, y, z$ are respectively: particle-hole and spin degrees of freedom. Being the Hamiltonian formed of mutually anticommuting matrices we can easily get the spectrum because: $H^2_{\mathrm{BdG}}(\boldsymbol{p}, \Delta) = (\epsilon(\boldsymbol{p})^2 + |\Delta|^2) I_{4x4}$ So the spectrum is:

$$E_\pm = \pm\sqrt{\epsilon(\boldsymbol{p})^2 + |\Delta|^2} \tag{A.11}$$

The spectrum has an energy gap whenever $|\Delta| \neq 0$ as shown in figure A.1.

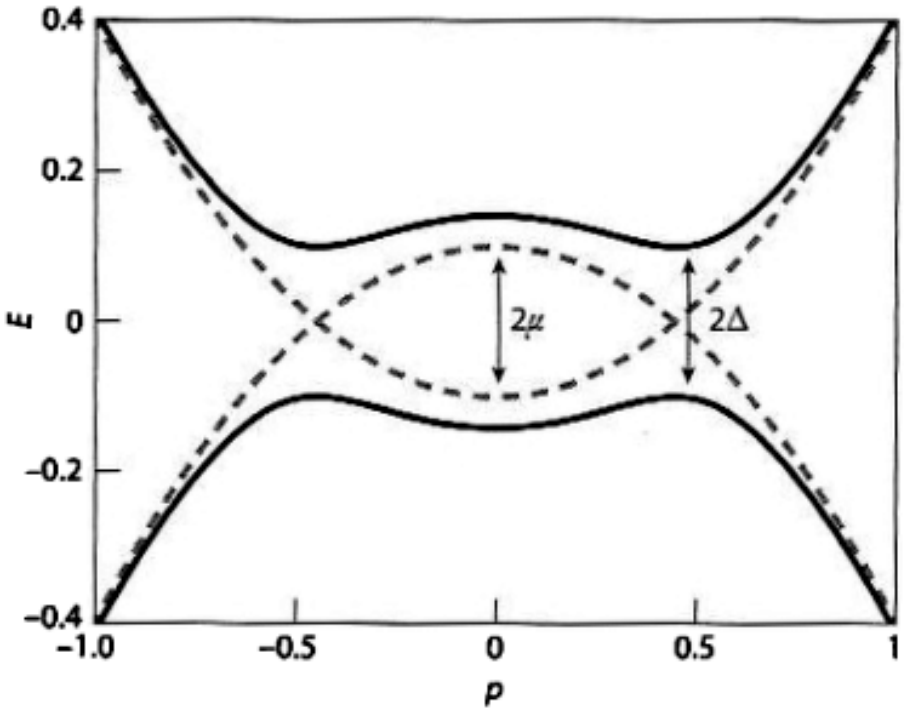

Figure A.1: Plot of the dispersion relation for an s-wave superconductor, taken from [17]

Appendix B

1D Lattice Fourier Transform and Bogoliubov Transformation

Let us start from the Hamiltonian (2.14):

$$H_{1D} = \sum_{j=1}^{N} \Big(-t(c_j^\dagger c_{j+1} + c_{j+1}^\dagger c_j) - \mu c_j^\dagger c_j + \Delta^* c_j c_{j+1} + \Delta c_{j+1}^\dagger c_j^\dagger \Big)$$

We consider a homogeneus real $\Delta = \Delta^*$ and assume the translational invariance of the system. After imposing some boundary conditions (PBC or APC) we can change $c_j^\dagger$, c_j with Fourier transformed fermion operators:

$$c_p = \frac{1}{\sqrt{N}} \sum_{j=1}^{N} e^{ipj} c_j \qquad c_p^\dagger = \frac{1}{\sqrt{N}} \sum_{j=1}^{N} e^{-ipj} c_j^\dagger \tag{B.1}$$

These are unitary transformations, thus invertible:

$$c_j = \frac{1}{\sqrt{N}} \sum_{p \in \text{B.Z.}} e^{-ipj} c_p \qquad c_j^\dagger = \frac{1}{\sqrt{N}} \sum_{p \in \text{B.Z.}} e^{ipj} c_p^\dagger \tag{B.2}$$

Here, the quasi-momenta p takes discrete values from the Brillouin zone. We can now evaluate the terms of the Hamiltonian:

$$\sum_j c_j^\dagger c_j = \sum_j \frac{1}{N} \sum_{pq} e^{ipj} e^{-iqj} c_p^\dagger c_q = \sum_p c_p^\dagger c_p \tag{B.3}$$

$$\sum_j (c_j^\dagger c_{j+1} + c_{j+1}^\dagger c_j) = \sum_j \frac{1}{N} \sum_{pq} e^{ipj} e^{-iq(j+1)} c_p^\dagger c_q + \text{h.c.} = \sum_p 2\cos(p) c_p^\dagger c_p \tag{B.4}$$

$$\sum_j c_j c_{j+1} = \sum_j \frac{1}{N} \sum_{pq} e^{-ipj} e^{-iq(j+1)} c_p c_q = \sum_p e^{-ip} c_{-p} c_p$$
$$\sum_j c_{j+1}^\dagger c_j^\dagger = \sum_j \frac{1}{N} \sum_{pq} e^{ip(j+1)} e^{iqj} c_p^\dagger c_q^\dagger = \sum_p e^{ip} c_p^\dagger c_{-p}^\dagger \tag{B.5}$$

Now we introduce new fermion operators which are a combination of the $q, -q$ components of (B.3) and (B.5) obtaining:

$$\sum_p c_p^\dagger c_p = \frac{1}{2} \sum_p (c_p^\dagger c_p - c_{-p} c_{-p}^\dagger) + \text{const.} \tag{B.6}$$

$$\sum_p 2\cos(p) c_p^\dagger c_p = \sum_p \cos(p)(c_p^\dagger c_p - c_{-p} c_{-p}^\dagger) + \text{const.} \tag{B.7}$$

$$\sum_j c_j c_{j+1} = \frac{1}{2} \sum_p (-e^{-ip} c_p c_{-p} + e^{ip} c_p c_{-p}) = \sum_p i \sin(p) c_p c_{-p}$$
$$\sum_j c_{j+1}^\dagger c_j^\dagger = \frac{1}{2} \sum_p (e^{ip} c_p^\dagger c_{-p}^\dagger - e^{-ip} c_p^\dagger c_{-p}^\dagger) = \sum_p i \sin(p) c_p^\dagger c_{-p}^\dagger \tag{B.8}$$

This is useful to write the Hamiltonian in the BdG formalism and then to diagonalize it. After dropping the const. terms the Hamiltonian is now:

$$H_{1D} = \frac{1}{2} \sum_p [(-2t\cos(p) - \mu)(c_p^\dagger c_p - c_{-p} c_{-p}^\dagger) + 2i\Delta \sin(p)(c_p c_{-p} + c_p^\dagger c_{-p}^\dagger) \tag{B.9}$$

that can be rewritten as:

$$H_{1D} = \frac{1}{2} \sum_p \begin{pmatrix} c_p^\dagger & c_{-p} \end{pmatrix} \begin{pmatrix} -2t\cos p - \mu & 2i\Delta \sin p \\ -2i\Delta \sin p & 2t\cos p + \mu \end{pmatrix} \begin{pmatrix} c_p \\ c_{-p}^\dagger \end{pmatrix} \tag{B.10}$$

The energy spectrumfor is $E_p = \sqrt{(-2t\cos p - \mu)^2 + (2|\Delta| \sin p)^2}$. This Hamiltonian can be diagonalized by means of a Bogoliubov transformation:

$$\begin{pmatrix} c_p \\ c_{-p}^\dagger \end{pmatrix} = U^\dagger \begin{pmatrix} \eta_p \\ \eta_{-p}^\dagger \end{pmatrix} \tag{B.11}$$

Where U is a unitary matrix:

$$U = \begin{pmatrix} \cos(\theta) & i\sin(\theta) \\ i\sin(\theta) & \cos(\theta) \end{pmatrix} \tag{B.12}$$

After this transformation the Hamiltonian is now:

$$H_{1D} = \frac{1}{2} \sum_p \{(-2t\cos(p) - \mu)[\cos(2\theta)(\eta_p^\dagger \eta_p - \eta_{-p} \eta_{-p}^\dagger) + i\sin(2\theta)(\eta_p \eta_{-p} + \eta_p^\dagger \eta_{-p}^\dagger)] +$$
$$+ 2i\Delta \sin(p)[\cos(2\theta)(\eta_p \eta_{-p} + \eta_p^\dagger \eta_{-p}^\dagger) + i\sin(2\theta)(\eta_p^\dagger \eta_p - \eta_{-p} \eta_p^\dagger)]\} \tag{B.13}$$

Then θ is given by the relation:

$$\tan(2\theta) = \frac{-2|\Delta|\sin(p)}{2t\cos(p) + \mu} \tag{B.14}$$

or equivalently by $\sin(2\theta) = \frac{-2|\Delta|\sin(p)}{E}$, $\cos(2\theta) = \frac{2t\cos(p)+\mu}{E}$ and finally H_{1D} in this basis becomes:

$$\sum_p E_p(\eta_p^\dagger \eta_p - \frac{1}{2}) \tag{B.15}$$

Appendix C

2D Long Range Models

C.1 Lattice Fourier Transform

Let us start from the Hamiltonian (3.13):

$$H = \sum_{\substack{m,n \\ r,s}}{}' \Big(-\frac{t}{d^\beta} c^\dagger_{m+r,n+s} c_{m,n} + \frac{\tilde{\Delta}(r,s)}{d^\alpha} c^\dagger_{m+r,n+s} c^\dagger_{m,n} + \text{h.c.} \Big) - (\mu - 4t) \sum_{m,n} c^\dagger_{m,n} c_{m,n}$$

After assuming the translational invariance of the system and imposing some boundary conditions (PBC for example) in both directions we can change $c^\dagger_{m,n}$, $c_{m,n}$ with Fourier transformed fermion operators:

$$c_{\boldsymbol{p}} = \frac{1}{\sqrt{N}} \sum_{\boldsymbol{l}} e^{i\boldsymbol{p}\cdot\boldsymbol{l}} c_{\boldsymbol{l}} \qquad c^\dagger_{\boldsymbol{p}} = \frac{1}{\sqrt{N}} \sum_{\boldsymbol{l}} e^{-i\boldsymbol{p}\cdot\boldsymbol{l}} c^\dagger_{\boldsymbol{l}} \qquad \boldsymbol{l} = (m,n) \qquad \boldsymbol{p} = (p_x, p_y) \tag{C.1}$$

These are unitary transformations, thus invertible:

$$c_{\boldsymbol{l}} = \frac{1}{\sqrt{N}} \sum_{\boldsymbol{p}} e^{-i\boldsymbol{p}\cdot\boldsymbol{l}} c_{\boldsymbol{p}} \qquad c^\dagger_{\boldsymbol{l}} = \frac{1}{\sqrt{N}} \sum_{\boldsymbol{p}} e^{i\boldsymbol{p}\cdot\boldsymbol{l}} c^\dagger_{\boldsymbol{p}} \tag{C.2}$$

Here, the quasi-momenta are taken to be:

$$\boldsymbol{p} = (\frac{2\pi}{L_x} i, \frac{2\pi}{L_y} j) \qquad i = 1, \dots, L_x \quad i \in \mathbb{N} \quad j = 1, \dots, L_y \quad i \in \mathbb{N}$$

Here L_x, L_y are the lattice lenghts along the x and y axes.

We can now evaluate the terms of the Hamiltonian:

- the first term is

$$-\sum_{\boldsymbol{l}}\sum_{\boldsymbol{d}}{}' \frac{t}{d^\beta}\Big(c^\dagger_{\boldsymbol{l}+\boldsymbol{d}}c_{\boldsymbol{l}} + \text{h.c.}\Big) = \tag{C.3}$$

$$-\sum_{\boldsymbol{p},\boldsymbol{q}}\sum_{\boldsymbol{d}}{}'\sum_{\boldsymbol{l}} \frac{t}{d^\beta}\frac{1}{N^2}\Big(e^{i(\boldsymbol{p}-\boldsymbol{q})\cdot\boldsymbol{l}}e^{i\boldsymbol{p}\boldsymbol{d}}c^\dagger_{\boldsymbol{p}}c_{\boldsymbol{q}} + \text{h.c.}\Big) = \tag{C.4}$$

$$-\sum_{\boldsymbol{p}}\sum_{\boldsymbol{d}}{}' \frac{t}{d^\beta}\Big(e^{i\boldsymbol{p}\boldsymbol{d}}c^\dagger_{\boldsymbol{p}}c_{\boldsymbol{p}} + \text{h.c.}\Big) = \tag{C.5}$$

$$-\sum_{\boldsymbol{p}}\sum_{\boldsymbol{d}}{}' \frac{t}{d^\beta}\Big(2\cos(\boldsymbol{p}\cdot\boldsymbol{d})c^\dagger_{\boldsymbol{p}}c_{\boldsymbol{p}}\Big) \tag{C.6}$$

- the second term is

$$\sum_{\boldsymbol{l}}\sum_{\boldsymbol{d}}{}' \Big(\frac{\tilde{\Delta}(r,s)}{d^\alpha}c^\dagger_{\boldsymbol{l}+\boldsymbol{d}}c^\dagger_{\boldsymbol{l}} + \text{h.c.}\Big) = \tag{C.7}$$

$$\sum_{\boldsymbol{p},\boldsymbol{q}}\sum_{\boldsymbol{d}}{}'\sum_{\boldsymbol{l}} \Big(\frac{\tilde{\Delta}(r,s)}{d^\alpha}\frac{1}{N^2}e^{i(\boldsymbol{p}-\boldsymbol{q})\cdot\boldsymbol{l}}e^{i\boldsymbol{p}\boldsymbol{d}}c^\dagger_{\boldsymbol{p}}c^\dagger_{\boldsymbol{q}} + \text{h.c.}\Big) = \tag{C.8}$$

$$\sum_{\boldsymbol{p}}\sum_{\boldsymbol{d}}{}' \Big(\frac{\tilde{\Delta}(r,s)}{d^\alpha}e^{i\boldsymbol{p}\boldsymbol{d}}c^\dagger_{\boldsymbol{p}}c^\dagger_{-\boldsymbol{p}} + \text{h.c.}\Big) \tag{C.9}$$

- the third term is

$$-(\mu-4t)\sum_{\boldsymbol{l}} c^\dagger_{\boldsymbol{l}}c_{\boldsymbol{l}} = -(\mu-4t)\sum_{\boldsymbol{p}} c^\dagger_{\boldsymbol{p}}c_{\boldsymbol{p}} \tag{C.10}$$

Now we introduce new operators depending both on $\boldsymbol{p}$,$-\boldsymbol{p}$ in (C.6), (C.9) and (C.10) obtaining:

- for the first term

$$\begin{aligned} &-\sum_{\boldsymbol{p}}\sum_{\boldsymbol{d}}{}' \frac{t}{d^\beta}\Big(2\cos(\boldsymbol{p}\cdot\boldsymbol{d})c^\dagger_{\boldsymbol{p}}c_{\boldsymbol{p}}\Big) = \\ &-\sum_{\boldsymbol{p}}\sum_{\boldsymbol{d}}{}' \frac{t}{d^\beta}\Big(\cos(\boldsymbol{p}\cdot\boldsymbol{d})(c^\dagger_{\boldsymbol{p}}c_{\boldsymbol{p}} - c_{-\boldsymbol{p}}c^\dagger_{-\boldsymbol{p}}\Big) + \text{const.} \end{aligned} \tag{C.11}$$

- for the second term

$$\sum_{\boldsymbol{p}}\sum_{\boldsymbol{d}}{}' \Big(\frac{\tilde{\Delta}(r,s)}{d^\alpha} e^{i\boldsymbol{pd}} c^\dagger_{\boldsymbol{p}} c^\dagger_{-\boldsymbol{p}} + \text{h.c.}\Big) = \tag{C.12}$$

$$\sum_{\boldsymbol{p}}\sum_{\boldsymbol{d}}{}' \Big(\frac{\tilde{\Delta}(r,s)}{d^\alpha} e^{i\boldsymbol{pd}} c^\dagger_{\boldsymbol{p}} c^\dagger_{-\boldsymbol{p}} + \frac{\tilde{\Delta}^*(r,s)}{d^\alpha} e^{-i\boldsymbol{pd}} c_{-\boldsymbol{p}} c_{\boldsymbol{p}}\Big) = \tag{C.13}$$

$$\sum_{\boldsymbol{p}}\sum_{\boldsymbol{d}}{}' \Big(\frac{\tilde{\Delta}(r,s)}{2d^\alpha}(e^{i\boldsymbol{pd}} - e^{-i\boldsymbol{pd}}) c^\dagger_{\boldsymbol{p}} c^\dagger_{-\boldsymbol{p}} - \frac{\tilde{\Delta}^*(r,s)}{2d^\alpha}(-e^{-i\boldsymbol{pd}} + e^{i\boldsymbol{pd}}) c_{-\boldsymbol{p}} c_{\boldsymbol{p}}\Big) = \tag{C.14}$$

$$\sum_{\boldsymbol{p}}\sum_{\boldsymbol{d}}{}' i\sin(\boldsymbol{p}\cdot\boldsymbol{d})\Big(\frac{\tilde{\Delta}(r,s)}{d^\alpha} c^\dagger_{\boldsymbol{p}} c^\dagger_{-\boldsymbol{p}} - \frac{\tilde{\Delta}^*(r,s)}{d^\alpha} c_{-\boldsymbol{p}} c_{\boldsymbol{p}}\Big) \tag{C.15}$$

- for the third term

$$-(\mu - 4t)\sum_{\boldsymbol{p}} c^\dagger_{\boldsymbol{p}} c_{\boldsymbol{p}} = -(\mu-4t)\frac{1}{2}\sum_{\boldsymbol{p}}(c^\dagger_{\boldsymbol{p}} c_{\boldsymbol{p}} - c_{-\boldsymbol{p}} c^\dagger_{-\boldsymbol{p}}) + \text{const.} \tag{C.16}$$

After dropping the const. terms the Hamiltonian can be rewritten as:

$$\begin{aligned} H = \frac{1}{2}\sum_{\boldsymbol{p}}\sum_{\boldsymbol{d}}{}' \Big(-\frac{2t}{d^\beta}\cos(\boldsymbol{p}\cdot\boldsymbol{d}) - (\mu-4t)\Big)\Big(c^\dagger_{\boldsymbol{p}} c_{\boldsymbol{p}} - c_{-\boldsymbol{p}} c^\dagger_{-\boldsymbol{p}}\Big) + \\ \frac{1}{2}\sum_{\boldsymbol{p}}\sum_{\boldsymbol{d}}{}' 2i\sin(\boldsymbol{p}\cdot\boldsymbol{d})\Big(\frac{\tilde{\Delta}(r,s)}{d^\alpha} c^\dagger_{\boldsymbol{p}} c^\dagger_{-\boldsymbol{p}} - \frac{\tilde{\Delta}^*(r,s)}{d^\alpha} c_{-\boldsymbol{p}} c_{\boldsymbol{p}}\Big) \end{aligned} \tag{C.17}$$

that in the BdG form is equal to:

$$H_{BdG} = \begin{pmatrix} -\sum_{\boldsymbol{d}}{}' \frac{2t}{d^\beta}\cos(\boldsymbol{p}\cdot\boldsymbol{d}) - (\mu-4t) & \sum_{\boldsymbol{d}}{}' 2i\sin(\boldsymbol{p}\cdot\boldsymbol{d})\frac{\Delta(r+is)}{d^{\alpha+1}} \\ -\sum_{\boldsymbol{d}}{}' 2i\sin(\boldsymbol{p}\cdot\boldsymbol{d})\frac{\Delta(r-is)}{d^{\alpha+1}} & \sum_{\boldsymbol{d}}{}' \frac{2t}{d^\beta}\cos(\boldsymbol{p}\cdot\boldsymbol{d}) + (\mu-4t) \end{pmatrix} \tag{C.18}$$

This can also be rewritten in the Bloch form:

$$H_{BdG} = \epsilon_\beta(\boldsymbol{p})\tau^z - 2\Delta f_\alpha(\boldsymbol{p})\tau^y - 2\Delta g_\alpha(\boldsymbol{p})\tau^x \tag{C.19}$$

$$\epsilon_\beta(\boldsymbol{p}) = -\sum_{\boldsymbol{d}}{}' \frac{2t}{d^\beta}\cos(\boldsymbol{p}\cdot\boldsymbol{d}) + (\mu-4t) \tag{C.20}$$

$$f_\alpha(\boldsymbol{p}) = \sum_{\boldsymbol{d}}{}' \sin(\boldsymbol{p}\cdot\boldsymbol{d})\frac{r}{d^{\alpha+1}} \tag{C.21}$$

$$g_\alpha(\boldsymbol{p}) = \sum_{\boldsymbol{d}}{}' \sin(\boldsymbol{p}\cdot\boldsymbol{d})\frac{s}{d^{\alpha+1}} \tag{C.22}$$

From the anticommutation properties of the τ matrices we find that the energy spectrum is given by:

$$E = \pm\sqrt{\epsilon_\beta(\boldsymbol{p})^2 + 4\Delta^2(f_\alpha(\boldsymbol{p})^2 + g_\alpha(\boldsymbol{p})^2)} \tag{C.23}$$

C.2 Study of $f_\alpha(\boldsymbol{p})$

We are now going to study the convergence properties of $f_\alpha(\boldsymbol{p})$, starting from its definition:

$$f_\alpha(\boldsymbol{p}) = {\sum_{\boldsymbol{d}}}' \sin(\boldsymbol{p}\cdot\boldsymbol{d})\frac{r}{d^{\alpha+1}}$$

where we set $\Delta = 1/2$ and the apostrophe stands for $\boldsymbol{d} \neq \boldsymbol{0}$. We will start from a general series studied by Born and Bradburn [33] which can be written as:

$$S_n^{\boldsymbol{x}}(\boldsymbol{p}) = \sum_{\boldsymbol{d}\neq 0} \frac{d_1^{x_1} d_2^{x_2} d_3^{x_3}}{d^n} \exp(-i\boldsymbol{d}\cdot\boldsymbol{x}) = i^{x_1+x_2+x_3}\frac{\partial^{x_1+x_2+x_3}}{\partial_{p_1}^{x_1}\partial_{p_2}^{x_2}\partial_{p_3}^{x_3}} S_n^{\boldsymbol{0}}(\boldsymbol{p}) \tag{C.24}$$

In this formalism our series can be written as:

$$f_\alpha(\boldsymbol{p}) = -\frac{\partial}{\partial p_x} f_\alpha^{\boldsymbol{0}}(\boldsymbol{p}) = -\frac{\partial}{\partial p_x}{\sum_{\boldsymbol{d}}}' \cos(\boldsymbol{p}\cdot\boldsymbol{d})\frac{1}{d^{\alpha+1}} \tag{C.25}$$

The modulus of the series $f_\alpha^{\boldsymbol{0}}(\boldsymbol{p})$ is bounded by:

$$|f_\alpha^{\boldsymbol{0}}(\boldsymbol{p})| \leq |{\sum_{\boldsymbol{d}}}' d^{-(\alpha+1)}|$$

that is a known series [34, 35] that converges absolutely for $\alpha > 1$ which is the case we are going to analyse. Using a Mellin transform [28] of the kind:

$$M[f^{-n}]\Gamma(s) = \int_0^\infty x^{n-1}\exp(-fx)\ \mathrm{d}x$$

where $\Gamma(s)$ is the Euler Gamma function, we can rewrite $f_\alpha^{\boldsymbol{0}}(\boldsymbol{p})$ as:

$$f_\alpha^{\boldsymbol{0}}(\boldsymbol{p}) = -\frac{1}{\Gamma((\alpha+1)/2)}\int_0^\infty x^{(\alpha+1)/2-1}{\sum_{\boldsymbol{d}}}' \cos(\boldsymbol{p}\cdot\boldsymbol{d})\exp(-d^2x)\ \mathrm{d}x \tag{C.26}$$

This will be the starting equation we aim to simplify.

C.2.1 Integral Form of $f_\alpha^{\mathbf{0}}(\boldsymbol{p})$

First we are going to split the (C.26) integral part in two $\int_0^1 + \int_1^\infty$ as the first part could either contain divergencies or be undefined:

$$\begin{aligned} f_\alpha^{\mathbf{0}}(\boldsymbol{p}) &= f_0 + f_1 \\ f_0 &= -\frac{1}{\Gamma((\alpha+1)/2)} \int_0^1 x^{(\alpha-1)/2} {\sum_{\boldsymbol{d}}}' \cos(\boldsymbol{p}\cdot\boldsymbol{d}) \exp(-d^2 x)\ \mathrm{d}x \\ f_1 &= -\frac{1}{\Gamma((\alpha+1)/2)} \int_1^\infty x^{(\alpha-1)/2} {\sum_{\boldsymbol{d}}}' \cos(\boldsymbol{p}\cdot\boldsymbol{d}) \exp(-d^2 x)\ \mathrm{d}x \end{aligned} \tag{C.27}$$

The f_1 term can be rewritten as:

$$\begin{aligned} f_1 = -\frac{1}{\Gamma((\alpha+1)/2)} \int_1^\infty x^{(\alpha-1)/2} {\sum_{\boldsymbol{d}}}' \cos(\boldsymbol{p}\cdot\boldsymbol{d}) \exp(-d^2 x)\ \mathrm{d}x = \\ -\frac{1}{\Gamma((\alpha+1)/2)} {\sum_{\boldsymbol{d}}}' \cos(\boldsymbol{p}\cdot\boldsymbol{d}) \int_1^\infty x^{(\alpha-1)/2} \exp(-d^2 x)\ \mathrm{d}x = \\ -\frac{1}{\Gamma((\alpha+1)/2)} {\sum_{\boldsymbol{d}}}' \cos(\boldsymbol{p}\cdot\boldsymbol{d})\ \Gamma((\alpha+1)/2, d^2) d^{-(\alpha+1)} = \\ -\frac{1}{\Gamma((\alpha+1)/2)} {\sum_{\boldsymbol{d}}}' \cos(\boldsymbol{p}\cdot\boldsymbol{d})\ \varphi_{(\alpha+1)/2}(d^2) = \\ \Re e\Big\{ -\frac{2}{\Gamma((\alpha+1)/2)} \sum_{\boldsymbol{d}>\mathbf{0}} \cos(\boldsymbol{p}\cdot\boldsymbol{d})\ \varphi_{(\alpha+1)/2}(d^2) \Big\} \end{aligned} \tag{C.28}$$

where $\Gamma((\alpha+1)/2, d^2)$ is the Incomplete Gamma function [28] defined as:

$$\Gamma(n, \tilde{x}) = \int_{\tilde{x}}^\infty x^{n-1} e^{-x} \mathrm{d}x$$

while $\varphi_{(\alpha+1)/2}(d^2)$ is a function introduced in [29]:

$$\varphi_n(x) = \int_1^\infty y^n \exp(-xy)\ \mathrm{d}y$$

which satisfies the following recurrence relation [36]:

$$\varphi_n(x) = \varphi_0(x) + \left(\frac{n}{x}\right) \varphi_{n-1}(x) \tag{C.29}$$

As shown in [36, 37] the infinite series f_1 is a rapidly convergent series. It encodes in fact the "short" range interactions. We can now move on to the f_0 term:

$$f_0 = -\frac{1}{\Gamma((\alpha+1)/2)} \int_0^1 x^{(\alpha-1)/2} {\sum_{\boldsymbol{d}}}' \cos(\boldsymbol{p}\cdot\boldsymbol{d}) \exp(-d^2 x)\ \mathrm{d}x =$$

$$\Re e\Big\{ -\frac{1}{\Gamma((\alpha+1)/2)} \int_0^1 x^{(\alpha-1)/2} [\sum_{\boldsymbol{d}} \exp(i\boldsymbol{p}\cdot\boldsymbol{d}) \exp(-d^2 x) - 1]\ \mathrm{d}x \Big\}$$

$$\Re e\Big\{ -\frac{1}{\Gamma((\alpha+1)/2)} \int_0^1 x^{(\alpha-1)/2} [\prod_{j=1}^{2} \Theta_3(p_j/2, e^{-x}) - 1]\ \mathrm{d}x \Big\} = \tag{C.30}$$

$$\Re e\Big\{ -\frac{1}{\Gamma((\alpha+1)/2)} \int_0^1 x^{(\alpha-1)/2} \prod_{j=1}^{2} \Theta_3(-p_j/2, e^{-x})\ \mathrm{d}x \Big\} +$$

$$+ \frac{1}{(\alpha+1)/2)\ \Gamma((\alpha+1)/2)}$$

Here $\Theta_3(-p_j/2, e^{-x})$ is the third Jacobi Theta Elliptic function [28] defined as:

$$\Theta_3(z,q) = \sum_n q^{n^2} e^{2niz}$$

and it will be useful for our calculation soon. Going back to (C.30) we see that it is the product of:

$$\Theta_3(p_x/2, e^{-x}) = \sum_r \exp(ip_x r) \exp(-r^2 x)$$

and

$$\Theta_3(p_y/2, e^{-x}) = \sum_s \exp(ip_y s) \exp(-s^2 x)$$

in fact:

$$\prod_{j=1}^{2} \Theta_3(p_j/2, e^{-x}) = \sum_{r,s} \exp\big(i(p_x r + p_y s)\big) \exp\big(-(r^2+s^2)\ x\big) \tag{C.31}$$

The last line term of (C.30) instead comes from:

$$\Re e\Big\{ \frac{1}{\Gamma((\alpha+1)/2)} \int_0^1 x^{(\alpha-1)/2}\ \mathrm{d}x \Big\} = \frac{1}{(\alpha+1)/2)\ \Gamma((\alpha+1)/2)}$$

We now use the Jacobi Imaginary Transformation of the third Theta Elliptic Function [35] defined as:

$$\Theta_3(z, e^{i\pi\tau}) = (-i\tau)^{-1/2} \exp(-iz^2/\pi\tau) \Theta(z/\tau, e^{-i\pi/\tau}) \tag{C.32}$$

where in our case $i\pi\tau = -x$ and $z = p_j/2$ so that (C.31) becomes:

$$\prod_{j=1}^{2}\Theta(p_j/2, e^{-x}) = \frac{\pi}{x}\prod_{j=1}^{2}\Theta(-i\pi p_j/2x, e^{-\pi^2/x})\exp(-p^2/4x) \tag{C.33}$$

Plugging this result in (C.30) we obtain:

$$\begin{aligned} f_0 - \frac{1}{(\alpha+1)/2)\ \Gamma((\alpha+1)/2)} = \\ \Re e\Big\{ -\frac{\pi}{\Gamma((\alpha+1)/2)}\int_0^1 x^{(\alpha-1)/2}\prod_{j=1}^{2}\Theta_3(-p_j/2, e^{-x})\ \mathrm{d}x\Big\} = \\ \Re e\Big\{ -\frac{\pi}{\Gamma((\alpha+1)/2)}\int_0^1 x^{(\alpha-1)/2-1}\sum_{\boldsymbol{d}}\exp\Big(-p^2/4x + (\pi/x)\ \boldsymbol{p}\cdot\boldsymbol{d} - \pi^2 d^2/x\Big)\ \mathrm{d}x\Big\} = \\ \Re e\Big\{ -\frac{\pi}{\Gamma((\alpha+1)/2)}\int_0^1 x^{(\alpha-3)/2}\sum_{\boldsymbol{d}}\exp\Big(-\frac{1}{x}(\boldsymbol{p}/2 - \pi\boldsymbol{d})^2\Big)\ \mathrm{d}x\Big\} \end{aligned} \tag{C.34}$$

We now have to change variables in order to obtain an integral from $1 \to \infty$ and this is done by sending $x \to \hat{x}^{-1}$ obtaining finally:

$$\begin{aligned} f_0 - \frac{1}{(\alpha+1)/2)\ \Gamma((\alpha+1)/2)} = \\ \Re e\Big\{ -\frac{\pi}{\Gamma((\alpha+1)/2)}\sum_{\boldsymbol{d}}\int_1^\infty \hat{x}^{(3-\alpha)/2-2}\exp\Big(-\hat{x}(\boldsymbol{p}/2 - \pi\boldsymbol{d})^2\Big)\ \mathrm{d}\hat{x}\Big\} \\ \Re e\Big\{ -\frac{\pi}{\Gamma((\alpha+1)/2)}\sum_{\boldsymbol{d}}(\boldsymbol{p}/2 - \pi\boldsymbol{d})^{2(\alpha-1)/2}\Gamma\Big((1-\alpha)/2, (\boldsymbol{p}/2 - \pi\boldsymbol{d})^2\Big)\Big\} = \\ \Re e\Big\{ -\frac{\pi}{\Gamma((\alpha+1)/2)}\sum_{\boldsymbol{d}}(\boldsymbol{p}/2 - \pi\boldsymbol{d})^{2(\frac{\alpha+1}{2}-1)}\Gamma\Big(1-(\alpha+1)/2, (\boldsymbol{p}/2 - \pi\boldsymbol{d})^2\Big)\Big\} = \\ \Re e\Big\{ -\frac{\pi}{\Gamma((\alpha+1)/2)}\sum_{\boldsymbol{d}}E_{(\alpha+1)/2}\big((\ \boldsymbol{p}/2 - \pi\boldsymbol{d})^2\big)\Big\} \end{aligned} \tag{C.35}$$

where $E_{(\alpha+1)/2}\big((\ \boldsymbol{p}/2 - \pi\boldsymbol{d})^2\big)$ is the Generalized Exponential Integral [28] defined as:

$$E_n(x) = x^{n-1}\Gamma(1-n, x)$$

Also this series, which encodes the "long range" interactions is rapidly convergent already in the $\alpha = 2$ case. We can see this by extracting the $\boldsymbol{d} = \boldsymbol{p} = \boldsymbol{0}$ exponential part which is the higher one:

$$E_{3/2}(0) = \frac{1}{3/2 - 1} = 2 \tag{C.36}$$

where we used the fact that $E_n(0) = \frac{1}{n-1}$ for $n > 1$. With this calculation that we will need in the next section, we have also implicitly studied $\epsilon_\beta(\boldsymbol{p})$ in fact we just need to set $\beta = \alpha + 1$ in the above description.

C.2.2 Convergence of $f_\alpha(\boldsymbol{p})$

Starting from the relation (C.25) we can now study the behaviour of $f_\alpha(\boldsymbol{p})$:

$$f_\alpha(\boldsymbol{p}) = \frac{\partial}{\partial p_x}(f_0 + f_1) \tag{C.37}$$

where:

$$\begin{aligned} \frac{\partial}{\partial p_x} f_0 = f_{0,p_x} &= \Re e\Big\{ \frac{\pi}{\Gamma((\alpha+1)/2)} \sum_{\boldsymbol{d}} (p_x/2 - \pi r) E_{(\alpha-1)/2}\big((\ \boldsymbol{p}/2 - \pi \boldsymbol{d})^2\big) \Big\} \\ \frac{\partial}{\partial p_x} f_1 = f_{1,p_x} &= \Re e\Big\{ \frac{2}{\Gamma((\alpha+1)/2)} \sum_{\boldsymbol{d}>\boldsymbol{0}} r \sin(\boldsymbol{p}\cdot\boldsymbol{d})\ \varphi_{(\alpha+1)/2}(d^2) \Big\} \end{aligned} \tag{C.38}$$

In the first line we used the relation:

$$\frac{\partial}{\partial x} E_n\big(f(x,y)\big) = -\Big(\frac{\partial}{\partial x} f(x,y)\Big)\ E_{n-1}\big(f(x,y)\big)$$

Also in this case the f_{1,p_x} component is absolutely convergent for $\alpha > 1$ and behaves in a smooth way for every $\boldsymbol{p}$. The f_{0,p_x} component instead in the limit $\boldsymbol{p} \to \boldsymbol{0}$ is not converging to 0 until $\alpha > 2$. In fact considering the $\boldsymbol{d} = \boldsymbol{0}$ term in the case $\alpha = 2$ (we have the same situation for $1 \le \alpha < 2$) we see that it is:

$$\propto p_x\ E_{(\alpha-1)/2}\Big(\frac{p_x^2 + p_y^2}{4}\Big) = p_x\ E_{1/2}\Big(\frac{p_x^2 + p_y^2}{4}\Big)$$

and:

$$\begin{aligned} \lim_{p_x \to 0^\pm} \lim_{p_y \to 0} p_x\ E_{1/2}\Big(\frac{p_x^2 + p_y^2}{4}\Big) &= \pm 2\sqrt{\pi} \\ \lim_{p_y \to 0} \lim_{p_x \to 0} p_x\ E_{1/2}\Big(\frac{p_x^2 + p_y^2}{4}\Big) &= 0 \end{aligned} \tag{C.39}$$

so the limit is undefined as it depends on the path. In the case $\alpha > 2 = 3$ e.g. (same situation for all the $\alpha > 2$) the $\boldsymbol{d} = \boldsymbol{0}$ term that is:

$$\propto p_x\ E_{(\alpha-1)/2}\Big(\frac{p_x^2 + p_y^2}{4}\Big) = p_x\ E_1\Big(\frac{p_x^2 + p_y^2}{4}\Big)$$

has now a well defined limit:

$$\lim_{(x,y)\to(0,0)} p_x\ E_{1/2}\Big(\frac{p_x^2 + p_y^2}{4}\Big) = 0 \tag{C.40}$$

So we can conclude that the series is absolutely convergent for $\alpha > 2$ and we recover all the short range critical lines.

C.3 Behaviour of $f_\alpha(\boldsymbol{p})$ for $\alpha < 2$ and $\boldsymbol{p} \to \mathbf{0}$

We will start from a general series studied by Barber [38] which reads:

$$S_\sigma(\boldsymbol{p}, \delta) = \sum_{\boldsymbol{d}>\mathbf{0}} d^{-\sigma} f(\boldsymbol{p}\cdot\boldsymbol{d}) \exp(-\delta d) \qquad \delta \geq 0 \; \boldsymbol{p} \geq 0 \tag{C.41}$$

This series converges uniformly for $\delta > 0$ and it can be differenciated term by term giving the relation:

$$\frac{\partial}{\partial \delta} \, S_\sigma(\boldsymbol{p}, \delta) = S_{\sigma-1}(\boldsymbol{p}, \delta) \tag{C.42}$$

Thus we can restrict the study of this series for $1 < \sigma < 2$ that is $0 < \alpha < 1$. We will start again from $f^{\mathbf{0}}_\alpha(\boldsymbol{p})$:

$$\begin{aligned} f^0_\alpha(\boldsymbol{p}, \delta) = {\sum_{\boldsymbol{d}}}' \frac{1}{d^{\alpha+1}} \cos(\boldsymbol{p}\cdot\boldsymbol{d}) \exp(-\delta d) = \\ 2 \sum_{\boldsymbol{d}>\mathbf{0}} \frac{1}{d^{\alpha+1}} \cos(\boldsymbol{p}\cdot\boldsymbol{d}) \exp(-\delta d) \end{aligned} \tag{C.43}$$

The idea now is to find a good approximation of (C.43) for $0 < \alpha < 1$ and then recover our original series in the $\delta \to 0$ limit. Then we will derive it and see that for $\alpha < 2$ the series is not convergent in $(0, 0)$. This can be done according to [34]. Let us define:

$$\gamma = \hat{\boldsymbol{p}} \cdot \hat{\boldsymbol{d}} \qquad \hat{\boldsymbol{p}} = \frac{\boldsymbol{p}}{|\boldsymbol{p}|} = \frac{\boldsymbol{p}}{p} \qquad \hat{\boldsymbol{d}} = \frac{\boldsymbol{d}}{|\boldsymbol{d}|} = \frac{\boldsymbol{d}}{d}$$

and introduce the Mellin transform:

$$M[\cos(\gamma p d) e^{-\delta d}] = \int_0^\infty x^{s-1} \cos(\gamma p x) e^{-\delta x} \, \mathrm{d}x = p^{-s} \; W(s; \delta/p, \gamma) \tag{C.44}$$

where:

$$W(s; \delta/p, \gamma) = p^{-s} \int_0^\infty y^{s-1} \cos(\gamma y) \exp\Big(-\frac{\delta}{p} y \Big) \mathrm{d}y \tag{C.45}$$

Inverting (C.44) and inserting it in (C.43) we obtain the integral representation:

$$f^0_\alpha(p, \delta) = \frac{1}{2\pi i} \int_{c-i\infty}^{c+i\infty} p^{-s} \Psi(s; \delta/p) dp \tag{C.46}$$

where:

$$\Psi(s; \delta/p) = 2 \sum_{\boldsymbol{d}>\mathbf{0}} d^{-s-(\alpha+1)} W(s; \delta/p, \gamma) \tag{C.47}$$

The contour in (C.46)is chosen to be

$$1 > c = \Re es > 2 - (\alpha + 1) \geq 0 \tag{C.48}$$

so that (C.44) and (C.47) converge. The asymptotic behaviour of $f^0_\alpha(\boldsymbol{p},\delta)$ for small p and $\delta/p = O(1)$ comes from the pole of (C.46) at $s = 2-(\alpha+1)$, when (C.47) diverges. Let us consider:

$$X_{\alpha+1}(\delta/p) = \lim_{s\to 2-(\alpha+1)^+}(s-2+(\alpha+1))\Psi(s;\delta/p) \tag{C.49}$$

where $X_{\alpha+1}(\delta/p)$ is called the cross-over function [38]. Apllying the Euler-Maclaurin expansion [28] to (C.43) leads us to write:

$$X_{\alpha+1}(\delta/p) = \lim_{s\to 2-(\alpha+1)^+} 2(s-2+(\alpha+1))\int_{d>d_0} \mathrm{d}^2 m\; m^{-s-(\alpha+1)} W(s;\delta/p,\gamma) \tag{C.50}$$

where $d_0 > 0$. The difference between the sum (C.47) and the integral (C.50) vanishes in this limit [38]. Introducing polar coordinates in the 2D space about the $\hat{\boldsymbol{p}}$ direction implies:

$$\begin{aligned} X_{\alpha+1}(\delta/p) = \\ \lim_{s\to 2-(\alpha+1)^+} K_{2D}\;(s-2+(\alpha+1)\;)\int_{d>d_0}\mathrm{d}m\; m^{1-s-(\alpha+1)}\int_0^1 \mathrm{d}\gamma(1-\gamma^2)^{-1/2}W(s;\delta/p,\gamma) = \\ = -K_2\int_0^1 \mathrm{d}\gamma(1-\gamma^2)^{-1/2}W(2-(\alpha+1);\delta/p,\gamma) \end{aligned} \tag{C.51}$$

where $K_{2D} = \frac{1}{2}\pi^{-1/2}/\Gamma[(1/2)]$ is a constant depending on the space dimensions. So we found a representation for the cross-over function first defined as a limit. This function is lattice independent having then a universal character and it describes the asymptotic behaviour of (C.43) for small p. In fact for $s \sim 2-(\alpha+1)$ we have that:

$$\Psi(s,\delta/p) = \frac{X_{\alpha+1}(\delta/p)}{s-2+(\alpha+1)} + o[(s-2+(\alpha+1)^{-1}] \tag{C.52}$$

Then C.46 implies that $f^0_\alpha(p,\delta)$ varies for $p\to 0$ as:

$$f^0_\alpha(p,\delta) = p^{(\alpha+1)-2}X_{\alpha+1}(\delta/p) + o(p^{(\alpha+1)-2}) \tag{C.53}$$

In our case it is also possible to find an exact form for (C.51) in the limit $\delta\to 0$, $p\to 0$. Starting from (C.45) that is a known Mellin transform, see [39]:

$$\begin{aligned} W(2-(\alpha+1);\gamma,\delta/p) = \\ \Gamma\big(2-(\alpha+1)\big)((\delta/p)^2+\gamma^2)^{((\alpha+1)-2)/2}\cos[(2-(\alpha+1))\tan^{-1}(\frac{\gamma}{\delta/p})] \end{aligned} \tag{C.54}$$

where we can already see that for $\alpha = 1$ the function diverges as $\Gamma(0) = \infty$. We can now write the cross-over function that is given by:

$$X_{\alpha+1}(\delta/p) = \\ -K_2\Gamma\big(2-(\alpha+1)\big)\int_0^1 \mathrm{d}\gamma(1-\gamma^2)^{-1/2}((\delta/p)^2+\gamma^2)^{((\alpha+1)-2)/2}\cos[(2-(\alpha+1))\tan^{-1}(\frac{\gamma}{\delta/p})] \tag{C.55}$$

Then in the limit we are considering we find, see [39]:

$$X_{\alpha+1}(0) = \frac{-1/2\ \pi^{-1/2}\Gamma(2-\big(\alpha+1)\big)}{\Gamma\big((\alpha+1)/2\big)\Gamma\big((3-(\alpha+1)\big)/2} \tag{C.56}$$

Thus (C.53) in this limit reads:

$$f^0_\alpha(p,0) = p^{(\alpha+1)-2}X_{\alpha+1}(0) + o(p^{(\alpha+1)-2}) \tag{C.57}$$

Finally deriving it with respect to p_x we obtain:

$$\frac{\partial}{\partial p_x}f^0_\alpha(p,0) = p_x\big((\alpha+1)-2\big)p^{(\alpha+1)-3}X_{\alpha+1}(0) + o(p^{(\alpha+1)-3}) \tag{C.58}$$

which is divergent for $p \to 0$ when $\alpha < 2$.

Bibliography

[1] D. C. Tsui, H. L. Stormer, and A. C. Gossard, "Two-dimensional magnetotransport in the extreme quantum limit. Phys. Rev. Lett., **48**, 1559, 1982

[2] G. Morandi, F. Napoli, E. Ercolessi, "Statistical Mechanics: An Intermediate Course", World Scientific, 2001

[3] T. D. Stanescu, "Introduction to Topological Quantum Matter and Quantum Computation" CRC Press, 2016

[4] J. Alicea, "New directions in the pursuit of Majorana fermions in solid state systems" Rep. Prog. Phys. **75**, 076501, 2012

[5] C Kallin, A J Berlinsky J. Phys., Condens. Matter **21**, 164210, 2009

[6] Alexei Yu. Kitaev, "Unpaired Majorana fermions in quantum wires", Physics Uspekhi **44**, 131, 2001

[7] J. Li et al., "Two-dimensional chiral topological superconductivity in Shiba lattice" Nature Communications **7**, 12297, 2016

[8] L. Fallani, A. Kastberg, "Cold atoms: A field enabled by light" EPL **110**, 53001

[9] European Laboratory for Non-Linear Spectroscopy, LENS

[10] D. Vodola, L. Lepori, E. Ercolessi, A. V. Gorshkov, G. Pupillo, "Kitaev Chains with Long-Range Pairing", Phys. Rev. Lett. **113**, 156402, 2014

[11] D. Vodola, L. Lepori, E. Ercolessi, G. Pupillo, "Long-range Ising and Kitaev models: phases, correlations and edge modes", New J. Phys. 18, 015001, 2016

[12] K. Huang, "Statistical Mechanics" Wiley, 1987

[13] S. Sachdev, "Quantum Phase Transitions, 2nd Edition", Cambridge University Press, 2011

[14] C. Chamon et al., "Topological Aspects of Condensed Matter Physics", Oxford University Press, 2017

[15] A. P. Schnyder et al. , "Classification of topological insulators and superconductors in three spatial dimensions", Phys. Rev. B **78**, 195125, 2008

[16] G. Morandi, "The Role of Topology in Classical and Quantum Physics" Lecture Notes in Physics Monographs, Springer, 1992

[17] A. Bernevig, T. L. Hughes, "Topological Insulators and Topological Superconductors", Princeton University Press, 2013

[18] D. Vodola, "Correlations and Quantum Dynamics of 1D Fermionic Models: New Results for the Kitaev Chain with Long-Range Pairing", Tesi di Dottorato, Università di Bologna, 2015

[19] S. Q. Shen, "Topological Insulators: Dirac Equation in Condensed Matters" Springer, 2013

[20] I. S. Gradshteyn, I. M. Ryzhik, "Tables of Integrals, Series, and Products", Academic, New York, 2007

[21] M. Abramowitz, I. A. Stegun, "Handbook of Mathematical Functions" National Bureau of Standards Applied Mathematics Series, 55, 1972

[22] E. Lieb, T. Schultz, D. Mattis, "Two soluble models of an antiferromagnetic chain", Annals of Physics **16**, 407, 1961

[23] Y. Tanaka, M. Sato, N. Nagaosa "Symmetry and Topology in Superconductors –Odd-Frequency Pairing and Edge States–" J. Phys. Soc. Jpn. **81**, 011013, 2012

[24] O. Viyuela, L. Fu, M. Delgado, "Chiral Topological Superconductors Enhanced by Long-Range Interactions" Phys. Rev. Lett. **120**, 017001, 2018

[25] L. Lepori, L. Dell'Anna, "Long-range topological insulators and weakened bulk-boundary correspondence" New J. Phys. **19**, 103030, 2017

[26] S. R. White, "Density matrix formulation for quantum renormalization groups," Phys. Rev. Lett. **69**, 2863, 1992.

[27] O. Viyuela, D. Vodola, G. Pupillo, M.A. Martin-Delgado, "Topological Massive Dirac Edge Modes and Long-Range Superconducting Hamiltonians" Phys. Rev. B **94**, 125121, 2016

[28] F. W. J. Olver, D. W. Lozier, R. F. Boisvert,C. W. Clark, "NIST Handbook of Mathematical Functions", Cambridge University Press, 2010

[29] R. D. Misra, "On the stability of crystal lattices.II" Proc. Cambridge Phil Soc. **36**, 173, 1940

[30] Wolfram Research, Inc., Mathematica, Version 11.3, Champaign, IL, 2018

[31] Python Software Foundation. Python Language Reference, version 3

[32] J. Bardeen, L. N. Cooper, R. Schrieffer, “Theory of superconductivity” , Phys. Rev. **108**, 1175, 1957

[33] M. Born and M. Bradburn, "The thermodynamics of crystal lattices. II.", Proc. Camb. Phil. Soc. **39**, 104, 1943

[34] M. N. Barber and A. H. Opie, "On the nature of anomalous terms in the dispersion relation at small wavenumber", J. Phys. C: Solid State Phys. **10**, 3717, 1977

[35] J. M. Borwein, M. L. Glasser, R. C. McPhedran, J. G. Wan, I. J. Zucker, "Lattice sums then and now", Cambridge University Press, 2013

[36] M. H. Cohen, F. Keffer, "Dipolar Sums in the Primitive Cubic Lattices", Phys. Rev. **99**, N. 4, 1955

[37] K. C. Gupta,R. M. Agrawal, R. P. S. Rathore, "Incomplete Gamma Functions and Lattice Sums for B.C.C. Structures" phys. stat. sol. (b) **118**, 399, 1983

[38] Michael N. Barber Cross-over phenomena in the asymptotic behaviour of lattice sums, J. Phys. A: Math. Gen. **10**, 2133, 1977

[39] H. Bateman, "Tables of Integral Transforms", A. Erdèlyi, 1954

Acknowledgements

I would like to express my gratitude to my thesis advisor Prof. Elisa Ercolessi which offered me the opportunity to study real interesting things and to get in touch with a group of competent and nice people to which I am thankful.
I also wanted to thank her for the constant help recieved and yet to always pushing me to go further.
I would then like to thank my supervisor Prof. Fabio Ortolani for sharing with me a little of his unvaluable experience and for his help.
I am also very thankful to Giuseppe Magnifico for his time and his important help.
Then I would like to thank Dr. Davide Vodola that I only met once but was able to give me the proper advice.
Thanks go to the University friends with whom I passed most of my time lately, as everyone helped me in someway and thanks go also to my other friends of everywhere.
My very special thanks go to my beloved Anna for her uncoditional love and neverending support.
I dedicate this work to my family. It is because of you that I have come this far.